Spin-orbit coupled states arising in the half-filled t_{2g} shell

Master thesis of

Marco Schönleber

December 18, 2023

Examiner: Prof. Dr. Maria Daghofer
Co-Examiner: Prof. Dr. Mathias Scheurer

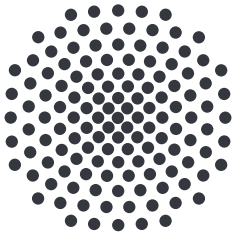

Institute for Functional Matter and Quantum Technologies
Universität Stuttgart
Pfaffenwaldring 57, 70550 Stuttgart

Contents

1 Introduction

1.1 Motivation

As early as the 18th century, physicists and mathematicians had to face the problem that the three-body problem of classical mechanics has no general, closed solution and can only be solved approximately using numerical approaches [1]. Many-particle systems such as solids with particle numbers in the order of 10^{23} therefore pose an obvious problem in physics. Over the past century, however, it has been shown that a surprisingly large number of materials can be described to a very good approximation by effective models of non-interacting fermions [2]. However, not all materials bow to the effectiveness of these approaches. In so-called strongly correlated materials, the correlations between the individual electrons cannot be ignored without leaving fundamental aspects of the real material unexplained [3]. Transition metal compounds are an important class of materials in which such correlation effects are prominent. The materials in this class are characterised by the fact that electrons in partially filled d orbitals are responsible for the dominant effects in the electronic structure [4]. Research into these materials is relevant because some of them are promising candidates for topologically non-trivial phases [5–9] as well as for unconventional superconductivity [4, 10, 11] and thus offer both scientific and technological potential. In this work, we will specifically investigate how four potentially relevant effects, Hund's coupling, spin-orbit coupling, superexchange and Jahn-Teller effect, affect the ground state in a half-filled t_{2g} shell. Previous studies, such as those by Streltsov and Khomskii [12], as well as more recent experimental studies based on their results [13], have not yet made any statement about the mutual relationship between the four effects, which is why the aim here is to investigate how they manifest themselves both in the spectrum and in the state characteristics.

1.2 Structure of the thesis

This thesis is divided into five chapters, which are briefly described below.

In Chapter 2, the theory underlying the problem under consideration is first elaborated. The fundamental difficulty of solving many-body problems is briefly explained and the specific effects in the case of strongly correlated electrons in transition metal compounds that will be relevant in this work are discussed.

Section 2.1 explains Hund's coupling and spin-orbit coupling, which can also influence the structure of individual atoms independently of the surrounding crystal.

Section 2.2 then explains the influence of the crystal surrounding the single ion on the system, in particular the energetic splitting of the d-shell. In addition, the Jahn-Teller effect is introduced, which in the context of this work has a similar effect to crystal field splitting and can cause a further symmetry reduction.

The final Section 2.3 describes the possibilities for exchanging electrons between individual sites and what influence these can have on the spectrum of the system. In addition, the cooperative Jahn-Teller effect of several sites is briefly discussed.

Chapter 3 explains the mathematical models used in this work. After a brief introduction to the considered Fock space in Section 3.1, Section 3.2 first explains how Hund's coupling can be described by the Kanamori-Hubbard Hamiltonian. Here, total angular momentum and total spin are introduced as good quantum numbers of the operator and the eigenstates of the ground state manifold are described.

The same is done in Section 3.3, where the spin-orbit coupling operator is derived and analysed.

Section 3.4 then shows how the Jahn-Teller effect can be implemented as a Hamiltonian operator. For this purpose, two normal modes are introduced, which describe the distortion of the crystal around the ion.

Finally, in Section 3.5, the possibility of electron hopping between individual sites by the superexchange mechanism is described, whereby the individual exchange terms between orbitals are discussed. In addition, the method of second-order perturbation theory is introduced, with which the solutions to the full problem will be analysed later.

The following results are divided into two chapters. Chapter 4 first explains all results concerning a single ion in the crystal. Section 4.1 shows exactly which energies and ground states the combination of Hund's coupling and spin-orbit coupling provides. Section 4.2 also considers the influence of the Jahn-Teller effect as an additional added term on the solution of the Hamiltonian operator. Here it can be shown that the ground state manifold is split depending on the magnitude of the magnetic quantum number, whereby the maximisation of it is slightly preferred.

Chapter 5 explains the effects that can occur when two neighbouring ions interact. Section 5.1 first discusses the applicability of perturbation theory to the problem. It was shown that although the energy gap between the supposed ground state and other states can disappear, this does not happen for physically relevant parameters, which ultimately validates its use. The two edge cases of vanishing spin-orbit coupling and Hund's coupling are then described analytically and the common region is analysed numerically. This shows that the perturbation-theoretic approach achieves almost perfect agreement with the exact solution. Section 5.1.2 then analyses the influence that the Jahn-Teller effect can have on the energy splitting. It is shown that this can cause a distortion even in a highly simplified system.

The following Chapter 6 then summarises and provides an outlook on possible subsequent research.

2 Theory

This chapter explains the theoretical principles required to understand the underlying physics and the methods and results based on it.

Section 2.1 describes the physics of isolated transition metal ions. It first explains how the description of multi-electron atoms works in the shell model and then goes into the two fundamental components in the Hamiltonian operator, namely Hund's coupling and spin-orbit coupling.

In Section 2.2, the effects that the ion experiences in the crystal are discussed. Firstly, the crystal field splitting of the d orbitals is explained and secondly, the reduction of the ground state energy through a further reduction of the symmetry, the so-called Jahn-Teller effect, is introduced.

Section 2.3 then describes how the interaction between the individual ions can manifest itself. On the one hand, this can occur through an exchange of electrons between the two ions, which takes place through the ligand atom in between. This mechanism is referred to as superexchange. Secondly, we briefly analyse how the Jahn-Teller effect manifests itself when the distortions on neighbouring ions are related to each other.

2.1 Isolated transition metal ions

Elements that have an incomplete d subshell or can form ions with an incomplete d subshell are referred to as transition metals.[14] This incomplete d subshell is a configuration in which correlation effects between individual electrons can become relevant, which is why the fundamental physical description is only possible using methods of many-body quantum mechanics. Neglecting relativistic effects, the Schrödinger equation can be described by

$$\left[-\sum_{i}^{n}\frac{\Delta_i}{2m}-\frac{\Delta_\alpha}{2M}-\sum_{i}^{n}\frac{Ze^2}{r_{i\alpha}}+\frac{1}{2}\sum_{i,j}^{n}\frac{e^2}{r_{ij}}-E_k\right]\psi_k\left(\{\vec{r_i}\}\right)=0 \tag{2.1}$$

where i indicates the n individual electrons of mass m, α indicates the atomic nucleus of mass M and atomic number Z and k indicates the possible eigenenergies and eigenstates of the operator. The solution of this equation (2.1) describes the wave function of all electrons under consideration and must also be completely antisymmetric under particle exchange according to the Pauli principle [15]. Equations of this form are generally not analytically solvable and must be replaced by simplified models [16]. A starting point for this can be to consider the solutions of equation (2.1) for a single electron, since this problem can be solved by eliminating the Coulomb interaction between individual particles. The mathematical elaboration of this problem is dealt with in detail in most standard textbooks on quantum mechanics [16–19], which is why only the results relevant to the following considerations will be explained here. The solutions of the eigenvalue problem can be separated in spherical coordinates by

$$\hat{H} R_{n,l}(r)\, Y_{l,m}(\phi,\theta) = E_n R_{n,l}(r)\, Y_{l,m}(\phi,\theta) \tag{2.2}$$

where the eigenvalues are given by

$$E_n = -Z^2 E_{\mathrm{Ry}} \frac{1}{n^2} \quad n \in \mathbb{N} \tag{2.3}$$

with the Rydberg energy E_{Ry}. For the remaining quantum numbers l and m the following relations

$$l < n \quad l \in \mathbb{N} \cup 0 \tag{2.4}$$

$$|m| \leq l \quad m \in \mathbb{Z} \tag{2.5}$$

apply, which results in a degeneration of the energy eigenvalues of

$$\# = n^2. \tag{2.6}$$

When naming the individual orbitals, it is usual to replace the secondary quantum number l with a corresponding lower case letter. The following relations

$$\begin{aligned} l = 0 &\;\widehat{=}\; s \\ l = 1 &\;\widehat{=}\; p \\ l = 2 &\;\widehat{=}\; d \\ l = 3 &\;\widehat{=}\; f. \end{aligned}$$

apply. The radial wave functions $R_{n,l}(r)$ are exclusively decisive for the expected distance between nucleus and electron, which is given by

$$\langle r \rangle = \int_0^\infty r R_{n,l}(r)\; r^2 dr. \tag{2.7}$$

It can be seen that this expectation value increases not only with increasing principal quantum number n, but also with increasing secondary quantum number l. If we now try to apply the knowledge gained to the multi-electron problem, the simplest approach is to use the calculated eigenstates of the single electron problem as the basis for the Fock space. If one now occupies the individual orbitals one after the other, starting with the lowest energy, it follows that the energy eigenvalues of the next highest orbitals must be influenced by this. If we make the simplifying assumption that the individual electrons shield the positively charged atomic nucleus radially symmetrically, the multi-electron problem can be solved for each additional orbital by an effective Hamiltonian of the form

$$\hat{H}_{\text{eff}} = \hat{H}_{\text{kin}} + \hat{V}_{\text{eff}}, \tag{2.8}$$

where the shielding of the nucleus by the already distributed electrons is implemented in $\hat{V}_{\text{eff}}$. Due to the l-dependence of the radial wave function and thus also the proportion of effective shielding, the $(n+1)$-s orbitals are now even below the n-d orbitals in terms of energy when the states are occupied. Even if this is not always true due to other effects that only become clear in a more detailed treatment of the problem, it can be assumed for the class of materials dealt with in this work that a configuration of the form $(n+1)s^2\, nd^k$ always exists for the individual atom.

Various spin configurations are now available within this electronic configuration. Depending on the exact problem, two different effects can play a role here, which influence the spin configuration in different ways.

Hund's rule is based on the fundamental assumption that electrons that are in the same orbital experience a greater Coulomb repulsion and thus an increase in energy than electrons that are in different orbitals. Since the symmetry of the occupied orbitals is directly linked to the total orbital angular momentum L and total spin S, the simple rules formulated by Hund [20] apply that the energetic ground state is always determined by the highest possible total spin S and, if this is fulfilled, the highest possible total orbital angular momentum L is also aimed for. A more mathematical description of these rules for the class of materials considered in this work is provided later on by the Kanamori-Hubbard Hamiltonian.

Spin-orbit coupling considers the interaction of the electron spin with its own orbital angular momentum. This interaction can be understood as a magnetic interaction, as in a semi-classical view, such as in the Bohr atomic model, the orbiting electron generates a magnetic field which can interact with the magnetic moment of the electron. In more precise physical terms, the interaction can be described as

$$\hat{H}_{\lambda} = \lambda \sum_{i} \vec{\hat{l}}_i \cdot \vec{\hat{s}}_i \tag{2.9}$$

where in the multi-electron problem the individual electrons, represented here by the index i, are added up. The spin-orbit coupling constant λ can be estimated with $\lambda \propto Z^4$ [4], where Z is the atomic number.

2.2 Influence of the surrounding crystal

2.2.1 Crystal field splitting

If a transition metal ion described in the previous section is viewed in a crystal, the physics changes fundamentally. The reason for this is that the full radial symmetry is reduced to that of the surrounding crystal. The influence of the cubic symmetry considered in this work, which is shown in Figure 2.1, is explained below.

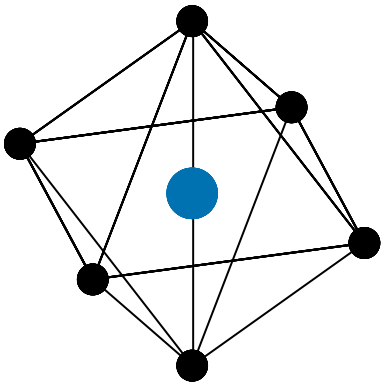

Figure 2.1: Shown is a single ion (blue) surrounded by ligands (black) in cubic crystal symmetry.

As can be seen in Figure 2.1, the ligands surrounding the transition metal ions in cubic crystals can be located on the classical Cartesian axes. If we combine this observation with the d orbitals considered in Figure 2.2, we can already intuitively see that the z^2 and $x^2 - y^2$ orbitals lying on the axes can be influenced differently than the yz, xz and xy orbitals that lie between the axes. This crystal field splitting of the orbitals can be physically explained by the Coulomb repulsion and the covalency between the electrons of the neighbouring ions. Since a detailed derivation is not necessary for the understanding of this work, only the result is considered here and reference is made to the literature.[4]

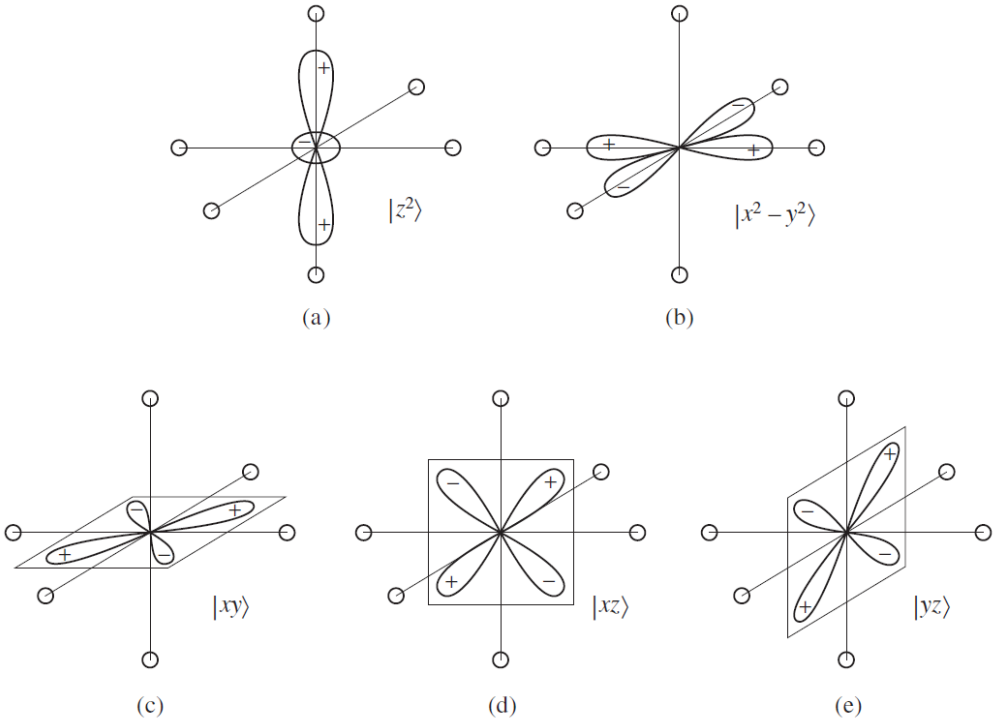

Figure 2.2: A possible basis of the d orbitals is shown. It can be seen that three of the states lie between, while the other two orbitals lie on the axes [4].

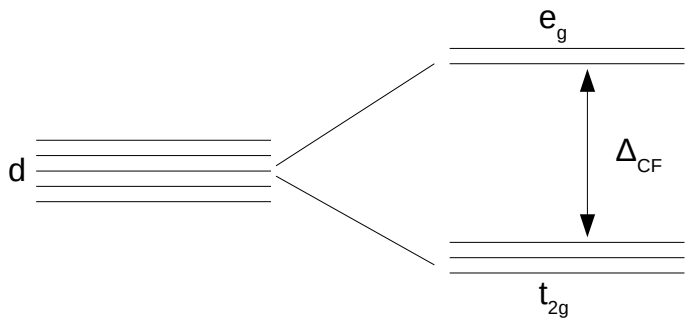

Figure 2.3: The crystal field splitting of the d orbitals in cubic symmetry is shown. The relevant triple degenerate t_{2g} shell in this work is energetically below the double degenerate e_g shell.

The result of the detailed calculation shows that the so-called t_{2g} orbitals, consisting of the yz, xz and xy orbitals, are lowered in energy, while the e_g orbitals consisting of the z^2 and $x^2 - y^2$ orbitals are increased. This energy splitting Δ_{CF}, which can usually be estimated with $1.5 - 3.5\,\mathrm{eV}$ [4], is shown in Figure 2.3.

Due to this relatively large energy splitting, it can be assumed that the hybridisation of the t_{2g} with the e_g orbitals can be neglected and only the t_{2g} orbitals need to be considered. If we consider the angular momentum of the d orbitals in matrix representation, we find that these matrices, projected onto the subspace spanned by the t_{2g} orbitals, are almost identical to those of the angular momentum of the p orbitals. This is shown in the following in the basis $\{d_{yz}, d_{xz}, d_{xy}, d_{3z^2-r^2}, d_{x^2-y^2}\}$ respectively $\{p_x, p_y, p_z\}$.

$$\hat{l}_d^x = \left[\begin{array}{ccc|cc} 0 & 0 & 0 & -\sqrt{3}i & -i \\ 0 & 0 & i & 0 & 0 \\ 0 & -i & 0 & 0 & 0 \\ \hline \sqrt{3}i & 0 & 0 & 0 & 0 \\ i & 0 & 0 & 0 & 0 \end{array}\right], \quad \hat{l}_p^x = \begin{pmatrix} 0 & 0 & 0 \\ 0 & 0 & -i \\ 0 & i & 0 \end{pmatrix}, \tag{2.10}$$

$$\hat{l}_d^y = \left[\begin{array}{ccc|cc} 0 & 0 & -i & 0 & 0 \\ 0 & 0 & 0 & \sqrt{3}i & -i \\ i & 0 & 0 & 0 & 0 \\ \hline 0 & -\sqrt{3}i & 0 & 0 & 0 \\ 0 & i & 0 & 0 & 0 \end{array}\right], \quad \hat{l}_p^y = \begin{pmatrix} 0 & 0 & i \\ 0 & 0 & 0 \\ -i & 0 & 0 \end{pmatrix}, \tag{2.11}$$

$$\hat{l}_d^z = \left[\begin{array}{ccc|cc} 0 & i & 0 & 0 & 0 \\ -i & 0 & 0 & 0 & 0 \\ 0 & 0 & 0 & 0 & 2i \\ \hline 0 & 0 & 0 & 0 & 0 \\ 0 & 0 & -2i & 0 & 0 \end{array}\right], \quad \hat{l}_p^z = \begin{pmatrix} 0 & -i & 0 \\ i & 0 & 0 \\ 0 & 0 & 0 \end{pmatrix}. \tag{2.12}$$

The only difference lies in the sign, which differs by one minus.

The angular momentum of the t_{2g} orbitals can therefore be described by an effective orbital angular momentum $l_{\text{eff}} = 1$, whereby the aforementioned negative sign must be taken into account in individual cases [21]. Accordingly, the following applies to the eigenstates

$$\hat{l}_{\text{eff}}^z \frac{1}{\sqrt{2}} \left(|yz\rangle + i\,|xz\rangle\right) = +\frac{1}{\sqrt{2}} \left(|yz\rangle + i\,|xz\rangle\right) \tag{2.13}$$

$$\hat{l}_{\text{eff}}^z |xy\rangle = 0 \tag{2.14}$$

$$\hat{l}_{\text{eff}}^z \frac{1}{\sqrt{2}} \left(|yz\rangle - i\,|xz\rangle\right) = -\frac{1}{\sqrt{2}} \left(|yz\rangle - i\,|xz\rangle\right). \tag{2.15}$$

2.2.2 Jahn-Teller effect

In addition to crystal field splitting, which is determined by the bonding-related symmetries of the crystal and here splits the d shell into t_{2g} and e_g orbitals, there are other similar effects that can be summarised under the term Jahn-Teller effect. As was shown with the Jahn-Teller theorem [22], the energy of the electronic ground state of a non-linear molecule or crystal can be lowered further and further by reducing the geometric symmetry until only the double Kramers degeneracy remains. Physically, this reduction in symmetry is manifested by a shift in the surrounding ligands, which can be described mathematically by generalised coordinates Q_i. If the potential energy in these coordinates is represented as a Taylor series, the result is

$$V(Q) = V_0 + \sum_k \frac{\partial V}{\partial Q_k} Q_k + \frac{1}{2} \sum_{k,l} \frac{\partial^2 V}{\partial Q_k \partial Q_l} Q_k Q_l + \cdots \tag{2.16}$$

where the square part can be understood as the energy required to distort the crystal against its compression modulus [23].

2.3 Interacting ions

2.3.1 Superexchange

If not only isolated ions are considered, but also ions in periodic crystal structures, these can interact with each other. In the class of materials considered in this thesis, the direct hybridisation of the orbitals of the transition metal ions is negligible. Instead, the electron exchange takes place mostly via superexchange interaction. This is characterised by the fact that the electrons in the d orbitals interact directly with the p orbitals of the ligand, whereby two ions that are not directly adjacent interact with each other through the ligand between them [24, 25]. The exchange can be described in general terms by a Hamiltonian of the form

$$\hat{H}_t = -t_{pd} \sum_i \left(\hat{c}^\dagger_{i\sigma} \hat{c}_{p\sigma} + \hat{c}^\dagger_{p\sigma} \hat{c}_{i\sigma} \right). \tag{2.17}$$

2.3.2 Cooperative Jahn-Teller effect

If several atoms are considered in a Jahn-Teller active crystal system, this results in a complex system with many possible interaction channels. The most important aspect is

that the individual displacements of the ligands can no longer occur independently of each other. If, for example, the crystal is compressed along the z-axis ($Q_3 < 0$) in the vicinity of a single ion, the crystal structure surrounding the ion above it must automatically be elongated along the z-axis ($Q_3 > 0$). In addition, the ions in the crystal can interact with each other via phonons, which has a direct influence on the distortions that characterise the Jahn-Teller effect. As the co-operative Jahn-Teller effect will only play a minor role in the following, this will suffice for the theoretical part. For more in-depth insights, one can find more detailed information in the literature [24, 26].

3 Models and methods

This chapter explains the models which were used to the describe the physical systems and the methods which were used to solve the resulting mathematical problems.

Section 3.1 introduces the Fock space on which all the calculations in this thesis are performed.

In Section 3.2 the Kanamori-Hubbard Hamiltonian is introduced, which gives a mathematical form to Hund's rules. The eigenenergies and the ground state manifold of the three electron case are given.

In Section 3.3 the mathematical implementation of the second relevant interaction, the spin-orbit coupling is introduced. As in Section 3.2, the ground state manifold of the three electron case is given.

Following this, the operator form of the Jahn-Teller effect and its corresponding normal modes are introduced in Section 3.4.

Lastly the superexchange mechanism and its implementation as a perturbation on the local Hamiltonian is explained in Section 3.5.

3.1 Fock space of the analysed model

In this thesis, we consider Fock spaces that describe half-filled t_{2g} shells. Here, a representation is chosen that is based on the underlying yz, xz and xy orbitals. Since each of these orbitals is doubly spin degenerate, there are three electrons distributed over six one-electron states, i.e. a $\binom{6}{3} = 20$ dimensional Fock space. As the standard basis used is shown in full in Appendix A, a brief example will suffice for a better understanding of the work.

$$|0,0,1,1,1,0\rangle = \left|\times,\uparrow\downarrow,\uparrow\right\rangle = c^\dagger_{xz\uparrow} c^\dagger_{xz\downarrow} c^\dagger_{xy\uparrow} |0\rangle \tag{3.1}$$

In addition, a two-site model will be considered in this work, in which the two identical ions are connected to each other via the z-axis. The resulting Fock space is therefore

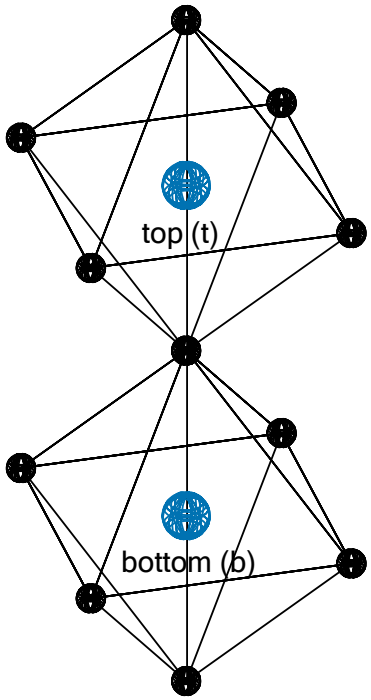

Figure 3.1: Shown is the structure considered in the second part of the thesis. The two octahedra share a corner on the z-axis.

$\binom{12}{6} = 924$ dimensional. States in this space are composed of the one-site states, whereby the upper (t) and lower (b) ions are indexed accordingly as is shown in figure 3.1

3.2 Kanamori-Hubbard Hamiltonian

The theoretical findings described in the previous chapter can be represented in the Kanamori form of the multi-orbital Hubbard Hamiltonian as a mathematical operator [27, 28]. This can be written in two forms, both of which contribute to understanding

and will therefore be explained here. On the one hand, the operator can be written as

$$\hat{H}_U = \sum_{\alpha,\beta} \hat{c}^\dagger_{\alpha\uparrow}\hat{c}^\dagger_{\alpha\downarrow}\left[U\delta_{\alpha,\beta} + J'\left(1-\delta_{\alpha,\beta}\right)\right]\hat{c}_{\beta\downarrow}\hat{c}_{\beta\uparrow} \tag{3.2}$$

$$+ \sum_{\alpha,\beta<\alpha}\sum_{\sigma,\sigma'} \hat{c}^\dagger_{\alpha\sigma}\hat{c}^\dagger_{\beta\sigma'}\left[U'\hat{c}_{\beta\sigma'}\hat{c}_{\alpha\sigma} - J_\mathrm{H}\hat{c}_{\beta\sigma}\hat{c}_{\alpha\sigma'}\right]. \tag{3.3}$$

Here U and U' represent the intra- and inter-orbital Coulomb repulsions between individual electrons, while J_H and J' represent the Hund's coupling and the pair-hopping exchange between individual orbitals respectively, whereby it can also be shown that $U' = U - 2J_\mathrm{H}$ and $J_\mathrm{H} = J'$ applies [29]. The Greek letters α and β stand for the three orbitals, while σ and σ' can represent spin up and down. In this form, you can directly see which microscopic aspects are taken into account in the model. Firstly, the energy increases with each additional electron due to Coulomb repulsion between the electrons. This is the essence of the Hubbard Hamiltonian. Secondly, there is a direct spin-spin interaction between the individual orbitals, which shows that a parallel alignment of the spins in the individual orbitals is favoured, exactly as predicted by Hund's rules. An alternative notation for the operator can be found by defining total orbital angular momentum and total spin as operators. If these operators are defined as follows

$$\hat{L}^2 = \sum_{i\in\{x,y,z\}}\left(\sum_n \hat{l}^i_n\right)^2 \tag{3.4}$$

$$\hat{S}^2 = \sum_{i\in\{x,y,z\}}\left(\sum_n \hat{s}^i_n\right)^2, \tag{3.5}$$

where n numbers the electrons and substituting them into the Kanamori-Hubbard Hamiltonian gives the intuitively understandable form

$$\hat{H}_U = \left(U - 3J_\mathrm{H}\right)\frac{\hat{N}(\hat{N}-1)}{2} - 2J_\mathrm{H}\hat{S}^2 - \frac{J_\mathrm{H}}{2}\hat{L}^2 + \frac{5}{2}J_\mathrm{H}\hat{N} \tag{3.6}$$

where $\hat{N}$ represents the particle number operator. Here you can see directly how the model relates to the well-known Hund's rules. First, the aim is to maximise the total spin, then to maximise the total orbital angular momentum. Accordingly, the eigenstates can be simply described by the usual quantum numbers S, L, m_S and m_L, where the degeneracy is given directly by $(2S+1)\cdot(2L+1)$. The eigenspaces and their energies are shown in Table 3.1, the states can be looked up in Appendix B.

In the following, only the most important states will be presented here, namely the fourfold degenerate $S = \frac{3}{2}, L = 0$ ground state manifold of the three-electron problem.

Table 3.1: Eigenenergies of the Kanamori-Hubbard Hamiltonian with three electrons

E	S	L	degeneracy
$3U-4J$	$\frac{1}{2}$	1	6
$3U-6J$	$\frac{1}{2}$	2	10
$3U-9J$	$\frac{3}{2}$	0	4

The states take the following form

$$\left|S_{+\frac{3}{2}}\right\rangle = \left|m_S = +\frac{3}{2}\right\rangle = |\uparrow,\uparrow,\uparrow\rangle \tag{3.7}$$

$$\left|S_{+\frac{1}{2}}\right\rangle = \left|m_S = +\frac{1}{2}\right\rangle = \frac{1}{\sqrt{3}}\left(|\downarrow,\uparrow,\uparrow\rangle + |\uparrow,\downarrow,\uparrow\rangle + |\uparrow,\uparrow,\downarrow\rangle\right) \tag{3.8}$$

$$\left|S_{-\frac{1}{2}}\right\rangle = \left|m_S = -\frac{1}{2}\right\rangle = \frac{1}{\sqrt{3}}\left(|\downarrow,\downarrow,\uparrow\rangle + |\downarrow,\uparrow,\downarrow\rangle + |\uparrow,\downarrow,\downarrow\rangle\right) \tag{3.9}$$

$$\left|S_{-\frac{3}{2}}\right\rangle = \left|m_S = -\frac{3}{2}\right\rangle = |\downarrow,\downarrow,\downarrow\rangle \tag{3.10}$$

where their energy is $3U - 9J_{\mathrm{H}}$.

3.3 Spin-orbit coupling

The spin-orbit coupling can be quantised with the help of the effective orbital angular momentum derived in Section 2.2 in second quantisation by

$$\begin{aligned}\hat{H}_\lambda &= \lambda \sum_{\alpha,\beta}\sum_{\sigma,\sigma'} \langle\alpha,\sigma|\,\vec{\hat{l}}_{t_{2g}}\cdot\vec{\hat{s}}\,|\beta,\sigma'\rangle\,\hat{c}^\dagger_{\alpha,\sigma}\hat{c}_{\beta,\sigma'} \\ &= -\lambda \sum_{\alpha,\beta}\sum_{\sigma,\sigma'} \langle\alpha|\,\vec{\hat{l}}_{p}\,|\beta\rangle\cdot\langle\sigma|\,\vec{\hat{s}}\,|\sigma'\rangle\,\hat{c}^\dagger_{\alpha,\sigma}\hat{c}_{\beta,\sigma'} \\ &= \frac{i\lambda}{2}\sum_{\alpha,\beta,\gamma}\sum_{\sigma,\sigma'} \epsilon_{\alpha,\beta,\gamma}\hat{\tau}^\gamma_{\sigma,\sigma'}\hat{c}^\dagger_{\alpha,\sigma}\hat{c}_{\beta,\sigma'}\end{aligned} \tag{3.11}$$

where the $\hat{\tau}^\gamma$ are the Pauli matrices [30]. The eigenstates of this operator can be represented as correspondingly antisymmetrised, direct products of the one-particle solution for any fixed number of particles. These are classified by the total angular momentum quantum numbers j and m_j. From the parameters for the single electron,

$s = \frac{1}{2}$ and $l = 1$, it follows that only $j = \frac{1}{2}$ and $j = \frac{3}{2}$ are possible. The eigenstates are therefore combined from

$$|j = 1/2, m_j = +1/2\rangle == \frac{1}{\sqrt{3}} |yz, \downarrow\rangle + \frac{i}{\sqrt{3}} |xz, \downarrow\rangle + \frac{1}{\sqrt{3}} |xy, \uparrow\rangle , \tag{3.12}$$

$$|j = 1/2, m_j = -1/2\rangle = \frac{1}{\sqrt{3}} |yz, \uparrow\rangle - \frac{i}{\sqrt{3}} |xz, \uparrow\rangle - \frac{1}{\sqrt{3}} |xy, \downarrow\rangle , \tag{3.13}$$

with energy $+\lambda$ and

$$|j = 3/2, m_j = +3/2\rangle = \frac{1}{\sqrt{2}} |yz, \uparrow\rangle + \frac{i}{\sqrt{2}} |xz, \uparrow\rangle , \tag{3.14}$$

$$|j = 3/2, m_j = +1/2\rangle = \frac{1}{\sqrt{6}} |yz, \downarrow\rangle + \frac{i}{\sqrt{6}} |xz, \downarrow\rangle - \sqrt{\frac{2}{3}} |xy, \uparrow\rangle , \tag{3.15}$$

$$|j = 3/2, m_j = -1/2\rangle = \frac{1}{\sqrt{6}} |yz, \uparrow\rangle - \frac{i}{\sqrt{6}} |xz, \uparrow\rangle + \sqrt{\frac{2}{3}} |xy, \downarrow\rangle , \tag{3.16}$$

$$|j = 3/2, m_j = -3/2\rangle = \frac{1}{\sqrt{2}} |yz, \downarrow\rangle - \frac{i}{\sqrt{2}} |xz, \downarrow\rangle , \tag{3.17}$$

with energy $-\frac{1}{2}\lambda$ and are listed in Appendix B.

In the following, only the most important states will be presented, namely the fourfold degenerate ground state manifold of the three-electron problem. The states take the following form

$$\left|j_{+\frac{3}{2}}\right\rangle = |j = 3/2, m_j = +3/2\rangle \, |j = 3/2, m_j = +1/2\rangle \, |j = 3/2, m_j = -1/2\rangle \tag{3.18}$$

$$\left|j_{+\frac{1}{2}}\right\rangle = |j = 3/2, m_j = +3/2\rangle \, |j = 3/2, m_j = +1/2\rangle \, |j = 3/2, m_j = -3/2\rangle \tag{3.19}$$

$$\left|j_{-\frac{1}{2}}\right\rangle = |j = 3/2, m_j = +3/2\rangle \, |j = 3/2, m_j = -1/2\rangle \, |j = 3/2, m_j = -3/2\rangle \tag{3.20}$$

$$\left|j_{-\frac{3}{2}}\right\rangle = |j = 3/2, m_j = +1/2\rangle \, |j = 3/2, m_j = -1/2\rangle \, |j = 3/2, m_j = -3/2\rangle \tag{3.21}$$

where their energy is $-\frac{3}{2}\lambda$.

3.4 Jahn-Teller effect

If the Taylor series (2.16) from 2.1 is broken off after the quadratic order, the Jahn-Teller effect can be described in the natural coordinates of the oscillation. For the octahedral

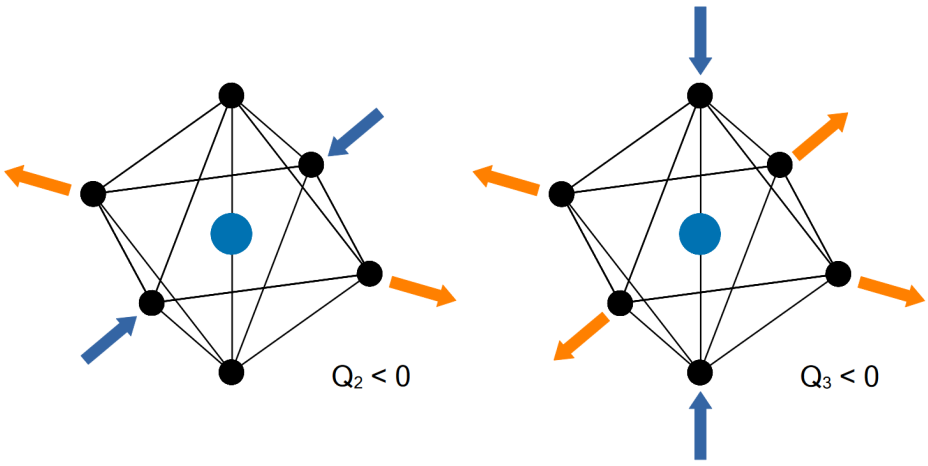

Figure 3.2: The Q_2 and Q_3 oscillation modes of the cubic system are shown.

system, only the oscillation modes Q_2 and Q_3 are relevant, which are represented by the vectors

$$Q_2 = \frac{1}{\sqrt{2}}(1,-1,0)^T \tag{3.22}$$

$$Q_3 = \frac{1}{\sqrt{6}}(-1,-1,2)^T \tag{3.23}$$

$$\tag{3.24}$$

and are shown in Figure 3.2.

The corresponding Hamiltonian can be written as

$$\hat{H}_{\mathrm{JT}} = -\frac{g}{\sqrt{3}}\sum_n \left[\left(\hat{l}_n^x\right)^2 - \left(\hat{l}_n^y\right)^2\right] Q_2 - g\sum_n \left[\left(\hat{l}_n^z\right)^2 - \frac{2}{3}\right] Q_3 + \frac{B}{2}\left(Q_2^2 + Q_3^2\right), \tag{3.25}$$

where g can be understood as the coupling of the electrons to the geometric distortion and B as the compression modulus of the crystal. The sums run over the individual electrons in the system [12].

If a single ion is considered, then if only the energy minima are of interest, even the value of Q_2 can be set to zero, since it can be shown that all local minima are equivalent and one always lies on the $Q_2 = 0$ axis. Although this argument cannot be maintained for the two-site problem, it is also assumed for this case in order to reduce the dimension of the parameter space that has to be analysed. In addition, the relationship $Q_3^{\mathrm{t}} = -Q_3^{\mathrm{b}}$ then results for two ions connected to the z-axis, since a compression of the crystal around

the upper ion is automatically accompanied by an elongation around the lower ion. As already mentioned in 2.3, all other possible interactions are neglected in this work.

3.5 Superexchange

The Hamilton operator described in (2.17) can be simplified in a first step by integrating out the occupations of the ligand orbitals within the framework of an effective theory [25]. If two transition metal ions lie in a line with a ligand, the Hamilton operator can be described similarly to the Hubbard Hamiltonian [28]. In its simplest form, this does not take any orbitals into account and reads

$$\hat{H}_{\mathrm{Hub}} = -t \sum_{i,\sigma} \left(\hat{c}^{\dagger}_{i,\sigma} \hat{c}_{i+1,\sigma} + \hat{c}^{\dagger}_{i+1,\sigma} \hat{c}_{i,\sigma} \right) + U \sum_{i} \hat{n}_{i\uparrow} \hat{n}_{i\downarrow}. \tag{3.26}$$

If, as is common in many transition metal compounds, $U \gg t$ applies, the kinetic part can be treated in perturbation theory. The Hubbard model with half filling can then be simplified to second order to a Heisenberg model of the form

$$\hat{H}_{\mathrm{Heis}} = \frac{4t^2}{U} \sum_{i} \left(\vec{\hat{S}}_i \cdot \vec{\hat{S}}_{i+1} - \frac{1}{4} \right). \tag{3.27}$$

The ground state of this model is an antiferromagnet. Due to the presence of individual orbitals, the system must be represented in a slightly more complex way, as the exchange between the orbitals is determined by their geometry. As can be seen from Figure 2.2, the xz and yz orbitals are equipped with lobes in the z-axis direction, while the xy orbital lies in the x-y plane. With a connection axis in the z direction, the dominant exchange terms are accordingly those that mediate between $xz - xz$ and $yz - yz$. For symmetry reasons, the relation

$$t_{yz,yz} = t_{xz,xz} = -t \tag{3.28}$$

applies, while for all other combinations

$$t_{\alpha,\beta} = 0 \tag{3.29}$$

can be assumed [31]. The corresponding kinetic Hamiltonian then takes the form

$$\hat{H}_t = -t \sum_{\alpha \in \{yz,xz\},\sigma} \left(\hat{c}^{\dagger}_{t,\alpha\sigma} \hat{c}_{b,\alpha\sigma} + \hat{c}^{\dagger}_{b,\alpha\sigma} \hat{c}_{t,\alpha\sigma} \right). \tag{3.30}$$

The local part of the full Hamiltonian is accordingly described by the two local interactions of Kanamori-Hubbard type (3.2) and spin-orbit coupling type (3.11). Anticipating the

results of the investigation of the single ion, it can be said that the ground state of the three-electron problem is fourfold degenerate at any time and has an energy gap to the states above it. It therefore makes sense to describe the physics with the aid of degenerate perturbation theory. Since $\hat{H}_t$ by definition describes a single hopping between the ions, it is clear that the perturbation series only contains the even-numbered terms. If we limit ourselves to the first relevant order, we arrive at a degenerate second-order perturbation theory, the derivation of which can be found in the standard textbooks [16, 19]. Effectively, it expresses itself in a Hamiltonian of the form

$$\left(\hat{H}_{t,\mathrm{eff}}\right)_{f,i} = \sum_{|v\rangle \in \mathrm{ES}} \frac{1}{E_{\mathrm{GS}} - E_{\mathrm{ES}}} \langle f| \hat{H}_t |v\rangle \langle v| \hat{H}_t |i\rangle \tag{3.31}$$

where is summed over a basis of excited eigenstates (ES) of the unperturbed Hamiltonian and $|i\rangle$ and $|f\rangle$ are chosen from a basis of the ground state manifold (GS) of the unperturbed Hamiltonian.

4 Single-ion results

In this chapter the results of the calculations of the single ion are presented. The chapter is separated into two sections.

In Section 4.1 the ground state manifold and its energy are calculated analytically for the Hamiltonian without Jahn-Teller effect, whereas the numerical results of the diagonalisation of the Hamiltonian with Jahn-Teller effect are shown in Section 4.2.

4.1 Interplay between Hund's rule and spin orbit coupling

If the operator composed of Kanamori-Hubbard and spin-orbit coupling Hamiltonian

$$\begin{aligned}\hat{H}_{\mathrm{loc}} = (U - 3J_{\mathrm{H}})\,\frac{\hat{N}(\hat{N}-1)}{2} - 2J_{\mathrm{H}}\hat{S}^2 - \frac{J_{\mathrm{H}}}{2}\hat{L}^2 + \frac{5}{2}J_{\mathrm{H}}\hat{N} \\ + \frac{i\lambda}{2}\sum_{\alpha,\beta,\gamma}\sum_{\sigma,\sigma'}\epsilon_{\alpha,\beta,\gamma}\hat{\tau}^{\gamma}_{\sigma,\sigma'}\hat{c}^{\dagger}_{\alpha,\sigma}\hat{c}_{\beta,\sigma'}\end{aligned} \tag{4.1}$$

is diagonalised under the constraint $N = 3$, the energy spectrum shown in Figure 4.1 is obtained [31].

It is noticeable that the ground state is clearly separated from the states above it regardless of the choice of J_{H} and λ and exhibits a fourfold degeneracy. To explain this spectrum, it is useful to introduce the total angular momentum J, which is defined by

$$\vec{\hat{J}} = \vec{\hat{L}} + \vec{\hat{S}}. \tag{4.2}$$

The corresponding operators

$$\hat{J}^2 = (\vec{\hat{L}} + \vec{\hat{S}})^2 = \hat{L}^2 + \hat{S}^2 + 2\vec{\hat{L}}\cdot\vec{\hat{S}} \tag{4.3}$$

and

$$\hat{J}_z = \hat{L}_z + \hat{S}_z \tag{4.4}$$

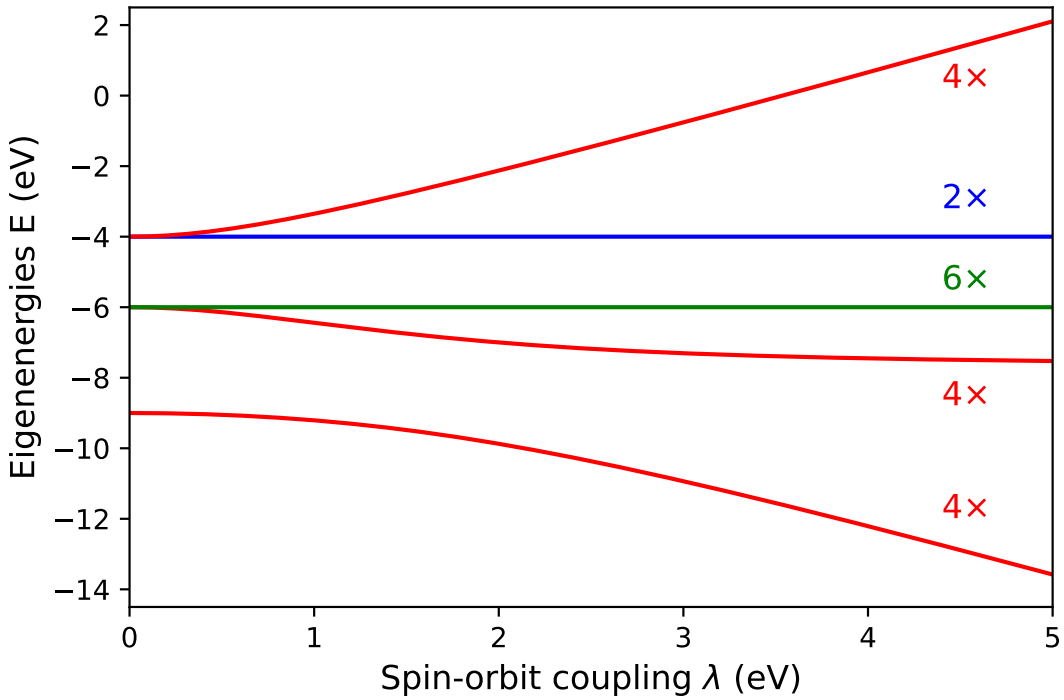

Figure 4.1: The spectrum of the Hamiltonian operator (4.1) for $U = 0$, $J_\mathrm{H} = 1$ is shown. The total angular momentum follows directly from the degeneracy, whereby $J = 1/2$ (blue), $J = 3/2$ (red) and $J = 5/2$ (green) are possible. It can be seen that the ground state manifold is always separated from the remaining states by an energy gap, regardless of λ.

with their corresponding quantum numbers J and m_J commute with the Hamilton operator 4.1 and are therefore useful for describing the states. However, they do not form a complete set of commuting observables. As can be seen, the ground state manifold as shown in Figure 4.1 corresponds to one of three branches with total angular momentum quantum number $J = \frac{3}{2}$. The ground state of the 20-dimensional Hamiltonian can therefore also be described as the ground state of each of the four possible three-dimensional $J = \frac{3}{2}$, $m_J \in \{-3/2, -1/2, +1/2, +3/2\}$ blocks. In SL-basis this matrix takes the form

$$H_{\mathrm{loc},J=+\frac{3}{2}} = \begin{bmatrix} -9J_\mathrm{H} & 0 & -\lambda \\ 0 & -6J_\mathrm{H} & -i\sqrt{\frac{5}{4}}\lambda \\ -\lambda & i\sqrt{\frac{5}{4}}\lambda & -4J_\mathrm{H}. \end{bmatrix} \tag{4.5}$$

The intrinsic energy of the ground state can then either be determined as the smallest

zero of the characteristic polynomial of the matrix, or formulated more elegantly as

$$E_{\mathrm{GS}} = -9J_{\mathrm{H}} - \sqrt{2}J_{\mathrm{H}}\gamma \tag{4.6}$$

where γ is the positive solution of

$$4x^3 + 16\sqrt{2}x^2 + \left(30 - \frac{9}{2}\left(\frac{\lambda}{J_{\mathrm{H}}}\right)^2\right)x - 3\sqrt{2}\left(\frac{\lambda}{J_{\mathrm{H}}}\right)^2 = 0. \tag{4.7}$$

Although exact representations exist for the zeros of such third-degree polynomials [32], these are not used in the following due to their exorbitant length. The eigenstate could now also be expressed in the selected SL-basis. However, the gain in knowledge of the description of the state in this basis is rather low, since the admixture of the energetically higher states does not provide any insight into the relevance of the j-like states. Instead, an alternative, non-orthogonal description can be chosen in which the vectors $|S_i\rangle$ and $|j_i\rangle$ each form a basis vector. This choice makes sense as it means that two of the entries of the states in the extreme cases $\lambda = 0$ and $\lambda \to \infty$ must be zero. The third vector for the complete description can now be selected, unique except for the prefactor, in such a way that it is orthogonal to the other two states. Since, by definition, it is only finite in the intermediate range, it is represented below as $|I_i\rangle$. The four selected states can be displayed as

$$\left|I_{+\frac{3}{2}}\right\rangle = \frac{1}{2}\left(-\left|\times,\uparrow,\uparrow\downarrow\right\rangle - \left|\uparrow\downarrow,\uparrow,\times\right\rangle + i\left|\uparrow,\times,\uparrow\downarrow\right\rangle + i\left|\uparrow,\uparrow\downarrow,\times\right\rangle\right) \tag{4.8}$$

$$\begin{aligned}\left|I_{+\frac{1}{2}}\right\rangle = \frac{1}{\sqrt{12}}\Big(&-\left|\times,\downarrow,\uparrow\downarrow\right\rangle - \left|\uparrow\downarrow,\downarrow,\times\right\rangle - 2i\left|\times,\uparrow\downarrow,\uparrow\right\rangle \\ &-2i\left|\uparrow\downarrow,\times,\uparrow\right\rangle + i\left|\downarrow,\times,\uparrow\downarrow\right\rangle + i\left|\downarrow,\uparrow\downarrow,\times\right\rangle\Big)\end{aligned} \tag{4.9}$$

$$\begin{aligned}\left|I_{+\frac{1}{2}}\right\rangle = \Big(&\frac{1}{\sqrt{12}} - \left|\times,\uparrow,\uparrow\downarrow\right\rangle - \left|\uparrow\downarrow,\uparrow,\times\right\rangle - 2i\left|\times,\uparrow\downarrow,\downarrow\right\rangle \\ &-2i\left|\uparrow\downarrow,\uparrow,\times\right\rangle - i\left|\uparrow,\times,\uparrow\downarrow\right\rangle - i\left|\uparrow,\uparrow\downarrow,\times\right\rangle\Big)\end{aligned} \tag{4.10}$$

$$\left|I_{-\frac{3}{2}}\right\rangle = \frac{1}{2}\left(-\left|\times,\downarrow,\uparrow\downarrow\right\rangle - \left|\uparrow\downarrow,\downarrow,\times\right\rangle - i\left|\downarrow,\times,\uparrow\downarrow\right\rangle - i\left|\downarrow,\uparrow\downarrow,\times\right\rangle\right) \tag{4.11}$$

in the standard base. In this form, the states can be described by

$$|GS_i\rangle = \alpha\,|S_i\rangle + \omega\,|I_i\rangle + \beta\,|j_i\rangle \tag{4.12}$$

where the parameters α, ω and β each depend on λ/J_{H} and are chosen so that the entire

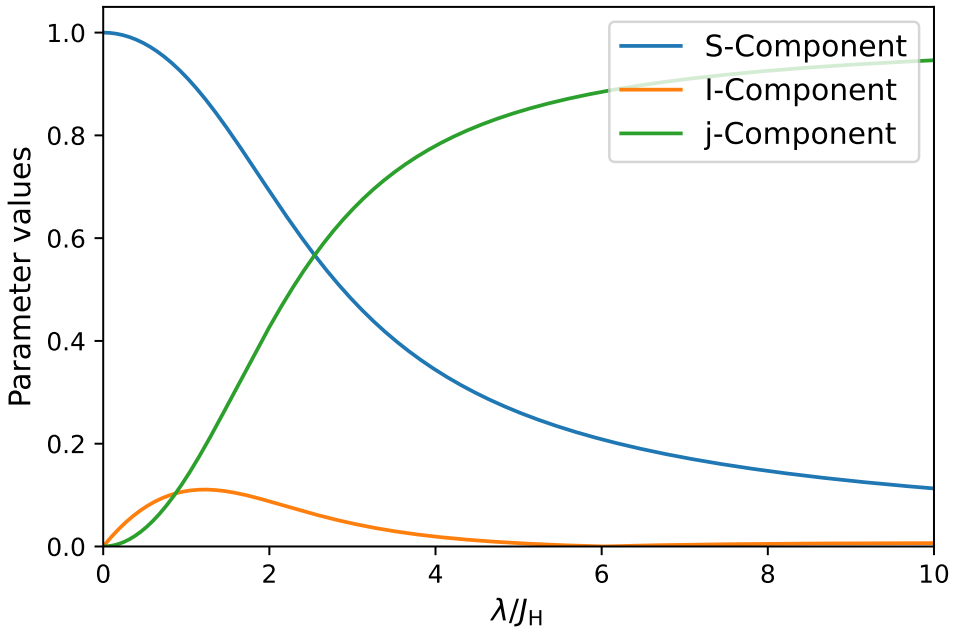

Figure 4.2: Shown are the amounts of the three components that make up the individual ground states, independent of m_J.

state is normalised. The following equations then result for the parameters

$$\alpha = \frac{1}{N} \tag{4.13}$$

$$\omega = \frac{1}{N}\omega' = \frac{-3\sqrt{2} - 2\gamma + \frac{3}{\sqrt{2}}\lambda}{3N\lambda}\gamma \tag{4.14}$$

$$\beta_{\pm\frac{3}{2}} = i\frac{\gamma}{N} \quad \beta_{\pm\frac{1}{2}} = -i\frac{\gamma}{N} \tag{4.15}$$

with the normalisation

$$N^2 = 1 + \gamma^2 + \omega'^2 - \sqrt{2}\gamma\omega' + \frac{2\sqrt{2}}{3}\gamma \tag{4.16}$$

which are plotted in Figure 4.2. It can be seen that the additional third component, which describes the orthogonal complement to the space spanned by $|S_i\rangle$ and $|j_i\rangle$, is particularly relevant in the area $\lambda \approx J_\mathrm{H}$.

4.2 Jahn-Teller effect

If the Jahn-Teller Hamiltonian from equation (3.25) is added as a further term to the local Hamiltonian (4.1), this results in a minimum energy that also depends on Q_2 and Q_3. This is plotted as an example for large λ in Figure 4.3.

It can be seen that the absolute minima are doubly degenerate at each point in time and that three equivalent minima exist within the $Q_2 - Q_3$ plane. Since one of these minima lies on the Q_3 axis regardless of the selected parameters, the analysis can be reduced to this axis in the following. The Jahn-Teller Hamiltonian thus takes the form

$$\hat{H}_{\mathrm{JT}} = -g \sum_n \left[\left(\hat{l}_n^z \right)^2 - \frac{2}{3} \right] Q_3 + \frac{B}{2} Q_3^2. \tag{4.17}$$

The minima of the resulting Hamiltonian were now analysed with variable spin-orbit coupling to determine how these two different interactions with the orbital angular momentum jointly influence the resulting ground state. For the free parameters, $J_{\mathrm{H}} = 0.5$, $g = 1$, $B = 1$ with variable λ was chosen. For the $\lambda = 0$ case, it can be shown that there can be no energetic advantage due to a distortion [12]. This is evident from the fact that in the ground state all three orbitals are equally occupied by an electron. Consequently, elongation and compression effects compensate each other, so that only the energy-increasing, quadratic part of the Jahn-Teller Hamiltonian takes part. By adding the Jahn-Teller term, the Hamiltonian no longer commutes with the $\hat{J}^2$ operator. Consequently, the problem can no longer be reduced to a three-dimensional subspace as before. However, it can be shown that the Hamiltonian still commutes with $\hat{J}_z$. A look back at Figure 4.1 shows that this results in three characteristically different block matrices that must be diagonalised. These are characterised by the magnitude of their magnetic quantum number and accordingly degenerate differently. Figure 4.1 also directly shows the dimension of these matrices as

$$\dim\left(\pm\frac{1}{2}\right) = 5 \tag{4.18}$$

$$\dim\left(\pm\frac{3}{2}\right) = 4 \tag{4.19}$$

$$\dim\left(\pm\frac{5}{2}\right) = 1. \tag{4.20}$$

The $\pm\frac{5}{2}$ case can therefore be ignored, as it cannot be influenced by the Jahn-Teller Hamiltonian except for the trivial, quadratic part. The other two block matrices can be represented explicitly with basis vectors of the form $|S, m_S, L, m_L\rangle$.

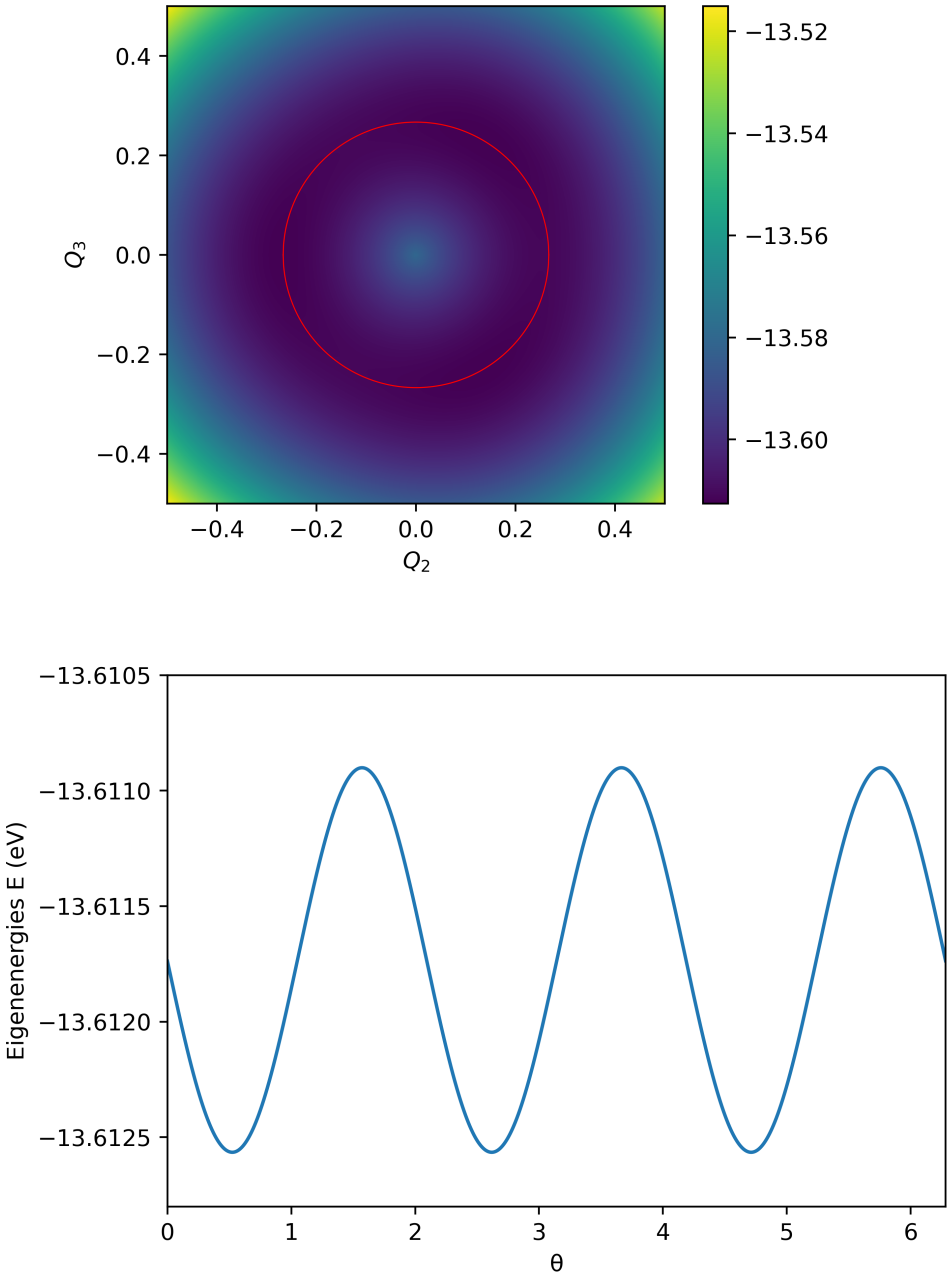

Figure 4.3: Shown is the ground state energy of the single-ion Hamiltonian with Jahn-Teller effect in the Q_2Q_3 plane and for $\sqrt{Q_2^2 + Q_3^2} = 0.267$ (red circle) against the angle to the Q_2 axis θ ($g = B = J = 1$, $\lambda = 5$). It can be seen that three equivalent minima are formed, with one of the minima lying on the Q_3 axis ($\theta = \frac{3}{2}\pi$).

For $J_z = +\frac{3}{2}$ one finds

$$\hat{H}_{\mathrm{loc+JT},+\frac{3}{2}} = \begin{bmatrix} -9J_{\mathrm{H}} & 0 & 0 & -\lambda \\ 0 & -6J_{\mathrm{H}} & 0 & i(\sqrt{\frac{1}{5}}gQ_3 - \sqrt{\frac{5}{4}}\lambda) \\ 0 & 0 & -6J_{\mathrm{H}} & i\sqrt{\frac{4}{5}}gQ_3 \\ -\lambda & -i(\sqrt{\frac{1}{5}}gQ_3 - \sqrt{\frac{5}{4}}\lambda) & -i\sqrt{\frac{4}{5}}gQ_3 & -4J_{\mathrm{H}} \end{bmatrix} + \frac{B}{2}Q_3^2 \tag{4.21}$$

in the basis

$$\left|\frac{3}{2}, +\frac{3}{2}, 0, 0\right\rangle \tag{4.22}$$

$$\sqrt{\frac{1}{5}}\left|\frac{1}{2}, +\frac{1}{2}, 2, +1\right\rangle + \sqrt{\frac{4}{5}}\left|\frac{1}{2}, -\frac{1}{2}, 2, +2\right\rangle \tag{4.23}$$

$$\sqrt{\frac{4}{5}}\left|\frac{1}{2}, +\frac{1}{2}, 2, +1\right\rangle - \sqrt{\frac{1}{5}}\left|\frac{1}{2}, -\frac{1}{2}, 2, +2\right\rangle \tag{4.24}$$

$$\left|\frac{1}{2}, +\frac{1}{2}, 1, +1\right\rangle \tag{4.25}$$

and for $J_z = +\frac{1}{2}$ one finds

$$\hat{H}_{\mathrm{loc+JT},+\frac{1}{2}} = \begin{bmatrix} -9J_\mathrm{H} & 0 & 0 & 0 & -\lambda \\ 0 & -6J_\mathrm{H} & 0 & -i\sqrt{\frac{2}{5}}gQ_3 & i(\sqrt{\frac{1}{5}}gQ_3 + \sqrt{\frac{5}{4}}\lambda) \\ 0 & 0 & -6J_\mathrm{H} & i\sqrt{\frac{4}{15}}gQ_3 & i\sqrt{\frac{2}{15}}gQ_3 \\ 0 & i\sqrt{\frac{2}{5}}gQ_3 & -i\sqrt{\frac{4}{15}}gQ_3 & -4J_\mathrm{H} & 0 \\ -\lambda & -i(\sqrt{\frac{1}{5}}gQ_3 + \sqrt{\frac{5}{4}}\lambda) & -i\sqrt{\frac{2}{15}}gQ_3 & 0 & -4J_\mathrm{H} \end{bmatrix} + \frac{B}{2}Q_3^2 \tag{4.26}$$

in the basis

$$\left|\frac{3}{2}, +\frac{1}{2}, 0, 0\right\rangle \tag{4.27}$$

$$\sqrt{\frac{2}{5}}\left|\frac{1}{2}, +\frac{1}{2}, 2, 0\right\rangle + \sqrt{\frac{3}{5}}\left|\frac{1}{2}, -\frac{1}{2}, 2, +1\right\rangle \tag{4.28}$$

$$\sqrt{\frac{3}{5}}\left|\frac{1}{2}, +\frac{1}{2}, 2, 0\right\rangle - \sqrt{\frac{2}{5}}\left|\frac{1}{2}, -\frac{1}{2}, 2, +1\right\rangle \tag{4.29}$$

$$\sqrt{\frac{2}{3}}\left|\frac{1}{2}, -\frac{1}{2}, 1, +1\right\rangle - \sqrt{\frac{1}{3}}\left|\frac{1}{2}, +\frac{1}{2}, 1, 0\right\rangle \tag{4.30}$$

$$\sqrt{\frac{1}{3}}\left|\frac{1}{2}, -\frac{1}{2}, 1, +1\right\rangle + \sqrt{\frac{2}{3}}\left|\frac{1}{2}, +\frac{1}{2}, 1, 0\right\rangle. \tag{4.31}$$

If these are diagonalised, it can be seen that the minimum for $m_J = \pm\frac{1}{2}$ is positive and that for $m_J = \pm\frac{3}{2}$ is negative Q_3. This is shown for various λ in Figure 4.4.

Consequently, the first maximum at $\frac{\pi}{2}$ shown in Figure 4.3 corresponds to the minimum of the $m_J = \pm\frac{1}{2}$ subspace, the actual minimum at $\frac{3\pi}{2}$ corresponds to the minimum of the $m_J = \pm\frac{3}{2}$ subspace.

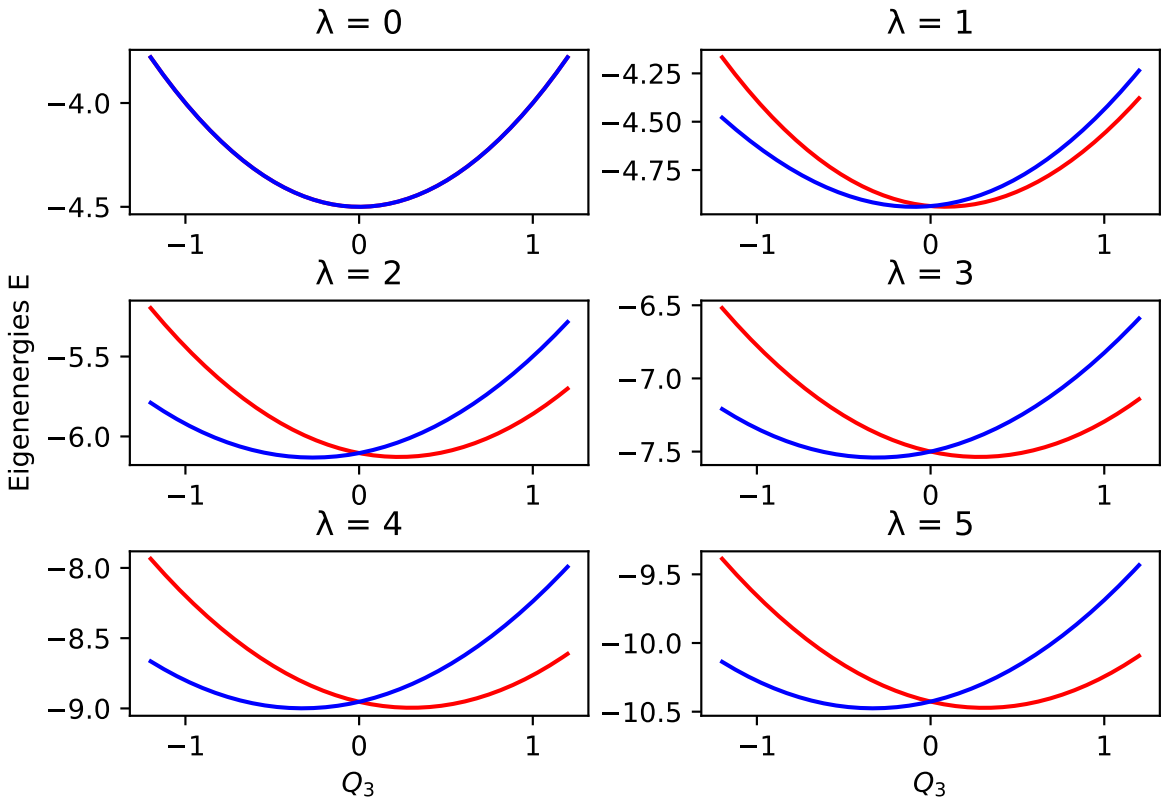

Figure 4.4: Shown is the ground state energy of the two subspaces ($m_J = \pm\frac{1}{2}$ in red, $m_J = \pm\frac{1}{2}$ in blue) as a function of Q_3. It can be seen that two almost equivalent minima are formed, with the one belonging to $m_J = \pm\frac{1}{2}$ at positive Q_3 and the one belonging to $m_J = \pm\frac{3}{2}$ at negative Q_3.

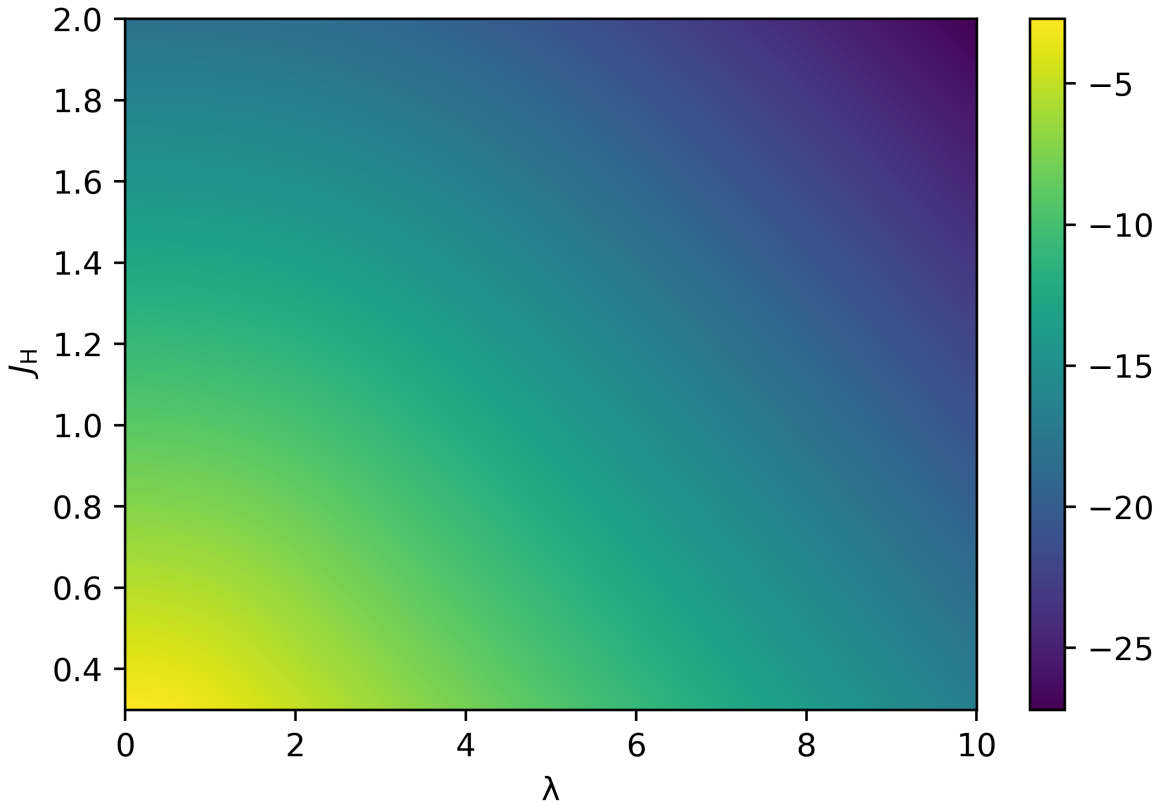

Figure 4.5: The ground state energy is shown as a function of λ and J_{H}, given by the energy minimum of the Hamiltonian belonging to the $m_J = \pm\frac{3}{2}$ subspace.

This results in the values shown in figures 4.5 and 4.6 for the energy and distortion of the ground state.

If the differences between the values of the two subspaces are examined more closely, it can be seen that the difference in energies almost disappears. This is shown in Figure 4.7.

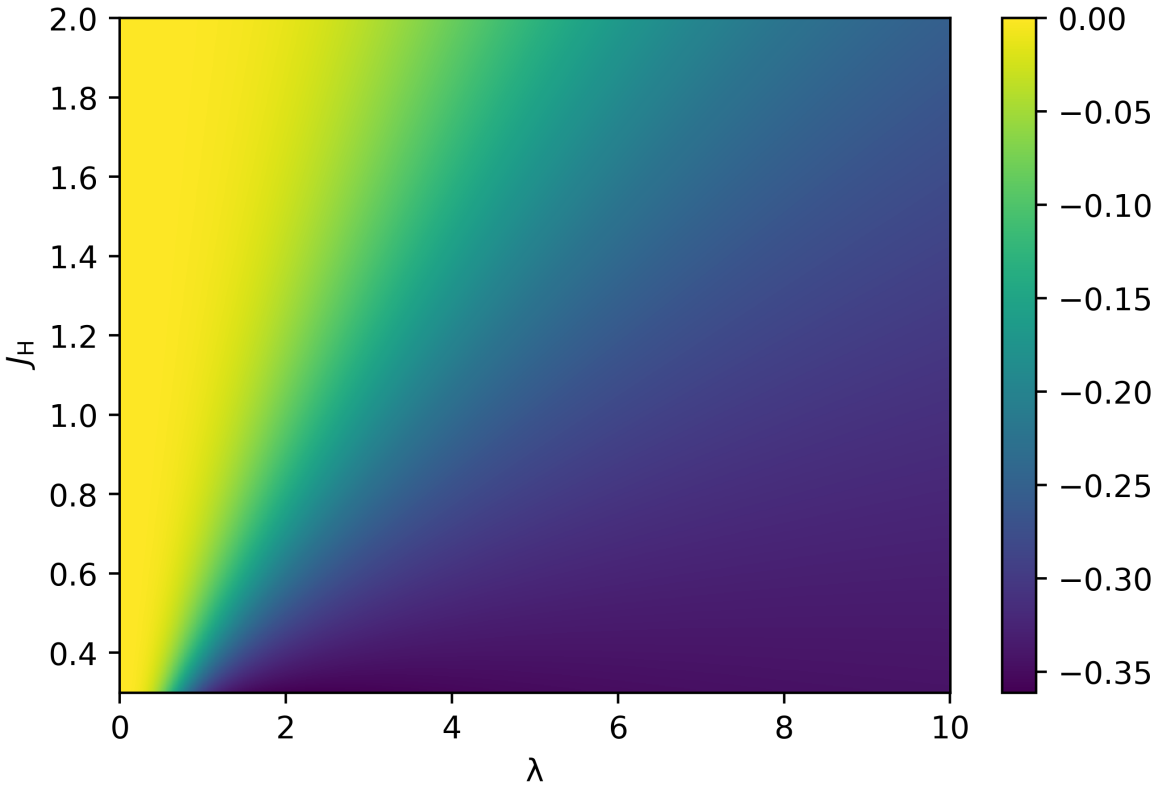

Figure 4.6: The optimal distortion $Q_{3,\min}$ is shown as a function of λ and J_{H}, given by the energy minimum of the Hamiltonian belonging to the $m_J = \pm\frac{3}{2}$ subspace.

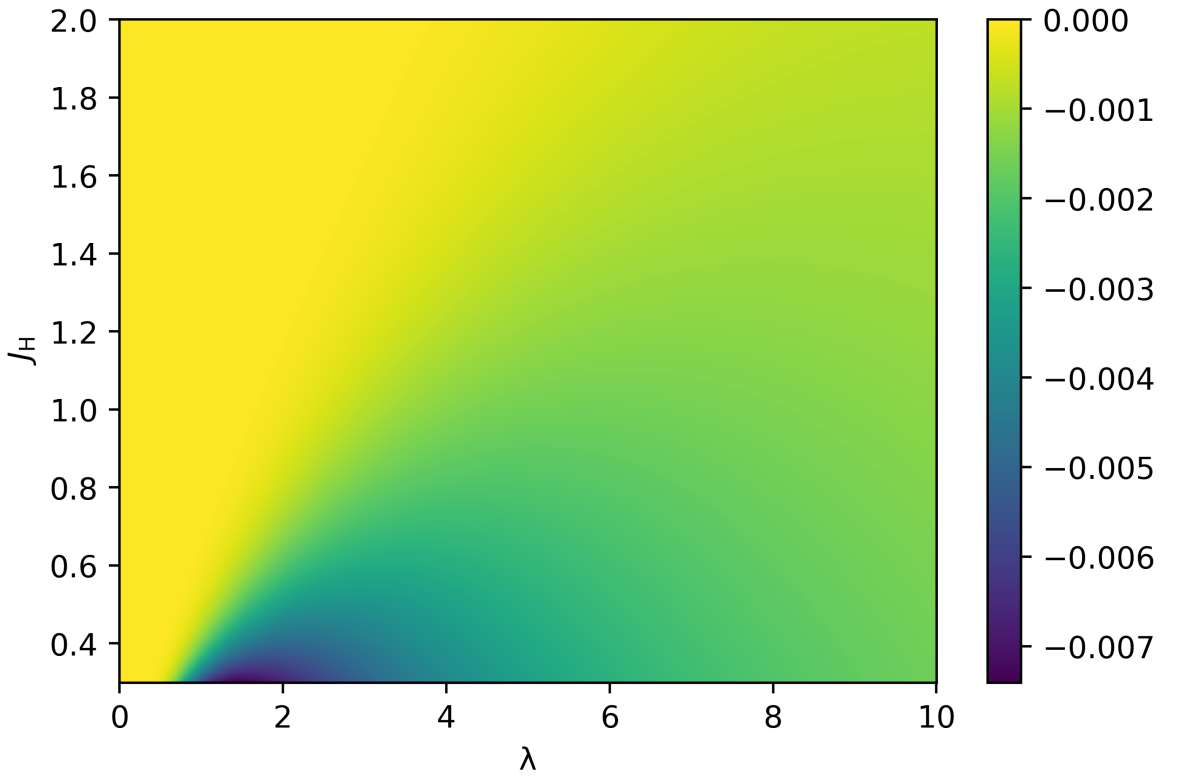

Figure 4.7: The difference between the minima of the ground state energy of the two subspaces $E_{\pm\frac{3}{2},\min} - E_{\pm\frac{1}{2},min}$ is shown as a function of λ and J_H. It can be seen that the energy associated with $m_J = \pm\frac{3}{2}$ is slightly lower.

In addition, the two minima are almost at the same Q_3 except for the difference in sign. This is shown in Figure 4.8.

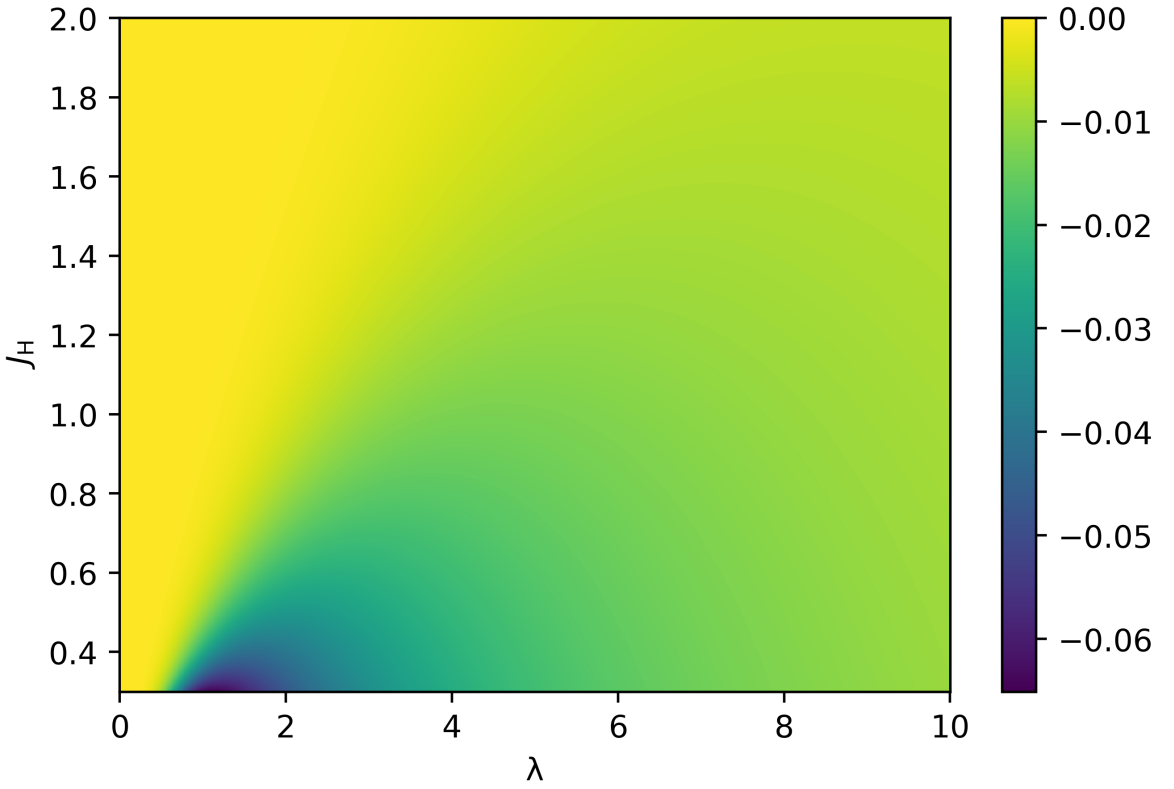

Figure 4.8: The difference in the position of the minima of the ground state energy of the two subspaces $Q_{\pm\frac{3}{2},\min} + Q_{\pm\frac{1}{2},\min}$ is shown as a function of λ and J_H. It can be seen that the minimum belonging to $m_J = \pm\frac{3}{2}$ is slightly further deflected.

This can be explained in more detail by plotting the contributions of the individual components in SL representation on the ground state vector. This is illustrated for the two relevant subspaces in the figures 4.9 and 4.10.

Here it can be seen that the additionally added component from the $J = \frac{1}{2}$ branch, which only takes part in the $m_J = \pm\frac{1}{2}$ subspace (component 4 in Figure 4.9), does not have a large share in the ground state in the energy minimum. This shows that although the minimum energy is given by the twofold degenerate ground state of the $m_J = \pm\frac{3}{2}$ subspace, the difference is so small that a qualitative statement by the approximation of truncating the Jahn-Teller Hamiltonian in second order is not sufficiently meaningful.

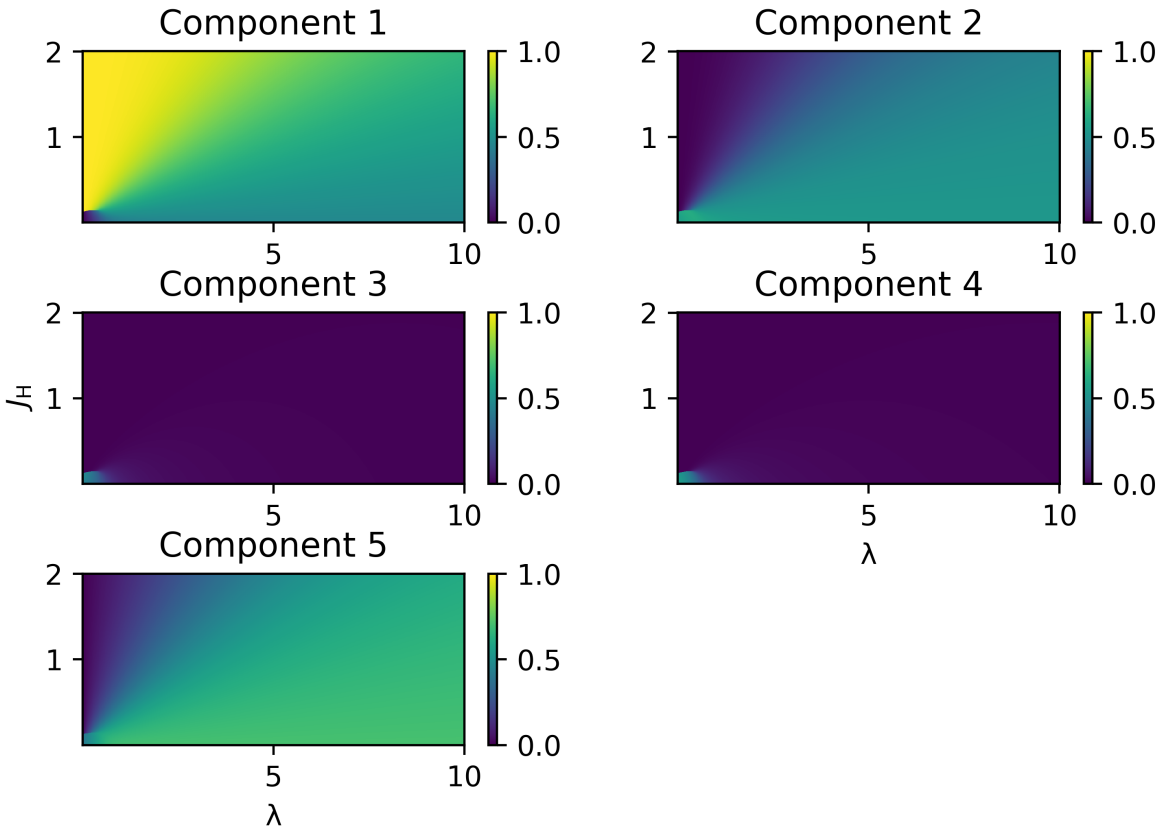

Figure 4.9: The magnitude of the individual components at the ground state of the $m_J = \pm\frac{1}{2}$ Hamiltonian in SL basis is shown. The fourth component corresponds to the contribution of the $J = \frac{1}{2}$ branch, which does not contribute for $m_J = \pm\frac{3}{2}$.

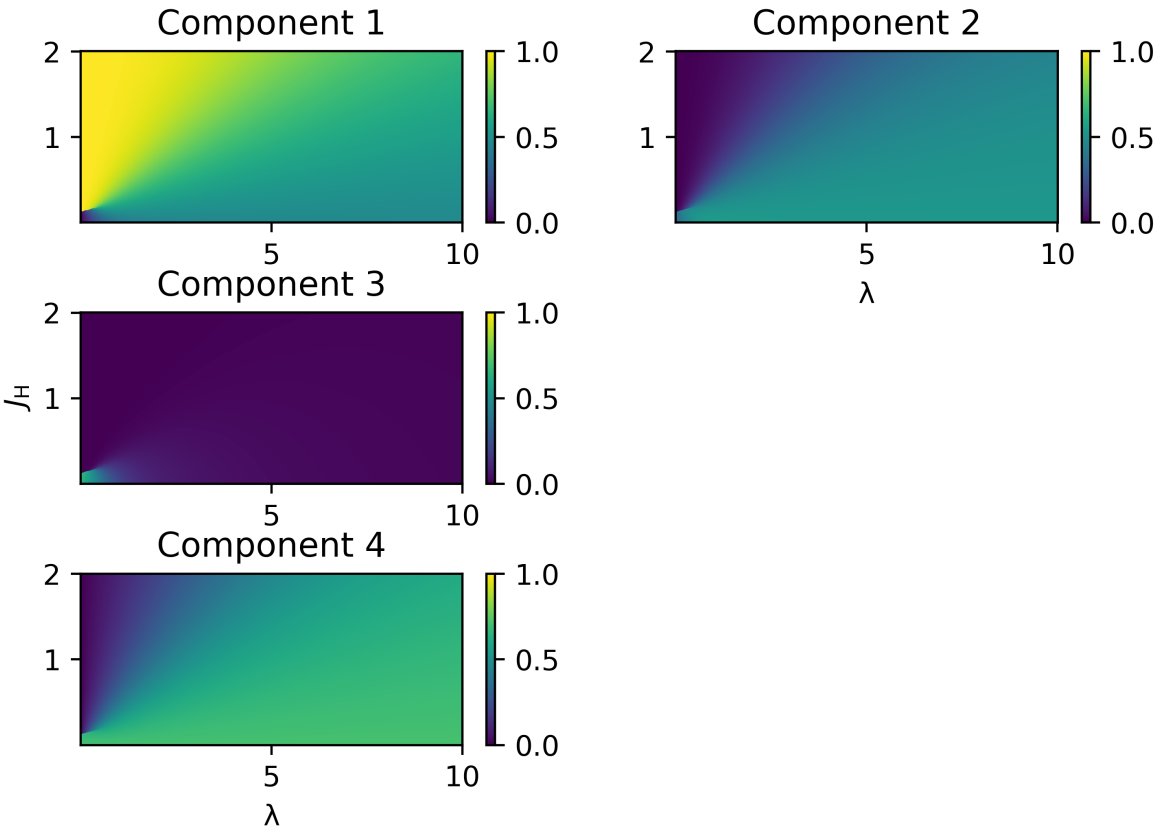

Figure 4.10: The magnitude of the individual components at the ground state of the $m_J = \pm\frac{3}{2}$ Hamiltonian in SL basis is shown. The differences to the $m_J = \pm\frac{1}{2}$ case from Figure 4.9 are minimal.

Also worth mentioning is the behaviour at very small J_{H} where it can be seen that the Jahn-Teller effect can also select a completely different state as the ground state. This is shown in Figure 4.11.

For $\lambda = 0$ this happens when

$$J_{\mathrm{H}} < (4 - \sqrt{15})\frac{g^2}{B} \tag{4.32}$$

is achieved. However, as this parameter range is not reached for the material class on which the Hamiltonian is based, it is more of a mathematical curiosity than a physically relevant case, so that the investigation of the phenomenon shall be discontinued here.

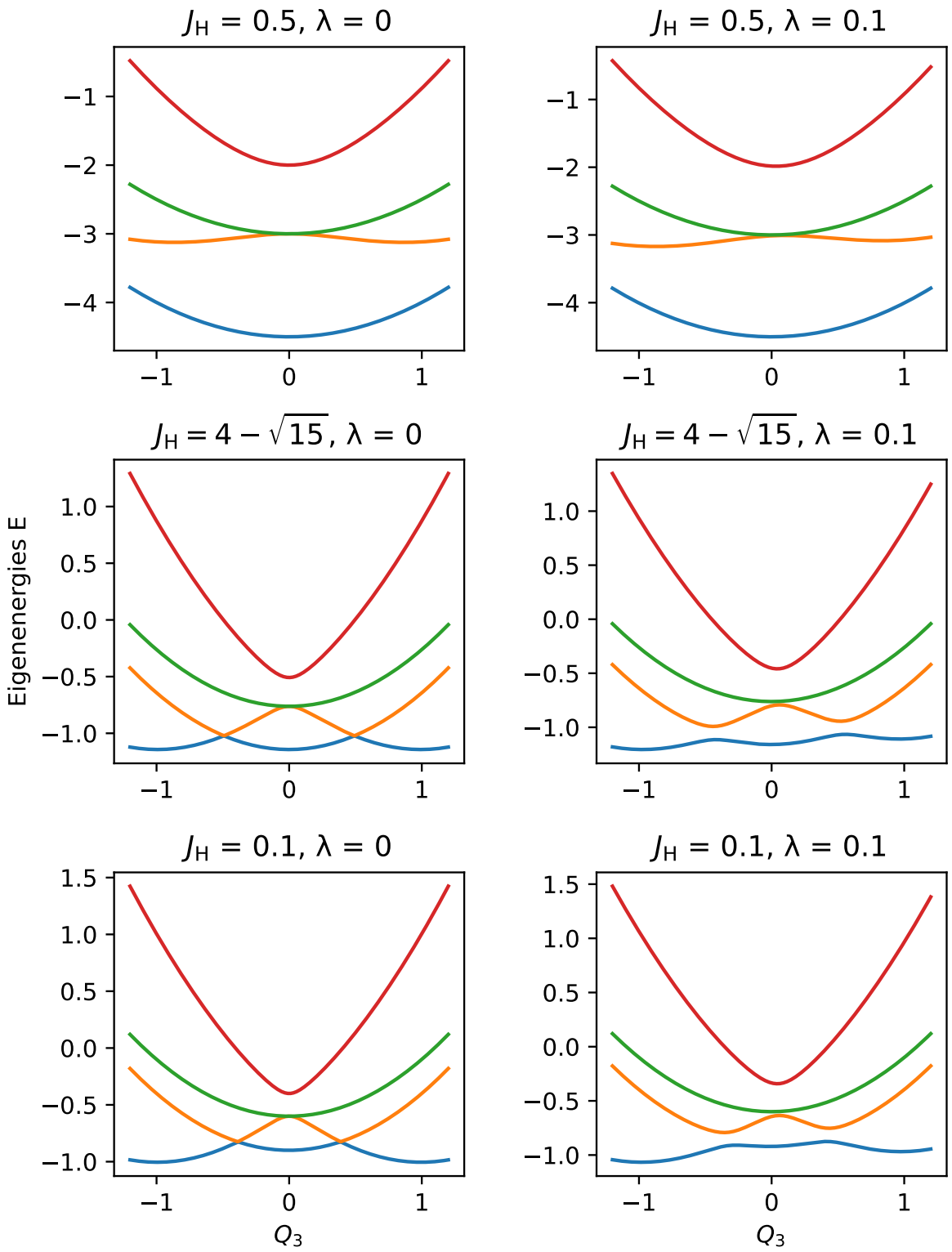

Figure 4.11: The behaviour of the eigenvalues of the $m_J = \pm\frac{3}{2}$ Hamiltonian is shown. At a critical value $J_H < (4 - \sqrt{15})$, the characteristic of the ground state changes.

5 Two-site results

In this chapter the results of the calculations of the two neighbouring ions are presented. The chapter is separated into two sections.

In Section 5.1 the results of adding the superexchange interaction to the local Hamiltonian are shown. Analytical expressions for the edge cases of the problems are presented and the behaviour in between those two is described numerically.

Lastly the cooperative Jahn-Teller effect is implemented in a simple form in Section 5.1.2, and its influence on the energy splitting is shown.

5.1 Superexchange

If two connected ions with six electrons are considered instead of a single ion with three electrons, the Hilbert space expands from

$$\binom{6}{3} = 20 \tag{5.1}$$

to

$$\binom{12}{6} = 924 \tag{5.2}$$

dimensions.

If the Jahn-Teller effect is neglected, the Hamiltonian

$$\hat{H} = \hat{H}_{\mathrm{loc,t}} + \hat{H}_{\mathrm{loc,b}} + \hat{H}_t \tag{5.3}$$

can be solved exactly, but the numerical effort is quite high. In the following, we will therefore analyse how well the results of the exact calculation can be reproduced by a perturbation-theoretic consideration of the ground state. The unperturbed Hamiltonian used here is the Hamiltonian completely solved in the previous section

$$\hat{H}_{\mathrm{loc}} = \hat{H}_U + \hat{H}_\lambda, \tag{5.4}$$

while the electron hopping between the two ions

$$\hat{H}_t = -t \sum_{\alpha\in\{yz,xz\},\sigma} \left(\hat{c}^\dagger_{\alpha\sigma,\mathrm{t}} \hat{c}_{\alpha\sigma,\mathrm{b}} + \hat{c}^\dagger_{\alpha\sigma,\mathrm{b}} \hat{c}_{\alpha\sigma,\mathrm{t}} \right) \tag{5.5}$$

is considered a perturbation. For the ground state manifold, it is assumed that it corresponds to the tensor product of the ground states of the solved one-site problem. The reason for this is that the ground state for $\lambda = 0$ lies at

$$E_{\mathrm{GS},3,3} = 6U - 18J_{\mathrm{H}} \tag{5.6}$$

and decreases for large λ with

$$\frac{dE_{\mathrm{GS},3,3}}{d\lambda} \to -3\lambda \tag{5.7}$$

if three electrons can be found at each of the two sites, while the ground state under the constraint of two electrons at one ion and four at the other ion lies for $\lambda = 0$ at

$$E_{\mathrm{GS},2,4} = 7U - 16J_{\mathrm{H}} \tag{5.8}$$

and decreases for large λ also with

$$\frac{dE_{\mathrm{GS},2,4}}{d\lambda} \to -3\lambda. \tag{5.9}$$

An exact description of these results is given in Appendix D. It is therefore reasonable to assume that the ground state with three electrons per site is separated by about $U + 2J_{\mathrm{H}}$ from the ground state of the system with two electrons on one ion and four electrons on the other. However, this assumption can be wrong for certain parameter values, as it ignores the curvature behaviour in the range of finite λ. Figure 5.1 shows this problem.

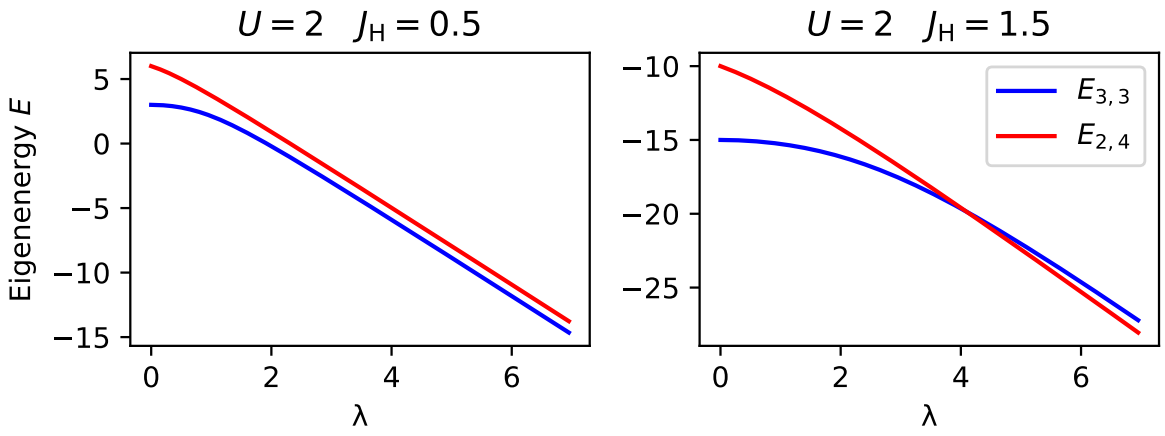

Figure 5.1: The behaviour of the ground state is shown for three electrons per site (blue) and two electrons on one, four electrons on the other ion (red). For $\frac{U}{J_\mathrm{H}} \lesssim 2.3$ the order can be reversed with increasing λ.

If the relation of U and J_H falls below

$$\frac{U}{J_\mathrm{H}} \lesssim 2.3 \tag{5.10}$$

the ground state may no longer described by the solutions from 4.1. However, this problem does not occur for physically realistic parameters $U > 3\,\mathrm{eV}$, $J_\mathrm{H} < 1\,\mathrm{eV}$, $\lambda < 1\,\mathrm{eV}$ [4, 33]. The relevant energy scales are therefore still defined by

$$U \gg t \tag{5.11}$$

which validates a perturbation-theoretic treatment.

This is done as described in Section 3.5 by an effective Hamiltonian of the form

$$\left(\hat{H}_{t,\mathrm{eff}}\right)_{f,i} = \sum_{|v\rangle \in \mathrm{ES}} \frac{1}{E_\mathrm{GS} - E_\mathrm{ES}} \langle f| \hat{H}_t |v\rangle \langle v| \hat{H}_t |i\rangle \,. \tag{5.12}$$

The initial and final states $|i\rangle$ and $|f\rangle$ form a 16-dimensional space dependent on $\frac{\lambda}{J_\mathrm{H}}$, which is spanned by the basis vectors derived in Chapter 4.1,

$$\left|+\frac{3}{2},+\frac{3}{2}\right\rangle, \left|+\frac{3}{2},+\frac{1}{2}\right\rangle, \ldots, \left|-\frac{3}{2},-\frac{1}{2}\right\rangle, \left|-\frac{3}{2},-\frac{3}{2}\right\rangle. \tag{5.13}$$

The sum over the possible intermediate states also runs over a space dependent on $\frac{\lambda}{J_\mathrm{H}}$, which is spanned by all states in which there are two electrons on one ion and four

electrons on the other. This sum therefore consists of

$$2\binom{6}{2}\binom{6}{4} = 450 \tag{5.14}$$

individual terms, which can be constructed from the single ion solutions described in Appendix D. First, the solutions for the two extreme cases $\lambda = 0$ and $J_{\mathrm{H}} = 0$, which can be described as exact Hamiltonians, are analysed.

5.1.1 The case $\lambda = 0$

Using the parameter $\lambda = 0$ this results in a spectrum which is given by

$$\Delta E = -\frac{t^2}{U + 2J_{\mathrm{H}}} \begin{cases} 0 & \times 7 \\ \frac{8}{3} & \times 5 \\ \frac{40}{9} & \times 3 \\ \frac{16}{3} & \times 1 \end{cases} . \tag{5.15}$$

An analysis of the ground states shows that these states are eigenstates of the total spin operator for both ions

$$\hat{S}^2_{\mathrm{ges}} = (\hat{S}_{\mathrm{t}} + \hat{S}_{\mathrm{b}})^2 = \hat{S}^2_{\mathrm{t}} + \hat{S}^2_{\mathrm{b}} + 2\vec{\hat{S}}_{\mathrm{t}} \cdot \vec{\hat{S}}_{\mathrm{b}}. \tag{5.16}$$

Since

$$\hat{S}^2_{\mathrm{t}} = \hat{S}^2_{\mathrm{b}} = 15/4 \tag{5.17}$$

applies to the ground state manifold, it follows that the Hamiltonian can be calculated as

$$\hat{H}_{t,\mathrm{eff},\lambda=0} = \frac{8}{9} \cdot \frac{t^2}{U + 2J_{\mathrm{H}}} \left(\vec{\hat{S}}_{\mathrm{t}} \cdot \vec{\hat{S}}_{\mathrm{b}} - \frac{9}{4} \right). \tag{5.18}$$

The eigenstates are shown in table 5.1.

Table 5.1: Eigenstates of the splitting with $\lambda = 0$

energy	degeneracy	state
0	7	$\left\vert+\frac{3}{2},+\frac{3}{2}\right\rangle$
		$\frac{1}{\sqrt{2}}\left(\left\vert+\frac{3}{2},+\frac{1}{2}\right\rangle+\left\vert+\frac{1}{2},+\frac{3}{2}\right\rangle\right)$
		$\frac{1}{\sqrt{5}}\left(\left\vert-\frac{1}{2},+\frac{3}{2}\right\rangle+\sqrt{3}\left\vert+\frac{1}{2},+\frac{1}{2}\right\rangle+\left\vert+\frac{3}{2},-\frac{1}{2}\right\rangle\right)$
		$\frac{1}{\sqrt{20}}\left(\left\vert+\frac{3}{2},-\frac{3}{2}\right\rangle+3\left\vert+\frac{1}{2},-\frac{1}{2}\right\rangle+3\left\vert-\frac{1}{2},+\frac{1}{2}\right\rangle\left\vert-\frac{3}{2},+\frac{3}{2}\right\rangle\right)$
		$\frac{1}{\sqrt{5}}\left(\left\vert+\frac{1}{2},-\frac{3}{2}\right\rangle+\sqrt{3}\left\vert-\frac{1}{2},-\frac{1}{2}\right\rangle+\left\vert-\frac{3}{2},+\frac{1}{2}\right\rangle\right)$
		$\frac{1}{\sqrt{2}}\left(\left\vert-\frac{3}{2},-\frac{1}{2}\right\rangle+\left\vert-\frac{1}{2},-\frac{3}{2}\right\rangle\right)$
		$\left\vert-\frac{3}{2},-\frac{3}{2}\right\rangle$
$-\frac{8}{3}\frac{t^2}{U+2J_\mathrm{H}}$	5	$\frac{1}{\sqrt{2}}\left(\left\vert+\frac{3}{2},+\frac{1}{2}\right\rangle-\left\vert+\frac{1}{2},+\frac{3}{2}\right\rangle\right)$
		$\frac{1}{\sqrt{2}}\left(\left\vert+\frac{3}{2},-\frac{1}{2}\right\rangle-\left\vert-\frac{1}{2},+\frac{3}{2}\right\rangle\right)$
		$\frac{1}{2}\left(\left\vert+\frac{3}{2},-\frac{3}{2}\right\rangle-\left\vert-\frac{3}{2},+\frac{3}{2}\right\rangle+\left\vert+\frac{1}{2},-\frac{1}{2}\right\rangle-\left\vert-\frac{1}{2},+\frac{1}{2}\right\rangle\right)$
		$\frac{1}{\sqrt{2}}\left(\left\vert+\frac{1}{2},-\frac{3}{2}\right\rangle-\left\vert-\frac{3}{2},+\frac{1}{2}\right\rangle\right)$
		$\frac{1}{\sqrt{2}}\left(\left\vert-\frac{3}{2},-\frac{1}{2}\right\rangle-\left\vert-\frac{1}{2},-\frac{3}{2}\right\rangle\right)$
$-\frac{40}{9}\frac{t^2}{U+2J_\mathrm{H}}$	3	$\frac{1}{\sqrt{10}}\left(\sqrt{3}\left\vert+\frac{3}{2},-\frac{1}{2}\right\rangle-2\left\vert+\frac{1}{2},+\frac{1}{2}\right\rangle+\sqrt{3}\left\vert-\frac{1}{2},+\frac{3}{2}\right\rangle\right)$
		$\frac{1}{\sqrt{20}}\left(3\left\vert+\frac{3}{2},-\frac{3}{2}\right\rangle+3\left\vert-\frac{3}{2},+\frac{3}{2}\right\rangle-\left\vert+\frac{1}{2},-\frac{1}{2}\right\rangle-\left\vert-\frac{1}{2},+\frac{1}{2}\right\rangle\right)$
		$\frac{1}{\sqrt{10}}\left(\sqrt{3}\left\vert-\frac{3}{2},+\frac{1}{2}\right\rangle-2\left\vert-\frac{1}{2},-\frac{1}{2}\right\rangle+\sqrt{3}\left\vert+\frac{1}{2},-\frac{3}{2}\right\rangle\right)$
$-\frac{16}{3}\frac{t^2}{U+2J_\mathrm{H}}$	1	$\frac{1}{2}\left(\left\vert+\frac{3}{2},-\frac{3}{2}\right\rangle-\left\vert-\frac{3}{2},+\frac{3}{2}\right\rangle-\left\vert+\frac{1}{2},-\frac{1}{2}\right\rangle+\left\vert-\frac{1}{2},+\frac{1}{2}\right\rangle\right)$

5.1.2 The case $J_{\mathrm{H}} = 0$

For the case $J_{\mathrm{H}} = 0$ it can be analysed, for which intermediate and ground states the overlap created by the perturbation

$$\langle \mathrm{ES} | \hat{H}_t | GS \rangle \neq 0 \tag{5.19}$$

holds. It turns out that only two energy terms become relevant. These are characterised by

$$\frac{1}{E_{\mathrm{ES}} - E_{\mathrm{GS}}} = \begin{cases} \frac{1}{U} \\ \frac{1}{U + \frac{3}{2}\lambda} \end{cases} . \tag{5.20}$$

The energies and their degeneracies are given by

$$\Delta E = -t^2 \begin{cases} \frac{4}{9}\frac{1}{U+\frac{3}{2}\lambda} & \times 3 \\ \frac{8}{9}\frac{1}{U+\frac{3}{2}\lambda} & \times 3 \\ \frac{4}{9U} + \frac{4}{9}\frac{1}{U+\frac{3}{2}\lambda} & \times 1 \\ \frac{4}{9U} + \frac{2}{3}\frac{1}{U+\frac{3}{2}\lambda} & \times 4 \\ \frac{16}{9U} + \frac{2}{3}\frac{1}{U+\frac{3}{2}\lambda} & \times 4 \\ \frac{4}{U} + \frac{8}{9}\frac{1}{U+\frac{3}{2}\lambda} & \times 1 \end{cases} \tag{5.21}$$

while the states are given in table 5.2.

The effective Hamiltonian can be described by a model in which at both sites the original quadruplet is considered as two doublets determined by the magnitude of m_j. It shall therefore apply that

$$\mathcal{H}_{\frac{3}{2}} = \mathrm{span}\left(\left| +\frac{3}{2} \right\rangle, \left| -\frac{3}{2} \right\rangle \right) \tag{5.22}$$

$$\mathcal{H}_{\frac{1}{2}} = \mathrm{span}\left(\left| +\frac{1}{2} \right\rangle, \left| -\frac{1}{2} \right\rangle \right) \tag{5.23}$$

$$\mathcal{H} = \mathcal{H}_{\frac{3}{2}} \otimes \mathcal{H}_{\frac{1}{2}}, \tag{5.24}$$

where the two subspaces are provided with the usual spin-1/2-algebra, so among other things

$$\sigma^{\mathrm{z}} \left| \pm\frac{3}{2} \right\rangle = \pm \left| \pm\frac{3}{2} \right\rangle \tag{5.25}$$

$$\sigma^{\mathrm{z}} \left| \pm\frac{1}{2} \right\rangle = \pm \left| \pm\frac{1}{2} \right\rangle, \tag{5.26}$$

Table 5.2: Eigenstates of the splitting with $J_{\mathrm{H}} = 0$

energy	degeneracy	state
$-t^2\left(\frac{4}{9}\frac{1}{U+\frac{3}{2}\lambda}\right)$	3	$\left\vert+\frac{1}{2},+\frac{1}{2}\right\rangle$
		$\frac{1}{\sqrt{2}}\left(\left\vert+\frac{1}{2},-\frac{1}{2}\right\rangle+\left\vert-\frac{1}{2},+\frac{1}{2}\right\rangle\right)$
		$\left\vert-\frac{1}{2},-\frac{1}{2}\right\rangle$
$-t^2\left(\frac{8}{9}\frac{1}{U+\frac{3}{2}\lambda}\right)$	3	$\left\vert+\frac{3}{2},+\frac{3}{2}\right\rangle$
		$\frac{1}{\sqrt{2}}\left(\left\vert+\frac{3}{2},-\frac{3}{2}\right\rangle+\left\vert-\frac{3}{2},+\frac{3}{2}\right\rangle\right)$
		$\left\vert-\frac{3}{2},-\frac{3}{2}\right\rangle$
$-t^2\left(\frac{4}{9U}+\frac{4}{9}\frac{1}{U+\frac{3}{2}\lambda}\right)$	1	$\frac{1}{\sqrt{2}}\left(\left\vert+\frac{1}{2},-\frac{1}{2}\right\rangle-\left\vert-\frac{1}{2},+\frac{1}{2}\right\rangle\right)$
$-t^2\left(\frac{4}{9U}+\frac{2}{3}\frac{1}{U+\frac{3}{2}\lambda}\right)$	4	$\frac{1}{\sqrt{2}}\left(\left\vert+\frac{3}{2},+\frac{1}{2}\right\rangle+\left\vert+\frac{1}{2},+\frac{3}{2}\right\rangle\right)$
		$\frac{1}{\sqrt{2}}\left(\left\vert+\frac{3}{2},-\frac{1}{2}\right\rangle+\left\vert-\frac{1}{2},+\frac{3}{2}\right\rangle\right)$
		$\frac{1}{\sqrt{2}}\left(\left\vert-\frac{3}{2},+\frac{1}{2}\right\rangle+\left\vert+\frac{1}{2},-\frac{3}{2}\right\rangle\right)$
		$\frac{1}{\sqrt{2}}\left(\left\vert-\frac{3}{2},-\frac{1}{2}\right\rangle+\left\vert-\frac{1}{2},-\frac{3}{2}\right\rangle\right)$
$-t^2\left(\frac{16}{9U}+\frac{2}{3}\frac{1}{U+\frac{3}{2}\lambda}\right)$	4	$\frac{1}{\sqrt{2}}\left(\left\vert+\frac{3}{2},+\frac{1}{2}\right\rangle-\left\vert+\frac{1}{2},+\frac{3}{2}\right\rangle\right)$
		$\frac{1}{\sqrt{2}}\left(\left\vert+\frac{3}{2},-\frac{1}{2}\right\rangle-\left\vert-\frac{1}{2},+\frac{3}{2}\right\rangle\right)$
		$\frac{1}{\sqrt{2}}\left(\left\vert-\frac{3}{2},+\frac{1}{2}\right\rangle-\left\vert+\frac{1}{2},-\frac{3}{2}\right\rangle\right)$
		$\frac{1}{\sqrt{2}}\left(\left\vert-\frac{3}{2},-\frac{1}{2}\right\rangle-\left\vert-\frac{1}{2},-\frac{3}{2}\right\rangle\right)$
$-t^2\left(\frac{4}{U}+\frac{8}{9}\frac{1}{U+\frac{3}{2}\lambda}\right)$	1	$\frac{1}{\sqrt{2}}\left(\left\vert+\frac{3}{2},-\frac{3}{2}\right\rangle-\left\vert-\frac{3}{2},+\frac{3}{2}\right\rangle\right)$

with the usual, associated definitions for $\sigma^{x,y}$. The two doublets in turn are also connected by a pseudo-spin-1/2-algebra, with the definition,

$$\tau^z \left|\pm\frac{3}{2}\right\rangle = + \left|\pm\frac{3}{2}\right\rangle \tag{5.27}$$

$$\tau^z \left|\pm\frac{1}{2}\right\rangle = - \left|\pm\frac{1}{2}\right\rangle, \tag{5.28}$$

with the usual, associated definitions for $\tau^{\pm}$. A detailed description of the operators is given in appendix E. In this formalism various projectors can be calculated by

$$P^{\text{singlet}} = \frac{1}{4}\left(1 - \vec{\sigma}_1 \cdot \vec{\sigma}_2\right) \tag{5.29}$$

$$P^{\text{triplet}} = \frac{1}{4}\left(\vec{\sigma}_1 \cdot \vec{\sigma}_2 - 3\right) \tag{5.30}$$

$$P^{\frac{3}{2}} = \frac{1}{4}\left(1 + \tau_1^z\right)\left(1 + \tau_2^z\right) \tag{5.31}$$

$$P^{\frac{1}{2}} = \frac{1}{4}\left(1 - \tau_1^z\right)\left(1 - \tau_2^z\right). \tag{5.32}$$

The effective Hamiltonian is then given by

$$\begin{aligned}\hat{H}_{\text{pert},J_H=0} = {} & \Omega_3 P^{\text{singlet}} P_1^{\frac{3}{2}} P_2^{\frac{3}{2}} + \Omega_1 P^{\text{singlet}} P_1^{\frac{1}{2}} P_2^{\frac{1}{2}} \\ & + E_1 \left(P_1^{\frac{1}{2}} P_2^{\frac{3}{2}} + P_1^{\frac{3}{2}} P_2^{\frac{1}{2}}\right) + E_2 \left(\tau_1^+ \tau_2^- + \tau_1^- \tau_2^+\right) \\ & + 2\Delta P^{\text{triplet}} P_1^{\frac{3}{2}} P_2^{\frac{3}{2}} + \Delta P^{\text{triplet}} P_1^{\frac{1}{2}} P_2^{\frac{1}{2}}\end{aligned} \tag{5.33}$$

with the parameters

$$\Omega_3 = -\frac{4}{U} - \frac{8}{9}\frac{1}{U + \frac{3}{2}\lambda} \tag{5.34}$$

$$\Omega_1 = -\frac{4}{9U} - \frac{4}{9}\frac{1}{U + \frac{3}{2}\lambda} \tag{5.35}$$

$$E_1 = -\frac{4}{U} - \frac{8}{9}\frac{1}{U + \frac{3}{2}\lambda} \tag{5.36}$$

$$E_2 = -\frac{2}{3U} \tag{5.37}$$

$$\Delta = -\frac{4}{9}\frac{1}{U + \frac{3}{2}\lambda}, \tag{5.38}$$

which is similar to models explaining d^1 systems [34, 35].

5.1.3 Intermediate behaviour

For $J_\mathrm{H} \neq 0$ and $\lambda \neq 0$ the behaviour is not so easily determined. However, if the matrix described in equation (5.12) is set up for different $\frac{\lambda}{J_\mathrm{H}}$ and diagonalised, the spectrum of the Hamiltonian can be represented. This is shown for $U = 4\,\mathrm{eV}$, $J_\mathrm{H} = 0.5\,\mathrm{eV}$, $t = 0.2\,\mathrm{eV}$ in Figure 5.2. The parameter values were selected so that they lie within the usual range for the materials under consideration [4].

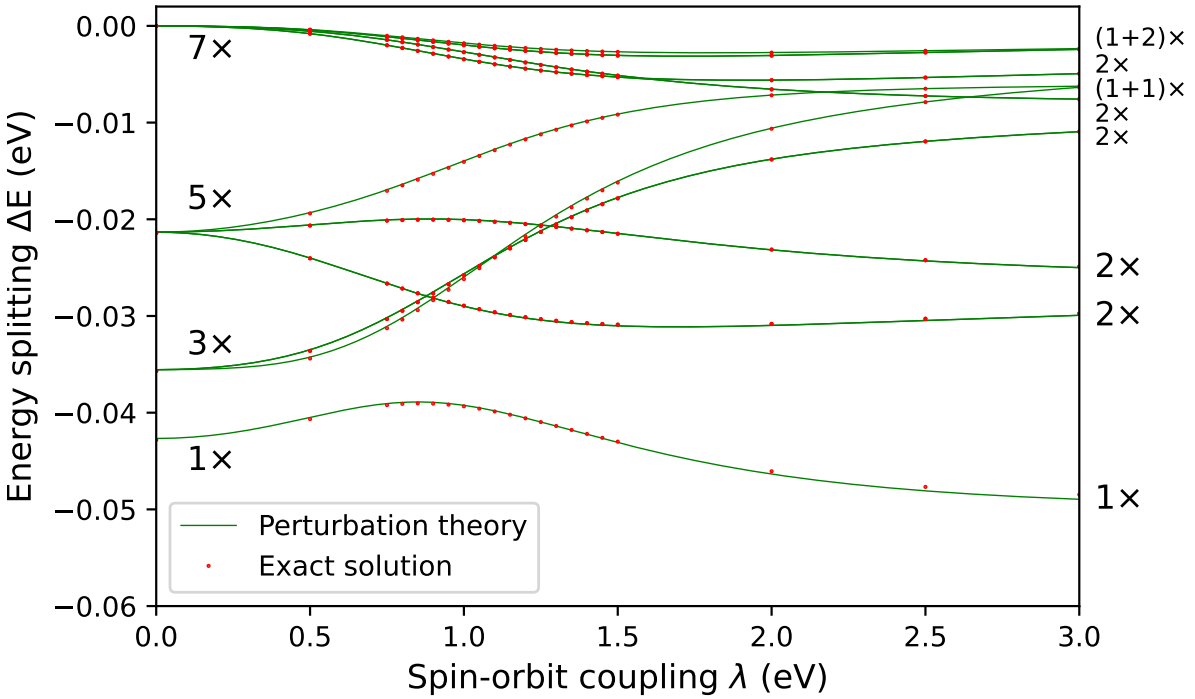

Figure 5.2: The energy splitting of the ground state for three electrons per site is shown. The degree of degeneracy is given for $\lambda = 0$ and $\lambda = 3$, where quasi-degeneracy ($\Delta\Delta E < 0.1\,\mathrm{meV}$) is described by the notation $(a + b)\times$.

In addition, the full Hamilton operator (5.3) was exactly diagonalised under the constraint of six electrons to serve as a reference for the quality of the approximated solution. It turns out that the perturbation-theoretic solution is almost indistinguishable from the exact solution. As can be seen in 5.2, the energies do not follow a simple course and thus elude a simple analysis. Nevertheless, some observations can be made. Firstly, the ground state is separated from the other states by an energy gap at all times. In addition, it can be seen that the ground state energy does not interpolate directly between $\Delta E\,(\lambda = 0)$ and $\Delta E\,(\lambda \to \infty)$, but first increases and then decreases again after a global maximum.

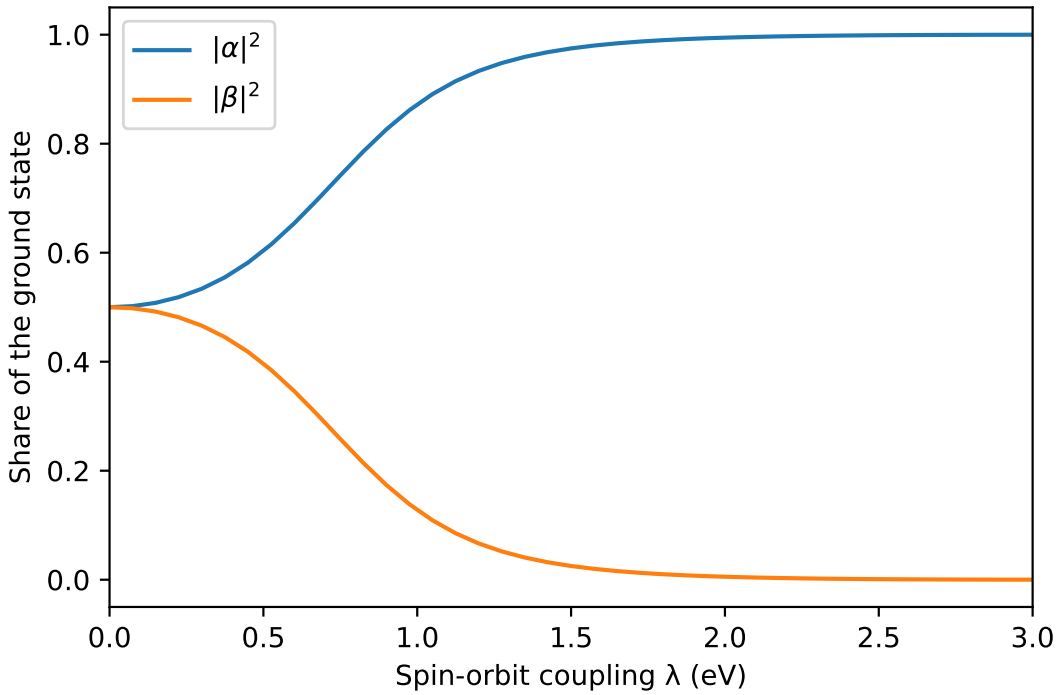

Figure 5.3: The two components at the ground state are shown. For increasing λ, the component α belonging to $\left|\pm\frac{3}{2}, \mp\frac{3}{2}\right\rangle$ dominates more and more over the component β belonging to $\left|\pm\frac{1}{2}, \mp\frac{1}{2}\right\rangle$.

It also shows that there is no observable level repulsion between the remaining states. This observation is also supported by the exact results. In the following, we will now analyze the course of the ground state vector between the edge cases already described. The analysis shows that only states of the form

$$\frac{\alpha}{\sqrt{2}}\left(\left|+\frac{3}{2},-\frac{3}{2}\right\rangle-\left|-\frac{3}{2},+\frac{3}{2}\right\rangle\right)+\frac{\beta}{\sqrt{2}}\left(\left|-\frac{1}{2},+\frac{1}{2}\right\rangle-\left|+\frac{1}{2},-\frac{1}{2}\right\rangle\right) \tag{5.39}$$

can be formed, where, as described in the previous sections, $\alpha(\lambda = 0) = 1$ and $\beta(J_\mathrm{H} = 0) = 1$. If these two parameters are plotted, the result is Figure 5.3.

As expected, α initially increases, while β decreases. For $J_\mathrm{H} \neq 0$, β for $\lambda \to \infty$ does not converge towards 0, but towards a small, negative value. There is therefore a change in the relative phase of α and β. For $J_\mathrm{H} = 0.5\,\mathrm{eV}$, however, this value is so small ($|\beta|^2 \approx 0.0025$) that this behaviour is not quantitatively relevant and was therefore not analysed in depth.

5.2 Cooperative Jahn-Teller effect

As explained in Section 2.3, the cooperative Jahn-Teller effect is an effect that depends on many factors. Nevertheless, it can be estimated to what extent the effect shown in Section 4.2 that for $\lambda > 0$ both $\left|\pm\frac{1}{2}\right\rangle$ and $\left|\pm\frac{3}{2}\right\rangle$ states can experience an almost identical energetic lowering can have an influence on the level splitting generated by the superexchange. It is to be expected that the Jahn-Teller Hamiltonian prefers a different ground state than the superexchange Hamiltonian, since under the condition $Q_3^{\mathrm{t}} = -Q_3^{\mathrm{b}}$ states that take the form $\left|\pm\frac{3}{2}, \pm\frac{1}{2}\right\rangle$ or $\left|\pm\frac{1}{2}, \pm\frac{3}{2}\right\rangle$ are energetically preferred. For this purpose, the Hamiltonian

$$\hat{H}_{t,\mathrm{JT,eff}} = \hat{H}_{t,\mathrm{eff}} + \hat{H}_{JT,\mathrm{eff}} \tag{5.40}$$

with

$$\hat{H}_{\mathrm{JT,eff,i,j}} = \langle i| H_{\mathrm{JT}} |j\rangle \tag{5.41}$$

was assumed and diagonalised under the constraints $Q_2 = 0$ and $Q_3^{\mathrm{t}} = -Q_3^{\mathrm{b}}$. With this approach, the $\pm\frac{1}{2}$ $\pm\frac{3}{2}$ subspaces are identical except for the sign, which is why it is sufficient to restrict the value range of Q_3 to $\mathbb{R}_0^+$. The results are shown in Figure 5.4.

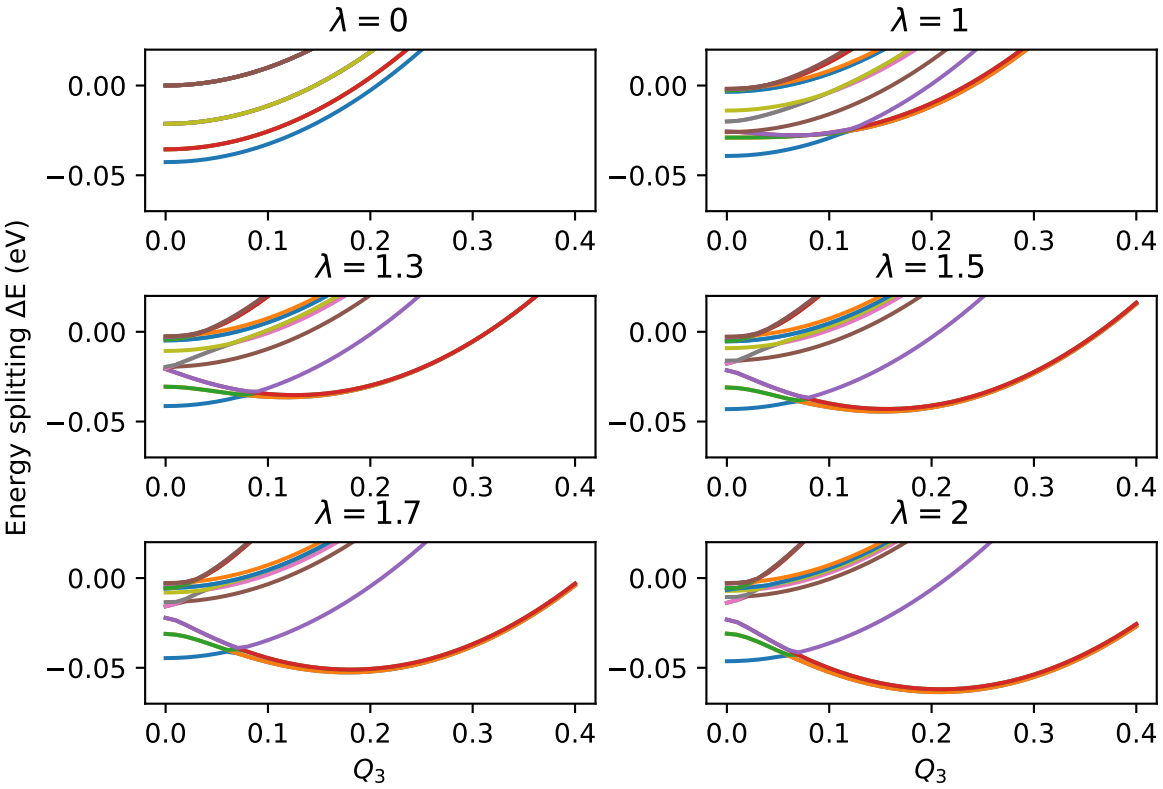

Figure 5.4: The spectra of the energy splitting are shown as a function of the distortion Q_3 ($g = B = 0.25$, $U = 2J_\mathrm{H} = 1$) for different λ. It can be seen that a distorted geometry is preferred for $\lambda \gtrsim 1.5$.

It turns out that the ground state determined by the superexchange can be replaced by the level above it at $\lambda \approx 1.5\,\mathrm{eV}$. Although this value is higher than the usually assumed $\lambda < 1\,\mathrm{eV}$ [33], it cannot be ruled out that the ground state in real materials can be influenced by the cooperative Jahn-Teller effect due to the highly simplified mathematical model. The Jahn-Teller distortion might therefore be more pronounced in crystals with superexchange than it was predicted in the purely one-site analysis of Section 4.2.

6 Conclusion and outlook

In the present work, a model Hamiltonian was investigated which can describe the properties of a half-filled t_{2g} shell in transition metal compounds. For this purpose, a one-site problem was first considered, in which the Hamiltonian can be composed of two components. On the one hand, the effects of Hund's coupling were described by a Kanamori-Hubbard Hamiltonian, and on the other hand, spin-orbit coupling was introduced by an interaction of spin and orbital angular momentum of the individual electrons. This showed that, regardless of the strength of the individual terms, a fourfold degenerate manifold always formed the ground state, the energy of which can be described by a zero of a third-degree polynomial. Furthermore, the ground state manifold was described completely, whereby it was shown that a basis of eigenstates of the two individual terms is not sufficient to describe the eigenstates of their sum.

It was then considered how the introduction of the Jahn-Teller effect, a coupling of the electronic states to the surrounding lattice, influences the states and whether the effect leads to a distortion of the ligands surrounding the transition metal ion. Here it was shown that the distortion increases with increasing spin-orbit coupling, whereby the compressed geometry is slightly preferable to the elongated geometry.

In the second part of the work, the influence of the possibility of electron exchange between neighbouring ions through superexchange on the ground state manifold was investigated. An analytical description was obtained for the two limiting cases of vanishing Hund's coupling and vanishing spin-orbit coupling. For the area of combined effects it could be shown that a perturbation-theoretical calculation does not always, but in the range of physically realistic parameters, achieve an almost perfect agreement with the exact diagonalisation of the Hamiltonian.

Furthermore, it was analysed to what extent the introduction of the superexchange changes the effects of the Jahn-Teller effect. In a highly simplified approach, it was shown that the symmetry reductions caused by the Jahn-Teller effect in the two-site model can already be noticeable with smaller spin-orbit coupling than in the one-site case.

Further research on the theoretical side should focus on implementing the model on a larger lattice with a stronger focus on the influence of the interplay between superexchange and the Jahn-Teller effect on the splitting of the ground state manifold. A further analysis

of the predicted states to conclude their magnetic properties also might return interesting results. Research on the experimental side could be done comparing the predicted single ion results with measured values in different materials. It could also prove useful to measure the splitting of the ground state manifold, as the predicted energy scale is still reasonably large.

A Second quantisation representation of t_{2g}

The simplest basis of the t_{2g} states can be given in second quantisation with the occupation numbers of the orbitals and electron spin quantum numbers.

$$|yz\uparrow, yz\downarrow, xz\uparrow, xz\downarrow, xy\uparrow, xy\downarrow,\rangle \tag{A.1}$$

In shorthand notation the states can be written by using just arrows to indicate spin with the positioning between commas indicating the orbit. As a third part, the state created by operators acting on the vacuum state $|0\rangle$ is also given.

Table A.1: Second quantisation representation of t_{2g}^1

occupation number notation	shorthand notation	creation operators notation
$\|0,0,0,0,0,1\rangle$	$\|\times,\times,\downarrow\rangle$	$c^\dagger_{xy\downarrow}\|0\rangle$
$\|0,0,0,0,1,0\rangle$	$\|\times,\times,\uparrow\rangle$	$c^\dagger_{xy\uparrow}\|0\rangle$
$\|0,0,0,1,0,0\rangle$	$\|\times,\downarrow,\times\rangle$	$c^\dagger_{xz\downarrow}\|0\rangle$
$\|0,0,1,0,0,0\rangle$	$\|\times,\uparrow,\times\rangle$	$c^\dagger_{xz\uparrow}\|0\rangle$
$\|0,1,0,0,0,0\rangle$	$\|\downarrow,\times,\times\rangle$	$c^\dagger_{yz\downarrow}\|0\rangle$
$\|1,0,0,0,0,0\rangle$	$\|\uparrow,\times,\times\rangle$	$c^\dagger_{yz\uparrow}\|0\rangle$

Table A.2: Second quantisation representation of t_{2g}^2

occupation number notation	shorthand notation	creation operators notation
$\|0,0,0,0,1,1\rangle$	$\|\times,\times,\uparrow\downarrow\rangle$	$c^\dagger_{xy\uparrow}c^\dagger_{xy\downarrow}\|0\rangle$
$\|0,0,0,1,0,1\rangle$	$\|\times,\downarrow,\downarrow\rangle$	$c^\dagger_{xz\downarrow}c^\dagger_{xy\downarrow}\|0\rangle$
$\|0,0,0,1,1,0\rangle$	$\|\times,\downarrow,\uparrow\rangle$	$c^\dagger_{xz\downarrow}c^\dagger_{xy\uparrow}\|0\rangle$
$\|0,0,1,0,0,1\rangle$	$\|\times,\uparrow,\downarrow\rangle$	$c^\dagger_{xz\uparrow}c^\dagger_{xy\downarrow}\|0\rangle$
$\|0,0,1,0,1,0\rangle$	$\|\times,\uparrow,\uparrow\rangle$	$c^\dagger_{xz\uparrow}c^\dagger_{xy\uparrow}\|0\rangle$
$\|0,0,1,1,0,0\rangle$	$\|\times,\uparrow\downarrow,\times\rangle$	$c^\dagger_{xz\uparrow}c^\dagger_{xz\downarrow}\|0\rangle$
$\|0,1,0,0,0,1\rangle$	$\|\downarrow,\times,\downarrow\rangle$	$c^\dagger_{yz\downarrow}c^\dagger_{xy\downarrow}\|0\rangle$
$\|0,1,0,0,1,0\rangle$	$\|\downarrow,\times,\uparrow\rangle$	$c^\dagger_{yz\downarrow}c^\dagger_{xy\uparrow}\|0\rangle$
$\|0,1,0,1,0,0\rangle$	$\|\downarrow,\downarrow,\times\rangle$	$c^\dagger_{yz\downarrow}c^\dagger_{xz\downarrow}\|0\rangle$
$\|0,1,1,0,0,0\rangle$	$\|\downarrow,\uparrow,\times\rangle$	$c^\dagger_{yz\downarrow}c^\dagger_{xz\uparrow}\|0\rangle$
$\|1,0,0,0,0,1\rangle$	$\|\uparrow,\times,\downarrow\rangle$	$c^\dagger_{yz\uparrow}c^\dagger_{xy\downarrow}\|0\rangle$
$\|1,0,0,0,1,0\rangle$	$\|\uparrow,\times,\uparrow\rangle$	$c^\dagger_{yz\uparrow}c^\dagger_{xy\uparrow}\|0\rangle$
$\|1,0,0,1,0,0\rangle$	$\|\uparrow,\downarrow,\times\rangle$	$c^\dagger_{yz\uparrow}c^\dagger_{xz\downarrow}\|0\rangle$
$\|1,0,1,0,0,0\rangle$	$\|\uparrow,\uparrow,\times\rangle$	$c^\dagger_{yz\uparrow}c^\dagger_{xz\uparrow}\|0\rangle$
$\|1,1,0,0,0,0\rangle$	$\|\uparrow\downarrow,\times,\times\rangle$	$c^\dagger_{yz\uparrow}c^\dagger_{yz\downarrow}\|0\rangle$

Table A.3: Second quantisation representation of t_{2g}^3

occupation number notation	shorthand notation	creation operators notation
$\|0,0,0,1,1,1\rangle$	$\left\|\times,\downarrow,\uparrow\downarrow\right\rangle$	$c^\dagger_{xz\downarrow}c^\dagger_{xy\uparrow}c^\dagger_{xy\downarrow}\|0\rangle$
$\|0,0,1,0,1,1\rangle$	$\left\|\times,\uparrow,\uparrow\downarrow\right\rangle$	$c^\dagger_{xz\uparrow}c^\dagger_{xy\uparrow}c^\dagger_{xy\downarrow}\|0\rangle$
$\|0,0,1,1,0,1\rangle$	$\left\|\times,\uparrow\downarrow,\downarrow\right\rangle$	$c^\dagger_{xz\uparrow}c^\dagger_{xz\downarrow}c^\dagger_{xy\downarrow}\|0\rangle$
$\|0,0,1,1,1,0\rangle$	$\left\|\times,\uparrow\downarrow,\uparrow\right\rangle$	$c^\dagger_{xz\uparrow}c^\dagger_{xz\downarrow}c^\dagger_{xy\uparrow}\|0\rangle$
$\|0,1,0,0,1,1\rangle$	$\left\|\downarrow,\times,\uparrow\downarrow\right\rangle$	$c^\dagger_{yz\downarrow}c^\dagger_{xy\uparrow}c^\dagger_{xy\downarrow}\|0\rangle$
$\|0,1,0,1,0,1\rangle$	$\|\downarrow,\downarrow,\downarrow\rangle$	$c^\dagger_{yz\downarrow}c^\dagger_{xz\downarrow}c^\dagger_{xy\downarrow}\|0\rangle$
$\|0,1,0,1,1,0\rangle$	$\|\downarrow,\downarrow,\uparrow\rangle$	$c^\dagger_{yz\downarrow}c^\dagger_{xz\downarrow}c^\dagger_{xy\uparrow}\|0\rangle$
$\|0,1,1,0,0,1\rangle$	$\|\downarrow,\uparrow,\downarrow\rangle$	$c^\dagger_{yz\downarrow}c^\dagger_{xz\uparrow}c^\dagger_{xy\downarrow}\|0\rangle$
$\|0,1,1,0,1,0\rangle$	$\|\downarrow,\uparrow,\uparrow\rangle$	$c^\dagger_{yz\downarrow}c^\dagger_{xz\uparrow}c^\dagger_{xy\uparrow}\|0\rangle$
$\|0,1,1,1,0,0\rangle$	$\left\|\downarrow,\uparrow\downarrow,\times\right\rangle$	$c^\dagger_{yz\downarrow}c^\dagger_{xz\uparrow}c^\dagger_{xz\downarrow}\|0\rangle$
$\|1,0,0,0,1,1\rangle$	$\left\|\uparrow,\times,\uparrow\downarrow\right\rangle$	$c^\dagger_{yz\uparrow}c^\dagger_{xy\uparrow}c^\dagger_{xy\downarrow}\|0\rangle$
$\|1,0,0,1,0,1\rangle$	$\|\uparrow,\downarrow,\downarrow\rangle$	$c^\dagger_{yz\uparrow}c^\dagger_{xz\downarrow}c^\dagger_{xy\downarrow}\|0\rangle$
$\|1,0,0,1,1,0\rangle$	$\|\uparrow,\downarrow,\uparrow\rangle$	$c^\dagger_{yz\uparrow}c^\dagger_{xz\downarrow}c^\dagger_{xy\uparrow}\|0\rangle$
$\|1,0,1,0,0,1\rangle$	$\|\uparrow,\uparrow,\downarrow\rangle$	$c^\dagger_{yz\uparrow}c^\dagger_{xz\uparrow}c^\dagger_{xy\downarrow}\|0\rangle$
$\|1,0,1,0,1,0\rangle$	$\|\uparrow,\uparrow,\uparrow\rangle$	$c^\dagger_{yz\uparrow}c^\dagger_{xz\uparrow}c^\dagger_{xy\uparrow}\|0\rangle$
$\|1,0,1,1,0,0\rangle$	$\left\|\uparrow,\uparrow\downarrow,\times\right\rangle$	$c^\dagger_{yz\uparrow}c^\dagger_{xz\uparrow}c^\dagger_{xz\downarrow}\|0\rangle$
$\|1,1,0,0,0,1\rangle$	$\left\|\uparrow\downarrow,\times,\downarrow\right\rangle$	$c^\dagger_{yz\uparrow}c^\dagger_{yz\downarrow}c^\dagger_{xy\downarrow}\|0\rangle$
$\|1,1,0,0,1,0\rangle$	$\left\|\uparrow\downarrow,\times,\uparrow\right\rangle$	$c^\dagger_{yz\uparrow}c^\dagger_{yz\downarrow}c^\dagger_{xy\uparrow}\|0\rangle$
$\|1,1,0,1,0,0\rangle$	$\left\|\uparrow\downarrow,\downarrow,\times\right\rangle$	$c^\dagger_{yz\uparrow}c^\dagger_{yz\downarrow}c^\dagger_{xz\downarrow}\|0\rangle$
$\|1,1,1,0,0,0\rangle$	$\left\|\uparrow\downarrow,\uparrow,\times\right\rangle$	$c^\dagger_{yz\uparrow}c^\dagger_{yz\downarrow}c^\dagger_{xz\uparrow}\|0\rangle$

Table A.4: Second quantisation representation of t_{2g}^4

occupation number notation	shorthand notation	creation operators notation
$\|0,0,1,1,1,1\rangle$	$\|\times,\uparrow\downarrow,\uparrow\downarrow\rangle$	$c^\dagger_{xz\uparrow}c^\dagger_{xz\downarrow}c^\dagger_{xy\uparrow}c^\dagger_{xy\downarrow}\|0\rangle$
$\|0,1,0,1,1,1\rangle$	$\|\downarrow,\downarrow,\uparrow\downarrow\rangle$	$c^\dagger_{yz\downarrow}c^\dagger_{xz\downarrow}c^\dagger_{xy\uparrow}c^\dagger_{xy\downarrow}\|0\rangle$
$\|0,1,1,0,1,1\rangle$	$\|\downarrow,\uparrow,\uparrow\downarrow\rangle$	$c^\dagger_{yz\downarrow}c^\dagger_{xz\uparrow}c^\dagger_{xy\uparrow}c^\dagger_{xy\downarrow}\|0\rangle$
$\|0,1,1,1,0,1\rangle$	$\|\downarrow,\uparrow\downarrow,\downarrow\rangle$	$c^\dagger_{yz\downarrow}c^\dagger_{xz\uparrow}c^\dagger_{xz\downarrow}c^\dagger_{xy\downarrow}\|0\rangle$
$\|0,1,1,1,1,0\rangle$	$\|\downarrow,\uparrow\downarrow,\uparrow\rangle$	$c^\dagger_{yz\downarrow}c^\dagger_{xz\uparrow}c^\dagger_{xz\downarrow}c^\dagger_{xy\uparrow}\|0\rangle$
$\|1,0,0,1,1,1\rangle$	$\|\uparrow,\downarrow,\uparrow\downarrow\rangle$	$c^\dagger_{yz\uparrow}c^\dagger_{xz\downarrow}c^\dagger_{xy\uparrow}c^\dagger_{xy\downarrow}\|0\rangle$
$\|1,0,1,0,1,1\rangle$	$\|\uparrow,\uparrow,\uparrow\downarrow\rangle$	$c^\dagger_{yz\uparrow}c^\dagger_{xz\uparrow}c^\dagger_{xy\uparrow}c^\dagger_{xy\downarrow}\|0\rangle$
$\|1,0,1,1,0,1\rangle$	$\|\uparrow,\uparrow\downarrow,\downarrow\rangle$	$c^\dagger_{yz\uparrow}c^\dagger_{xz\uparrow}c^\dagger_{xz\downarrow}c^\dagger_{xy\downarrow}\|0\rangle$
$\|1,0,1,1,1,0\rangle$	$\|\uparrow,\uparrow\downarrow,\uparrow\rangle$	$c^\dagger_{yz\uparrow}c^\dagger_{xz\uparrow}c^\dagger_{xz\downarrow}c^\dagger_{xy\uparrow}\|0\rangle$
$\|1,1,0,0,1,1\rangle$	$\|\uparrow\downarrow,\times,\uparrow\downarrow\rangle$	$c^\dagger_{yz\uparrow}c^\dagger_{yz\downarrow}c^\dagger_{xy\uparrow}c^\dagger_{xy\downarrow}\|0\rangle$
$\|1,1,0,1,0,1\rangle$	$\|\uparrow\downarrow,\downarrow,\downarrow\rangle$	$c^\dagger_{yz\uparrow}c^\dagger_{yz\downarrow}c^\dagger_{xz\downarrow}c^\dagger_{xy\downarrow}\|0\rangle$
$\|1,1,0,1,1,0\rangle$	$\|\uparrow\downarrow,\downarrow,\uparrow\rangle$	$c^\dagger_{yz\uparrow}c^\dagger_{yz\downarrow}c^\dagger_{xz\downarrow}c^\dagger_{xy\uparrow}\|0\rangle$
$\|1,1,1,0,0,1\rangle$	$\|\uparrow\downarrow,\uparrow,\downarrow\rangle$	$c^\dagger_{yz\uparrow}c^\dagger_{yz\downarrow}c^\dagger_{xz\uparrow}c^\dagger_{xy\downarrow}\|0\rangle$
$\|1,1,1,0,1,0\rangle$	$\|\uparrow\downarrow,\uparrow,\uparrow\rangle$	$c^\dagger_{yz\uparrow}c^\dagger_{yz\downarrow}c^\dagger_{xz\uparrow}c^\dagger_{xy\uparrow}\|0\rangle$
$\|1,1,1,1,0,0\rangle$	$\|\uparrow\downarrow,\uparrow\downarrow,\times\rangle$	$c^\dagger_{yz\uparrow}c^\dagger_{yz\downarrow}c^\dagger_{xz\uparrow}c^\dagger_{xz\downarrow}\|0\rangle$

Table A.5: Second quantisation representation of t_{2g}^5

occupation number notation	shorthand notation	creation operators notation
$\|0,1,1,1,1,1\rangle$	$\|\downarrow,\uparrow\downarrow,\uparrow\downarrow\rangle$	$c^\dagger_{yz\downarrow}c^\dagger_{xz\uparrow}c^\dagger_{xz\downarrow}c^\dagger_{xy\uparrow}c^\dagger_{xy\downarrow}\|0\rangle$
$\|1,0,1,1,1,1\rangle$	$\|\uparrow,\uparrow\downarrow,\uparrow\downarrow\rangle$	$c^\dagger_{yz\uparrow}c^\dagger_{xz\uparrow}c^\dagger_{xz\downarrow}c^\dagger_{xy\uparrow}c^\dagger_{xy\downarrow}\|0\rangle$
$\|1,1,0,1,1,1\rangle$	$\|\uparrow\downarrow,\downarrow,\uparrow\downarrow\rangle$	$c^\dagger_{yz\uparrow}c^\dagger_{yz\downarrow}c^\dagger_{xz\downarrow}c^\dagger_{xy\uparrow}c^\dagger_{xy\downarrow}\|0\rangle$
$\|1,1,1,0,1,1\rangle$	$\|\uparrow\downarrow,\uparrow,\uparrow\downarrow\rangle$	$c^\dagger_{yz\uparrow}c^\dagger_{yz\downarrow}c^\dagger_{xz\uparrow}c^\dagger_{xy\uparrow}c^\dagger_{xy\downarrow}\|0\rangle$
$\|1,1,1,1,0,1\rangle$	$\|\uparrow\downarrow,\uparrow\downarrow,\downarrow\rangle$	$c^\dagger_{yz\uparrow}c^\dagger_{yz\downarrow}c^\dagger_{xz\uparrow}c^\dagger_{xz\downarrow}c^\dagger_{xy\downarrow}\|0\rangle$
$\|1,1,1,1,1,0\rangle$	$\|\uparrow\downarrow,\uparrow\downarrow,\uparrow\rangle$	$c^\dagger_{yz\uparrow}c^\dagger_{yz\downarrow}c^\dagger_{xz\uparrow}c^\dagger_{xz\downarrow}c^\dagger_{xy\uparrow}\|0\rangle$

B Eigenstates of the Kanamori-Hubbard Hamiltonian

The eigenstates of the Kanamori-Hubbard Hamiltonian

$$H_{\text{int}} = (U - 3J)\frac{N(N-1)}{2} - 2JS^2 - \frac{1}{2}JL^2 + \frac{5}{2}JN$$

are shown for different numbers of electrons. The states can be characterised by the usual quantum numbers S, L, m_S, m_L. the degeneracy is therefore given by

$$\# = (2S + 1) \cdot (2L + 1).$$

B.1 t_{2g}^1

For one electron there is one combination of S and L.

Table B.1: Eigenenergies and eigenstates of the Kanamori-Hubbard Hamiltonian with 1 electron

E	S	L	m_S	m_L	state
0	$\frac{1}{2}$	1	$+\frac{1}{2}$	$+1$	$\frac{1}{\sqrt{2}}\left(\left\|\times,\uparrow,\times\right\rangle - i\left\|\uparrow,\times,\times\right\rangle\right)$
			$+\frac{1}{2}$	0	$\left\|\times,\times,\uparrow\right\rangle$
			$+\frac{1}{2}$	-1	$\frac{1}{\sqrt{2}}\left(\left\|\times,\uparrow,\times\right\rangle + i\left\|\uparrow,\times,\times\right\rangle\right)$
			$-\frac{1}{2}$	$+1$	$\frac{1}{\sqrt{2}}\left(\left\|\times,\downarrow,\times\right\rangle - i\left\|\downarrow,\times,\times\right\rangle\right)$
			$-\frac{1}{2}$	0	$\left\|\times,\times,\downarrow\right\rangle$
			$-\frac{1}{2}$	-1	$\frac{1}{\sqrt{2}}\left(\left\|\times,\downarrow,\times\right\rangle - i\left\|\downarrow,\times,\times\right\rangle\right)$

B.2 t_{2g}^2

For two electrons there are three different combinations of S and L.

Table B.2: Eigenenergies and eigenstates of the Kanamori-Hubbard Hamiltonian with 2 electrons

E	S	L	m_S	m_L	state
$U+2J$	0	0	0	0	$\frac{1}{\sqrt{3}}\left(\left\|\times,\times,\uparrow\downarrow\right\rangle+\left\|\times,\uparrow\downarrow,\times\right\rangle+\left\|\uparrow\downarrow,\times,\times\right\rangle\right)$
$U-J$	0	2	0	+2	$\frac{1}{2}\left(\left\|\times,\uparrow\downarrow,\times\right\rangle+i\left\|\downarrow,\uparrow,\times\right\rangle-i\left\|\uparrow,\downarrow,\times\right\rangle-\left\|\uparrow\downarrow,\times,\times\right\rangle\right)$
			0	+1	$\frac{1}{2}\left(\left\|\times,\downarrow,\uparrow\right\rangle-\left\|\times,\uparrow,\downarrow\right\rangle-i\left\|\downarrow,\times,\uparrow\right\rangle+i\left\|\uparrow,\times,\downarrow\right\rangle\right)$
			0	0	$\frac{1}{\sqrt{6}}\left(2\cdot\left\|\times,\times,\uparrow\downarrow\right\rangle-\left\|\times,\uparrow\downarrow,\times\right\rangle-\left\|\uparrow\downarrow,\times,\times\right\rangle\right)$
			0	-1	$\frac{1}{2}\left(\left\|\times,\downarrow,\uparrow\right\rangle-\left\|\times,\uparrow,\downarrow\right\rangle+i\left\|\downarrow,\times,\uparrow\right\rangle-i\left\|\uparrow,\times,\downarrow\right\rangle\right)$
			0	-2	$\frac{1}{2}\left(\left\|\times,\uparrow\downarrow,\times\right\rangle-i\left\|\downarrow,\uparrow,\times\right\rangle+i\left\|\uparrow,\downarrow,\times\right\rangle-\left\|\uparrow\downarrow,\times,\times\right\rangle\right)$
$U-3J$	1	1	+1	+1	$\frac{1}{\sqrt{2}}\left(\left\|\times,\uparrow,\uparrow\right\rangle-i\left\|\uparrow,\times,\uparrow\right\rangle\right)$
			+1	0	$\left\|\uparrow,\uparrow,\times\right\rangle$
			+1	-1	$\frac{1}{\sqrt{2}}\left(\left\|\times,\uparrow,\uparrow\right\rangle+i\left\|\uparrow,\times,\uparrow\right\rangle\right)$
			0	+1	$\frac{1}{2}\left(\left\|\times,\downarrow,\uparrow\right\rangle+\left\|\times,\uparrow,\downarrow\right\rangle-i\left\|\downarrow,\times,\uparrow\right\rangle-i\left\|\uparrow,\times,\downarrow\right\rangle\right)$
			0	0	$\frac{1}{\sqrt{2}}\left(\left\|\downarrow,\uparrow,\times\right\rangle+\left\|\uparrow,\downarrow,\times\right\rangle\right)$
			0	-1	$\frac{1}{2}\left(\left\|\times,\downarrow,\uparrow\right\rangle+\left\|\times,\uparrow,\downarrow\right\rangle+i\left\|\downarrow,\times,\uparrow\right\rangle+i\left\|\uparrow,\times,\downarrow\right\rangle\right)$
			−1	+1	$\frac{1}{\sqrt{2}}\left(\left\|\times,\downarrow,\downarrow\right\rangle-i\left\|\downarrow,\times,\downarrow\right\rangle\right)$
			−1	0	$\left\|\downarrow,\downarrow,\times\right\rangle$
			−1	-1	$\frac{1}{\sqrt{2}}\left(\left\|\times,\downarrow,\downarrow\right\rangle+i\left\|\downarrow,\times,\downarrow\right\rangle\right)$

B.3 t_{2g}^3

For three electrons there are three different combinations of S and L.

Table B.3: Eigenenergies and eigenstates of the Kanamori-Hubbard Hamiltonian with 3 electrons

E	S	L	m_S	m_L	state
$3U-4J$	$\frac{1}{2}$	1	$+\frac{1}{2}$	+1	$\frac{1}{2}\left(\left\vert\times,\uparrow,\uparrow\downarrow\right\rangle - i\left\vert\uparrow,\times,\uparrow\downarrow\right\rangle - i\left\vert\uparrow,\uparrow\downarrow,\times\right\rangle + \left\vert\uparrow\downarrow,\uparrow,\times\right\rangle\right)$
			$+\frac{1}{2}$	0	$\frac{1}{\sqrt{2}}\left(\left\vert\times,\uparrow\downarrow,\uparrow\right\rangle + \left\vert\uparrow\downarrow,\times,\uparrow\right\rangle\right)$
			$+\frac{1}{2}$	-1	$\frac{1}{2}\left(\left\vert\times,\uparrow,\uparrow\downarrow\right\rangle + i\left\vert\uparrow,\times,\uparrow\downarrow\right\rangle + i\left\vert\uparrow,\uparrow\downarrow,\times\right\rangle + \left\vert\uparrow\downarrow,\uparrow,\times\right\rangle\right)$
			$-\frac{1}{2}$	+1	$\frac{1}{2}\left(\left\vert\times,\downarrow,\uparrow\downarrow\right\rangle - i\left\vert\downarrow,\times,\uparrow\downarrow\right\rangle - i\left\vert\downarrow,\uparrow\downarrow,\times\right\rangle + \left\vert\uparrow\downarrow,\downarrow,\times\right\rangle\right)$
			$-\frac{1}{2}$	0	$\frac{1}{\sqrt{2}}\left(\left\vert\times,\uparrow\downarrow,\downarrow\right\rangle + \left\vert\uparrow\downarrow,\times,\downarrow\right\rangle\right)$
			$-\frac{1}{2}$	-1	$\frac{1}{2}\left(\left\vert\times,\downarrow,\uparrow\downarrow\right\rangle + i\left\vert\downarrow,\times,\uparrow\downarrow\right\rangle + i\left\vert\downarrow,\uparrow\downarrow,\times\right\rangle + \left\vert\uparrow\downarrow,\downarrow,\times\right\rangle\right)$
$3U-6J$	$\frac{1}{2}$	2	$+\frac{1}{2}$	+2	$\frac{1}{2}\left(\left\vert\times,\uparrow\downarrow,\uparrow\right\rangle + i\left\vert\downarrow,\uparrow,\uparrow\right\rangle - i\left\vert\uparrow,\downarrow,\uparrow\right\rangle - \left\vert\uparrow\downarrow,\times,\uparrow\right\rangle\right)$
			$+\frac{1}{2}$	+1	$\frac{1}{2}\left(\left\vert\times,\uparrow,\uparrow\downarrow\right\rangle - i\left\vert\uparrow,\times,\uparrow\downarrow\right\rangle + i\left\vert\uparrow,\uparrow\downarrow,\times\right\rangle - \left\vert\uparrow\downarrow,\uparrow,\times\right\rangle\right)$
			$+\frac{1}{2}$	0	$\frac{1}{\sqrt{6}}\left(\left\vert\downarrow,\uparrow,\uparrow\right\rangle + \left\vert\uparrow,\downarrow,\uparrow\right\rangle - 2\cdot\left\vert\uparrow,\uparrow,\downarrow\right\rangle\right)$
			$+\frac{1}{2}$	-1	$\frac{1}{2}\left(\left\vert\times,\uparrow,\uparrow\downarrow\right\rangle + i\left\vert\uparrow,\times,\uparrow\downarrow\right\rangle - i\left\vert\uparrow,\uparrow\downarrow,\times\right\rangle - \left\vert\uparrow\downarrow,\uparrow,\times\right\rangle\right)$
			$+\frac{1}{2}$	-2	$\frac{1}{2}\left(\left\vert\times,\uparrow\downarrow,\uparrow\right\rangle - i\left\vert\downarrow,\uparrow,\uparrow\right\rangle + i\left\vert\uparrow,\downarrow,\uparrow\right\rangle - \left\vert\uparrow\downarrow,\times,\uparrow\right\rangle\right)$
			$-\frac{1}{2}$	+2	$\frac{1}{2}\left(\left\vert\times,\uparrow\downarrow,\downarrow\right\rangle + i\left\vert\downarrow,\uparrow,\downarrow\right\rangle - i\left\vert\uparrow,\downarrow,\downarrow\right\rangle - \left\vert\uparrow\downarrow,\times,\downarrow\right\rangle\right)$
			$-\frac{1}{2}$	+1	$\frac{1}{2}\left(\left\vert\times,\downarrow,\uparrow\downarrow\right\rangle - i\left\vert\downarrow,\times,\uparrow\downarrow\right\rangle + i\left\vert\downarrow,\uparrow\downarrow,\times\right\rangle - \left\vert\uparrow\downarrow,\downarrow,\times\right\rangle\right)$
			$-\frac{1}{2}$	0	$\frac{1}{\sqrt{6}}\left(2\cdot\left\vert\downarrow,\downarrow,\uparrow\right\rangle - \left\vert\downarrow,\uparrow,\downarrow\right\rangle - \left\vert\uparrow,\downarrow,\downarrow\right\rangle\right)$
			$-\frac{1}{2}$	-1	$\frac{1}{2}\left(\left\vert\times,\downarrow,\uparrow\downarrow\right\rangle + i\left\vert\downarrow,\times,\uparrow\downarrow\right\rangle - i\left\vert\downarrow,\uparrow\downarrow,\times\right\rangle - \left\vert\uparrow\downarrow,\downarrow,\times\right\rangle\right)$
			$-\frac{1}{2}$	-2	$\frac{1}{2}\left(\left\vert\times,\uparrow\downarrow,\downarrow\right\rangle - i\left\vert\downarrow,\uparrow,\downarrow\right\rangle + i\left\vert\uparrow,\downarrow,\downarrow\right\rangle - \left\vert\uparrow\downarrow,\times,\downarrow\right\rangle\right)$
$3U-9J$	$\frac{3}{2}$	0	$+\frac{3}{2}$	0	$\left\vert\uparrow,\uparrow,\uparrow\right\rangle$
			$+\frac{1}{2}$	0	$\frac{1}{\sqrt{3}}\left(\left\vert\downarrow,\uparrow,\uparrow\right\rangle + \left\vert\uparrow,\downarrow,\uparrow\right\rangle + \left\vert\uparrow,\uparrow,\downarrow\right\rangle\right)$
			$-\frac{1}{2}$	0	$\frac{1}{\sqrt{3}}\left(\left\vert\downarrow,\downarrow,\uparrow\right\rangle + \left\vert\downarrow,\uparrow,\downarrow\right\rangle + \left\vert\uparrow,\downarrow,\downarrow\right\rangle\right)$
			$-\frac{3}{2}$	0	$\left\vert\downarrow,\downarrow,\downarrow\right\rangle$

B.4 t_{2g}^4

For four electrons there are three different combinations of S and L.

Table B.4: Eigenenergies and eigenstates of the Kanamori-Hubbard Hamiltonian with 4 electrons

E	S	L	m_S	m_L	state
$6U-8J$	0	0	0	0	$\frac{1}{\sqrt{3}}\left(\left\vert\times,\uparrow\downarrow,\uparrow\downarrow\right\rangle+\left\vert\uparrow\downarrow,\times,\uparrow\downarrow\right\rangle+\left\vert\uparrow\downarrow,\uparrow\downarrow,\times\right\rangle\right)$
$6U-11J$	0	2	0	+2	$\frac{1}{2}\left(\left\vert\times,\uparrow\downarrow,\uparrow\downarrow\right\rangle+i\left\vert\downarrow,\uparrow,\uparrow\downarrow\right\rangle-i\left\vert\uparrow,\downarrow,\uparrow\downarrow\right\rangle-\left\vert\uparrow\downarrow,\uparrow\downarrow,\times\right\rangle\right)$
			0	+1	$\frac{1}{2}\left(\left\vert\downarrow,\uparrow\downarrow,\uparrow\right\rangle-\left\vert\uparrow,\uparrow\downarrow,\downarrow\right\rangle+i\left\vert\uparrow\downarrow,\downarrow,\uparrow\right\rangle-i\left\vert\uparrow\downarrow,\uparrow,\downarrow\right\rangle\right)$
			0	0	$\frac{1}{\sqrt{6}}\left(\left\vert\times,\uparrow\downarrow,\uparrow\downarrow\right\rangle+\left\vert\uparrow\downarrow,\times,\uparrow\downarrow\right\rangle-2\cdot\left\vert\uparrow\downarrow,\uparrow\downarrow,\times\right\rangle\right)$
			0	-1	$\frac{1}{2}\left(\left\vert\downarrow,\uparrow\downarrow,\uparrow\right\rangle-\left\vert\uparrow,\uparrow\downarrow,\downarrow\right\rangle-i\left\vert\uparrow\downarrow,\downarrow,\uparrow\right\rangle+i\left\vert\uparrow\downarrow,\uparrow,\downarrow\right\rangle\right)$
			0	-2	$\frac{1}{2}\left(\left\vert\times,\uparrow\downarrow,\uparrow\downarrow\right\rangle-i\left\vert\downarrow,\uparrow,\uparrow\downarrow\right\rangle+i\left\vert\uparrow,\downarrow,\uparrow\downarrow\right\rangle-\left\vert\uparrow\downarrow,\uparrow\downarrow,\times\right\rangle\right)$
$6U-13J$	1	1	+1	+1	$\frac{1}{\sqrt{2}}\left(\left\vert\uparrow,\uparrow\downarrow,\uparrow\right\rangle+i\left\vert\uparrow\downarrow,\uparrow,\uparrow\right\rangle\right)$
			+1	0	$\left\vert\uparrow,\uparrow,\uparrow\downarrow\right\rangle$
			+1	-1	$\frac{1}{\sqrt{2}}\left(\left\vert\uparrow,\uparrow\downarrow,\uparrow\right\rangle-i\left\vert\uparrow\downarrow,\uparrow,\uparrow\right\rangle\right)$
			0	+1	$\frac{1}{2}\left(\left\vert\downarrow,\uparrow\downarrow,\uparrow\right\rangle+\left\vert\uparrow,\uparrow\downarrow,\downarrow\right\rangle+i\left\vert\uparrow\downarrow,\downarrow,\uparrow\right\rangle+i\left\vert\uparrow\downarrow,\uparrow,\downarrow\right\rangle\right)$
			0	0	$\frac{1}{\sqrt{2}}\left(\left\vert\downarrow,\uparrow,\uparrow\downarrow\right\rangle+\left\vert\uparrow,\downarrow,\uparrow\downarrow\right\rangle\right)$
			0	-1	$\frac{1}{2}\left(\left\vert\downarrow,\uparrow\downarrow,\uparrow\right\rangle+\left\vert\uparrow,\uparrow\downarrow,\downarrow\right\rangle-i\left\vert\uparrow\downarrow,\downarrow,\uparrow\right\rangle-i\left\vert\uparrow\downarrow,\uparrow,\downarrow\right\rangle\right)$
			−1	+1	$\frac{1}{\sqrt{2}}\left(\left\vert\downarrow,\uparrow\downarrow,\downarrow\right\rangle+i\left\vert\uparrow\downarrow,\downarrow,\downarrow\right\rangle\right)$
			−1	0	$\left\vert\downarrow,\downarrow,\uparrow\downarrow\right\rangle$
			−1	-1	$\frac{1}{\sqrt{2}}\left(\left\vert\downarrow,\uparrow\downarrow,\downarrow\right\rangle-i\left\vert\uparrow\downarrow,\downarrow,\downarrow\right\rangle\right)$

B.5 t_{2g}^5

For five electrons there is one combination of S and L.

Table B.5: Eigenenergies and eigenstates of the Kanamori-Hubbard Hamiltonian with 5 electrons

E	S	L	m_S	m_L	state
10U - 20J	$\frac{1}{2}$	1	$+\frac{1}{2}$	+1	$\frac{1}{\sqrt{2}}\left(\lvert\uparrow,\uparrow\downarrow,\uparrow\downarrow\rangle + i\lvert\uparrow\downarrow,\uparrow,\uparrow\downarrow\rangle\right)$
			$+\frac{1}{2}$	0	$\lvert\uparrow\downarrow,\uparrow\downarrow,\uparrow\rangle$
			$+\frac{1}{2}$	-1	$\frac{1}{\sqrt{2}}\left(\lvert\uparrow,\uparrow\downarrow,\uparrow\downarrow\rangle - i\lvert\uparrow\downarrow,\uparrow,\uparrow\downarrow\rangle\right)$
			$-\frac{1}{2}$	+1	$\frac{1}{\sqrt{2}}\left(\lvert\downarrow,\uparrow\downarrow,\uparrow\downarrow\rangle + i\lvert\uparrow\downarrow,\downarrow,\uparrow\downarrow\rangle\right)$
			$-\frac{1}{2}$	0	$\lvert\uparrow\downarrow,\uparrow\downarrow,\downarrow\rangle$
			$-\frac{1}{2}$	-1	$\frac{1}{\sqrt{2}}\left(\lvert\downarrow,\uparrow\downarrow,\uparrow\downarrow\rangle - i\lvert\uparrow\downarrow,\downarrow,\uparrow\downarrow\rangle\right)$

C Eigenstates of the spin-orbit coupling Hamiltonian

The eigenstates of the spin-orbit coupling Hamiltonian

$$H_\lambda = \frac{i\lambda}{2} \sum_{\alpha,\beta,\gamma} \sum_{\sigma,\sigma'} \epsilon_{\alpha,\beta,\gamma} \tau^{\gamma}_{\sigma,\sigma'} c^{\dagger}_{\alpha,\sigma} c_{\beta,\sigma'} \tag{C.1}$$

are shown for different numbers of electrons. The states can be characterised by their composition of one-electron states with the quantum numbers j, m_j. Those having the form

$$|j = 1/2, m_j = +1/2\rangle == \frac{1}{\sqrt{3}} |yz, \downarrow\rangle + \frac{i}{\sqrt{3}} |xz, \downarrow\rangle + \frac{1}{\sqrt{3}} |xy, \uparrow\rangle , \tag{C.2}$$

$$|j = 1/2, m_j = -1/2\rangle = \frac{1}{\sqrt{3}} |yz, \uparrow\rangle - \frac{i}{\sqrt{3}} |xz, \uparrow\rangle - \frac{1}{\sqrt{3}} |xy, \downarrow\rangle , \tag{C.3}$$

with energy $+\lambda$ and

$$|j = 3/2, m_j = +3/2\rangle = \frac{1}{\sqrt{2}} |yz, \uparrow\rangle + \frac{i}{\sqrt{2}} |xz, \uparrow\rangle , \tag{C.4}$$

$$|j = 3/2, m_j = +1/2\rangle = \frac{1}{\sqrt{6}} |yz, \downarrow\rangle + \frac{i}{\sqrt{6}} |xz, \downarrow\rangle - \sqrt{\frac{2}{3}} |xy, \uparrow\rangle , \tag{C.5}$$

$$|j = 3/2, m_j = -1/2\rangle = \frac{1}{\sqrt{6}} |yz, \uparrow\rangle - \frac{i}{\sqrt{6}} |xz, \uparrow\rangle + \sqrt{\frac{2}{3}} |xy, \downarrow\rangle , \tag{C.6}$$

$$|j = 3/2, m_j = -3/2\rangle = \frac{1}{\sqrt{2}} |yz, \downarrow\rangle - \frac{i}{\sqrt{2}} |xz, \downarrow\rangle , \tag{C.7}$$

with energy $-\frac{1}{2}\lambda$, the degeneracies can be deduced from the possible combinatorics.

C.1 t_{2g}^1

For one electron, the states are given by the one-electron states.

C.2 t_{2g}^2

For two electrons there are three different combinations of j_1 and j_2.

Table C.1: Eigenenergies and eigenstates of the SOC-Hamiltonian with 2 electrons

E	j_1	j_2	m_{j_1}	m_{j_2}	state
2λ	$\frac{1}{2}$	$\frac{1}{2}$	$+\frac{1}{2}$	$-\frac{1}{2}$	$c^\dagger_{\frac{1}{2},+\frac{1}{2}} c^\dagger_{\frac{1}{2},-\frac{1}{2}} \lvert 0\rangle$
$\frac{1}{2}\lambda$	$\frac{1}{2}$	$\frac{3}{2}$	$+\frac{1}{2}$	$+\frac{3}{2}$	$c^\dagger_{\frac{1}{2},+\frac{1}{2}} c^\dagger_{\frac{3}{2},+\frac{3}{2}} \lvert 0\rangle$
			$+\frac{1}{2}$	$+\frac{1}{2}$	$c^\dagger_{\frac{1}{2},+\frac{1}{2}} c^\dagger_{\frac{3}{2},+\frac{1}{2}} \lvert 0\rangle$
			$+\frac{1}{2}$	$-\frac{1}{2}$	$c^\dagger_{\frac{1}{2},+\frac{1}{2}} c^\dagger_{\frac{3}{2},-\frac{1}{2}} \lvert 0\rangle$
			$+\frac{1}{2}$	$-\frac{3}{2}$	$c^\dagger_{\frac{1}{2},+\frac{1}{2}} c^\dagger_{\frac{3}{2},-\frac{3}{2}} \lvert 0\rangle$
			$-\frac{1}{2}$	$+\frac{3}{2}$	$c^\dagger_{\frac{1}{2},-\frac{1}{2}} c^\dagger_{\frac{3}{2},+\frac{3}{2}} \lvert 0\rangle$
			$-\frac{1}{2}$	$+\frac{1}{2}$	$c^\dagger_{\frac{1}{2},-\frac{1}{2}} c^\dagger_{\frac{3}{2},+\frac{1}{2}} \lvert 0\rangle$
			$-\frac{1}{2}$	$-\frac{1}{2}$	$c^\dagger_{\frac{1}{2},-\frac{1}{2}} c^\dagger_{\frac{3}{2},-\frac{1}{2}} \lvert 0\rangle$
			$-\frac{1}{2}$	$-\frac{3}{2}$	$c^\dagger_{\frac{1}{2},-\frac{1}{2}} c^\dagger_{\frac{3}{2},-\frac{3}{2}} \lvert 0\rangle$
$-\lambda$	$\frac{3}{2}$	$\frac{3}{2}$	$+\frac{3}{2}$	$+\frac{1}{2}$	$c^\dagger_{\frac{3}{2},+\frac{3}{2}} c^\dagger_{\frac{3}{2},+\frac{1}{2}} \lvert 0\rangle$
			$+\frac{3}{2}$	$-\frac{1}{2}$	$c^\dagger_{\frac{3}{2},+\frac{3}{2}} c^\dagger_{\frac{3}{2},-\frac{1}{2}} \lvert 0\rangle$
			$+\frac{3}{2}$	$-\frac{3}{2}$	$c^\dagger_{\frac{3}{2},+\frac{3}{2}} c^\dagger_{\frac{3}{2},-\frac{3}{2}} \lvert 0\rangle$
			$+\frac{1}{2}$	$-\frac{1}{2}$	$c^\dagger_{\frac{3}{2},+\frac{1}{2}} c^\dagger_{\frac{3}{2},-\frac{1}{2}} \lvert 0\rangle$
			$+\frac{1}{2}$	$-\frac{3}{2}$	$c^\dagger_{\frac{3}{2},+\frac{1}{2}} c^\dagger_{\frac{3}{2},-\frac{3}{2}} \lvert 0\rangle$
			$-\frac{1}{2}$	$-\frac{3}{2}$	$c^\dagger_{\frac{3}{2},-\frac{1}{2}} c^\dagger_{\frac{3}{2},-\frac{3}{2}} \lvert 0\rangle$

C.3 t_{2g}^3

For three electrons there are three different combinations j_1, j_2 and j_3.

Table C.2: Eigenenergies and eigenstates of the SOC-Hamiltonian with 3 electrons

E	j_1	j_2	j_3	m_{j_1}	m_{j_2}	m_{j_3}	state
$\frac{3}{2}\lambda$	$\frac{1}{2}$	$\frac{1}{2}$	$\frac{3}{2}$	$+\frac{1}{2}$	$-\frac{1}{2}$	$+\frac{3}{2}$	$c^\dagger_{\frac{1}{2},+\frac{1}{2}} c^\dagger_{\frac{1}{2},-\frac{1}{2}} c^\dagger_{\frac{3}{2},+\frac{3}{2}} \lvert 0\rangle$
				$+\frac{1}{2}$	$-\frac{1}{2}$	$+\frac{3}{2}$	$c^\dagger_{\frac{1}{2},+\frac{1}{2}} c^\dagger_{\frac{1}{2},-\frac{1}{2}} c^\dagger_{\frac{3}{2},+\frac{1}{2}} \lvert 0\rangle$
				$+\frac{1}{2}$	$-\frac{1}{2}$	$+\frac{3}{2}$	$c^\dagger_{\frac{1}{2},+\frac{1}{2}} c^\dagger_{\frac{1}{2},-\frac{1}{2}} c^\dagger_{\frac{3}{2},-\frac{1}{2}} \lvert 0\rangle$
				$+\frac{1}{2}$	$-\frac{1}{2}$	$+\frac{3}{2}$	$c^\dagger_{\frac{1}{2},+\frac{1}{2}} c^\dagger_{\frac{1}{2},-\frac{1}{2}} c^\dagger_{\frac{3}{2},-\frac{3}{2}} \lvert 0\rangle$
0	$\frac{1}{2}$	$\frac{3}{2}$	$\frac{3}{2}$	$+\frac{1}{2}$	$+\frac{3}{2}$	$+\frac{1}{2}$	$c^\dagger_{\frac{1}{2},+\frac{1}{2}} c^\dagger_{\frac{3}{2},+\frac{3}{2}} c^\dagger_{\frac{3}{2},+\frac{1}{2}} \lvert 0\rangle$
				$+\frac{1}{2}$	$+\frac{3}{2}$	$-\frac{1}{2}$	$c^\dagger_{\frac{1}{2},+\frac{1}{2}} c^\dagger_{\frac{3}{2},+\frac{3}{2}} c^\dagger_{\frac{3}{2},-\frac{1}{2}} \lvert 0\rangle$
				$+\frac{1}{2}$	$+\frac{3}{2}$	$-\frac{3}{2}$	$c^\dagger_{\frac{1}{2},+\frac{1}{2}} c^\dagger_{\frac{3}{2},+\frac{3}{2}} c^\dagger_{\frac{3}{2},-\frac{3}{2}} \lvert 0\rangle$
				$+\frac{1}{2}$	$+\frac{1}{2}$	$-\frac{1}{2}$	$c^\dagger_{\frac{1}{2},+\frac{1}{2}} c^\dagger_{\frac{3}{2},+\frac{1}{2}} c^\dagger_{\frac{3}{2},-\frac{1}{2}} \lvert 0\rangle$
				$+\frac{1}{2}$	$+\frac{1}{2}$	$-\frac{3}{2}$	$c^\dagger_{\frac{1}{2},+\frac{1}{2}} c^\dagger_{\frac{3}{2},+\frac{1}{2}} c^\dagger_{\frac{3}{2},-\frac{3}{2}} \lvert 0\rangle$
				$+\frac{1}{2}$	$-\frac{1}{2}$	$-\frac{3}{2}$	$c^\dagger_{\frac{1}{2},+\frac{1}{2}} c^\dagger_{\frac{3}{2},-\frac{1}{2}} c^\dagger_{\frac{3}{2},-\frac{3}{2}} \lvert 0\rangle$
				$-\frac{1}{2}$	$+\frac{3}{2}$	$+\frac{1}{2}$	$c^\dagger_{\frac{1}{2},-\frac{1}{2}} c^\dagger_{\frac{3}{2},+\frac{3}{2}} c^\dagger_{\frac{3}{2},+\frac{1}{2}} \lvert 0\rangle$
				$-\frac{1}{2}$	$+\frac{3}{2}$	$-\frac{1}{2}$	$c^\dagger_{\frac{1}{2},-\frac{1}{2}} c^\dagger_{\frac{3}{2},+\frac{3}{2}} c^\dagger_{\frac{3}{2},-\frac{1}{2}} \lvert 0\rangle$
				$-\frac{1}{2}$	$+\frac{3}{2}$	$-\frac{3}{2}$	$c^\dagger_{\frac{1}{2},-\frac{1}{2}} c^\dagger_{\frac{3}{2},+\frac{3}{2}} c^\dagger_{\frac{3}{2},-\frac{3}{2}} \lvert 0\rangle$
				$-\frac{1}{2}$	$+\frac{1}{2}$	$-\frac{1}{2}$	$c^\dagger_{\frac{1}{2},-\frac{1}{2}} c^\dagger_{\frac{3}{2},+\frac{1}{2}} c^\dagger_{\frac{3}{2},-\frac{1}{2}} \lvert 0\rangle$
				$-\frac{1}{2}$	$+\frac{1}{2}$	$-\frac{3}{2}$	$c^\dagger_{\frac{1}{2},-\frac{1}{2}} c^\dagger_{\frac{3}{2},+\frac{1}{2}} c^\dagger_{\frac{3}{2},-\frac{3}{2}} \lvert 0\rangle$
				$-\frac{1}{2}$	$-\frac{1}{2}$	$-\frac{3}{2}$	$c^\dagger_{\frac{1}{2},-\frac{1}{2}} c^\dagger_{\frac{3}{2},-\frac{1}{2}} c^\dagger_{\frac{3}{2},-\frac{3}{2}} \lvert 0\rangle$
$-\frac{3}{2}\lambda$	$\frac{3}{2}$	$\frac{3}{2}$	$\frac{3}{2}$	$+\frac{3}{2}$	$+\frac{1}{2}$	$-\frac{1}{2}$	$c^\dagger_{\frac{3}{2},+\frac{3}{2}} c^\dagger_{\frac{3}{2},+\frac{1}{2}} c^\dagger_{\frac{3}{2},-\frac{1}{2}} \lvert 0\rangle$
				$+\frac{3}{2}$	$+\frac{1}{2}$	$-\frac{3}{2}$	$c^\dagger_{\frac{3}{2},+\frac{3}{2}} c^\dagger_{\frac{3}{2},+\frac{1}{2}} c^\dagger_{\frac{3}{2},-\frac{3}{2}} \lvert 0\rangle$
				$+\frac{3}{2}$	$-\frac{1}{2}$	$-\frac{3}{2}$	$c^\dagger_{\frac{3}{2},+\frac{3}{2}} c^\dagger_{\frac{3}{2},-\frac{1}{2}} c^\dagger_{\frac{3}{2},-\frac{3}{2}} \lvert 0\rangle$
				$+\frac{1}{2}$	$-\frac{1}{2}$	$-\frac{3}{2}$	$c^\dagger_{\frac{3}{2},+\frac{3}{2}} c^\dagger_{\frac{3}{2},-\frac{1}{2}} c^\dagger_{\frac{3}{2},-\frac{3}{2}} \lvert 0\rangle$

C.4 t_{2g}^4

For four electrons there are three different combinations of j_1, j_2, j_3 and j_4.

Table C.3: Eigenenergies and eigenstates of the SOC-Hamiltonian with 4 electrons

E	j_1	j_2	j_3	j_4	m_{j_1}	m_{j_2}	m_{j_3}	m_{j_4}	state
λ	$\frac{1}{2}$	$\frac{1}{2}$	$\frac{3}{2}$	$\frac{3}{2}$	$+\frac{1}{2}$	$-\frac{1}{2}$	$+\frac{3}{2}$	$+\frac{1}{2}$	$c^\dagger_{\frac{1}{2},+\frac{1}{2}} c^\dagger_{\frac{1}{2},-\frac{1}{2}} c^\dagger_{\frac{3}{2},+\frac{3}{2}} c^\dagger_{\frac{3}{2},+\frac{1}{2}} \lvert 0\rangle$
					$+\frac{1}{2}$	$-\frac{1}{2}$	$+\frac{3}{2}$	$-\frac{1}{2}$	$c^\dagger_{\frac{1}{2},+\frac{1}{2}} c^\dagger_{\frac{1}{2},-\frac{1}{2}} c^\dagger_{\frac{3}{2},+\frac{3}{2}} c^\dagger_{\frac{3}{2},-\frac{1}{2}} \lvert 0\rangle$
					$+\frac{1}{2}$	$-\frac{1}{2}$	$+\frac{3}{2}$	$-\frac{3}{2}$	$c^\dagger_{\frac{1}{2},+\frac{1}{2}} c^\dagger_{\frac{1}{2},-\frac{1}{2}} c^\dagger_{\frac{3}{2},+\frac{3}{2}} c^\dagger_{\frac{3}{2},-\frac{3}{2}} \lvert 0\rangle$
					$+\frac{1}{2}$	$-\frac{1}{2}$	$+\frac{1}{2}$	$-\frac{1}{2}$	$c^\dagger_{\frac{1}{2},+\frac{1}{2}} c^\dagger_{\frac{1}{2},-\frac{1}{2}} c^\dagger_{\frac{3}{2},+\frac{1}{2}} c^\dagger_{\frac{3}{2},-\frac{1}{2}} \lvert 0\rangle$
					$+\frac{1}{2}$	$-\frac{1}{2}$	$+\frac{1}{2}$	$-\frac{3}{2}$	$c^\dagger_{\frac{1}{2},+\frac{1}{2}} c^\dagger_{\frac{1}{2},-\frac{1}{2}} c^\dagger_{\frac{3}{2},+\frac{1}{2}} c^\dagger_{\frac{3}{2},-\frac{3}{2}} \lvert 0\rangle$
					$+\frac{1}{2}$	$-\frac{1}{2}$	$-\frac{1}{2}$	$-\frac{3}{2}$	$c^\dagger_{\frac{1}{2},+\frac{1}{2}} c^\dagger_{\frac{1}{2},-\frac{1}{2}} c^\dagger_{\frac{3}{2},-\frac{1}{2}} c^\dagger_{\frac{3}{2},-\frac{3}{2}} \lvert 0\rangle$
$-\frac{1}{2}\lambda$	$\frac{1}{2}$	$\frac{3}{2}$	$\frac{3}{2}$	$\frac{3}{2}$	$+\frac{1}{2}$	$+\frac{3}{2}$	$+\frac{1}{2}$	$-\frac{1}{2}$	$c^\dagger_{\frac{1}{2},+\frac{1}{2}} c^\dagger_{\frac{3}{2},+\frac{3}{2}} c^\dagger_{\frac{3}{2},+\frac{1}{2}} c^\dagger_{\frac{3}{2},-\frac{1}{2}} \lvert 0\rangle$
					$+\frac{1}{2}$	$+\frac{3}{2}$	$+\frac{1}{2}$	$-\frac{3}{2}$	$c^\dagger_{\frac{1}{2},+\frac{1}{2}} c^\dagger_{\frac{3}{2},+\frac{3}{2}} c^\dagger_{\frac{3}{2},+\frac{1}{2}} c^\dagger_{\frac{3}{2},-\frac{3}{2}} \lvert 0\rangle$
					$+\frac{1}{2}$	$+\frac{3}{2}$	$-\frac{1}{2}$	$-\frac{3}{2}$	$c^\dagger_{\frac{1}{2},+\frac{1}{2}} c^\dagger_{\frac{3}{2},+\frac{3}{2}} c^\dagger_{\frac{3}{2},-\frac{1}{2}} c^\dagger_{\frac{3}{2},-\frac{3}{2}} \lvert 0\rangle$
					$+\frac{1}{2}$	$+\frac{1}{2}$	$-\frac{1}{2}$	$-\frac{3}{2}$	$c^\dagger_{\frac{1}{2},+\frac{1}{2}} c^\dagger_{\frac{3}{2},+\frac{1}{2}} c^\dagger_{\frac{3}{2},-\frac{1}{2}} c^\dagger_{\frac{3}{2},-\frac{3}{2}} \lvert 0\rangle$
					$-\frac{1}{2}$	$+\frac{3}{2}$	$+\frac{1}{2}$	$-\frac{1}{2}$	$c^\dagger_{\frac{1}{2},-\frac{1}{2}} c^\dagger_{\frac{3}{2},+\frac{3}{2}} c^\dagger_{\frac{3}{2},+\frac{1}{2}} c^\dagger_{\frac{3}{2},-\frac{1}{2}} \lvert 0\rangle$
					$-\frac{1}{2}$	$+\frac{3}{2}$	$+\frac{1}{2}$	$-\frac{3}{2}$	$c^\dagger_{\frac{1}{2},-\frac{1}{2}} c^\dagger_{\frac{3}{2},+\frac{3}{2}} c^\dagger_{\frac{3}{2},+\frac{1}{2}} c^\dagger_{\frac{3}{2},-\frac{3}{2}} \lvert 0\rangle$
					$-\frac{1}{2}$	$+\frac{3}{2}$	$-\frac{1}{2}$	$-\frac{3}{2}$	$c^\dagger_{\frac{1}{2},-\frac{1}{2}} c^\dagger_{\frac{3}{2},+\frac{3}{2}} c^\dagger_{\frac{3}{2},-\frac{1}{2}} c^\dagger_{\frac{3}{2},-\frac{3}{2}} \lvert 0\rangle$
					$-\frac{1}{2}$	$+\frac{1}{2}$	$-\frac{1}{2}$	$-\frac{3}{2}$	$c^\dagger_{\frac{1}{2},-\frac{1}{2}} c^\dagger_{\frac{3}{2},+\frac{1}{2}} c^\dagger_{\frac{3}{2},-\frac{1}{2}} c^\dagger_{\frac{3}{2},-\frac{3}{2}} \lvert 0\rangle$
-2λ	$\frac{3}{2}$	$\frac{3}{2}$	$\frac{3}{2}$	$\frac{3}{2}$	$+\frac{3}{2}$	$+\frac{1}{2}$	$-\frac{1}{2}$	$-\frac{3}{2}$	$c^\dagger_{\frac{3}{2},+\frac{3}{2}} c^\dagger_{\frac{3}{2},+\frac{1}{2}} c^\dagger_{\frac{3}{2},-\frac{1}{2}} c^\dagger_{\frac{3}{2},-\frac{3}{2}} \lvert 0\rangle$

C.5 t_{2g}^5

For five electrons there are two different combinations of j_1, j_2, j_3, j_4 and j_5.

Table C.4: Eigenenergies and eigenstates of the SOC-Hamiltonian with 5 electrons

E	j_1	j_2	j_3	j_4	j_5	m_{j_1}	m_{j_2}	m_{j_3}	m_{j_4}	m_{j_5}	state
$\frac{1}{2}\lambda$	$\frac{1}{2}$	$\frac{1}{2}$	$\frac{3}{2}$	$\frac{3}{2}$	$\frac{3}{2}$	$+\frac{1}{2}$	$-\frac{1}{2}$	$+\frac{3}{2}$	$+\frac{1}{2}$	$-\frac{1}{2}$	$c^\dagger_{\frac{1}{2},+\frac{1}{2}} c^\dagger_{\frac{1}{2},-\frac{1}{2}} c^\dagger_{\frac{3}{2},+\frac{3}{2}} c^\dagger_{\frac{3}{2},+\frac{1}{2}} c^\dagger_{\frac{3}{2},-\frac{1}{2}} \lvert 0\rangle$
						$+\frac{1}{2}$	$-\frac{1}{2}$	$+\frac{3}{2}$	$+\frac{1}{2}$	$-\frac{3}{2}$	$c^\dagger_{\frac{1}{2},+\frac{1}{2}} c^\dagger_{\frac{1}{2},-\frac{1}{2}} c^\dagger_{\frac{3}{2},+\frac{3}{2}} c^\dagger_{\frac{3}{2},+\frac{1}{2}} c^\dagger_{\frac{3}{2},-\frac{3}{2}} \lvert 0\rangle$
						$+\frac{1}{2}$	$-\frac{1}{2}$	$+\frac{3}{2}$	$-\frac{1}{2}$	$-\frac{3}{2}$	$c^\dagger_{\frac{1}{2},+\frac{1}{2}} c^\dagger_{\frac{1}{2},-\frac{1}{2}} c^\dagger_{\frac{3}{2},+\frac{3}{2}} c^\dagger_{\frac{3}{2},-\frac{1}{2}} c^\dagger_{\frac{3}{2},-\frac{3}{2}} \lvert 0\rangle$
						$+\frac{1}{2}$	$-\frac{1}{2}$	$+\frac{1}{2}$	$-\frac{1}{2}$	$-\frac{3}{2}$	$c^\dagger_{\frac{1}{2},+\frac{1}{2}} c^\dagger_{\frac{1}{2},-\frac{1}{2}} c^\dagger_{\frac{3}{2},+\frac{1}{2}} c^\dagger_{\frac{3}{2},-\frac{1}{2}} c^\dagger_{\frac{3}{2},-\frac{3}{2}} \lvert 0\rangle$
$-\lambda$	$\frac{1}{2}$	$\frac{3}{2}$	$\frac{3}{2}$	$\frac{3}{2}$	$\frac{3}{2}$	$+\frac{1}{2}$	$+\frac{3}{2}$	$+\frac{1}{2}$	$-\frac{1}{2}$	$-\frac{3}{2}$	$c^\dagger_{\frac{1}{2},+\frac{1}{2}} c^\dagger_{\frac{3}{2},+\frac{3}{2}} c^\dagger_{\frac{3}{2},+\frac{1}{2}} c^\dagger_{\frac{3}{2},-\frac{1}{2}} c^\dagger_{\frac{3}{2},-\frac{3}{2}} \lvert 0\rangle$
						$-\frac{1}{2}$	$+\frac{3}{2}$	$+\frac{1}{2}$	$-\frac{1}{2}$	$-\frac{3}{2}$	$c^\dagger_{\frac{1}{2},-\frac{1}{2}} c^\dagger_{\frac{3}{2},+\frac{3}{2}} c^\dagger_{\frac{3}{2},+\frac{1}{2}} c^\dagger_{\frac{3}{2},-\frac{1}{2}} c^\dagger_{\frac{3}{2},-\frac{3}{2}} \lvert 0\rangle$

D Intermediate regime

For $J_{\mathrm{H}} \neq 0$ and $\lambda \neq 0$ the states can be described by their total angular momentum quantum numbers J and m_J. However, those do not form a complete set of commuting observables. The resulting eigenenergies are listed below.

D.1 t_{2g}^1

As shown in figure D.1, there is one doubly degenerate($J = 1/2$) and one fourfold degenerate ($J = 3/2$) branch. The energies of the states can be described by the linear functions

$$E_{J=\frac{1}{2}} = \lambda \tag{D.1}$$

$$E_{J=\frac{3}{2}} = -\frac{1}{2}\lambda. \tag{D.2}$$

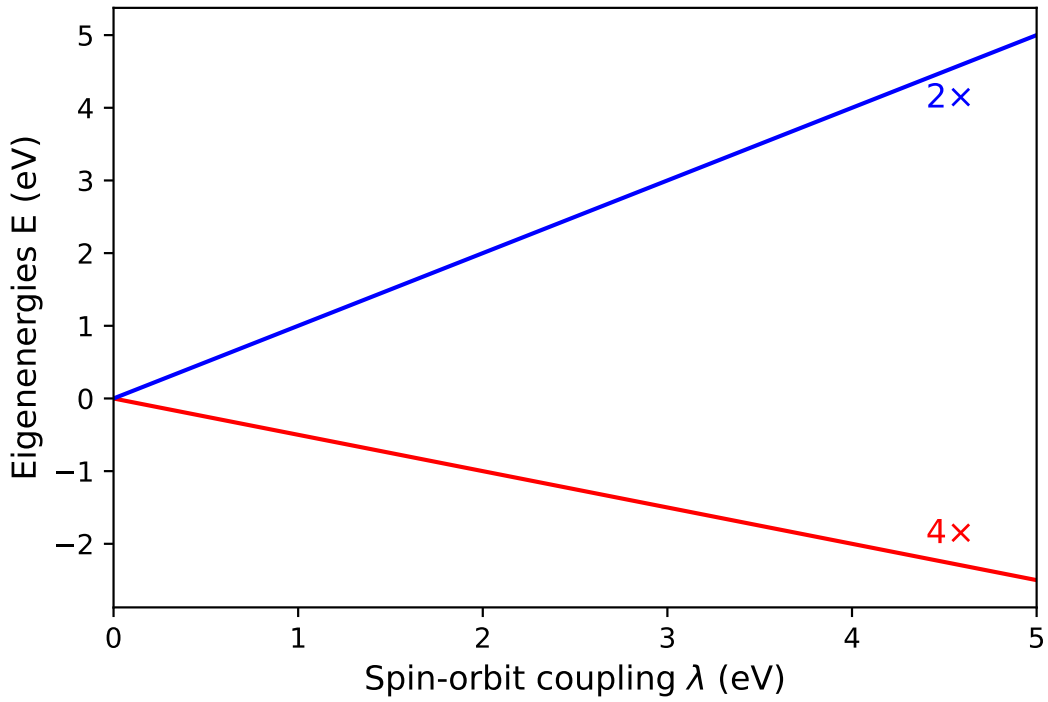

Figure D.1: The eigenenergies of the one electron case are shown for $U = 0, J_{\mathrm{H}} = 1$.

D.2 t_{2g}^2

As shown in figure D.2, there are two nondegenerate ($J = 0$), two fivefold degenerate ($J = 2$) and one threefold degenerate ($J = 1$) branch.

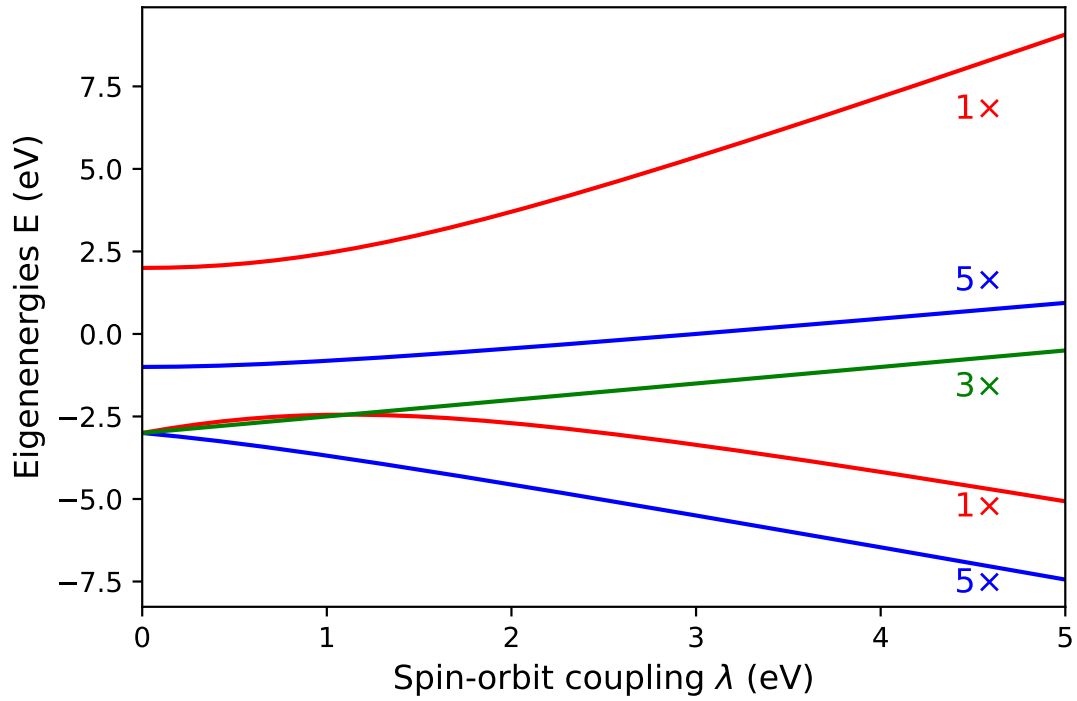

Figure D.2: The eigenenergies of the two electron case are shown for $U = 0, J_{\mathrm{H}} = 1$.

The energies of the states can be described by the functions

$$E_{J=0,upper} = J_{\mathrm{H}} \left(-\frac{1}{2} + \frac{1}{2}\frac{\lambda}{J_{\mathrm{H}}} + \frac{1}{2}\sqrt{9\left(\frac{\lambda}{J_{\mathrm{H}}}\right)^2 - 10\frac{\lambda}{J_{\mathrm{H}}} + 25} \right) \tag{D.3}$$

$$E_{J=2,upper} = J_{\mathrm{H}} \left(-2 - \frac{1}{4}\frac{\lambda}{J_{\mathrm{H}}} + \frac{1}{2}\sqrt{\frac{9}{4}\left(\frac{\lambda}{J_{\mathrm{H}}}\right)^2 + 2\frac{\lambda}{J_{\mathrm{H}}} + 4} \right) \tag{D.4}$$

$$E_{J=1} = -3J_{\mathrm{H}} + \frac{1}{2}\lambda \tag{D.5}$$

$$E_{J=0,lower} = J_{\mathrm{H}} \left(-\frac{1}{2} + \frac{1}{2}\frac{\lambda}{J_{\mathrm{H}}} - \frac{1}{2}\sqrt{9\left(\frac{\lambda}{J_{\mathrm{H}}}\right)^2 - 10\frac{\lambda}{J_{\mathrm{H}}} + 25} \right) \tag{D.6}$$

$$E_{J=2,lower} = J_{\mathrm{H}} \left(-2 - \frac{1}{4}\frac{\lambda}{J_{\mathrm{H}}} - \frac{1}{2}\sqrt{\frac{9}{4}\left(\frac{\lambda}{J_{\mathrm{H}}}\right)^2 + 2\frac{\lambda}{J_{\mathrm{H}}} + 4} \right). \tag{D.7}$$

D.3 t_{2g}^3

As shown in figure D.3, there are three fourfold degenerate ($J = 3/2$), one doubly degenerate ($J = 1/2$) and one sixfold degenerate ($J = 5/2$) branch.

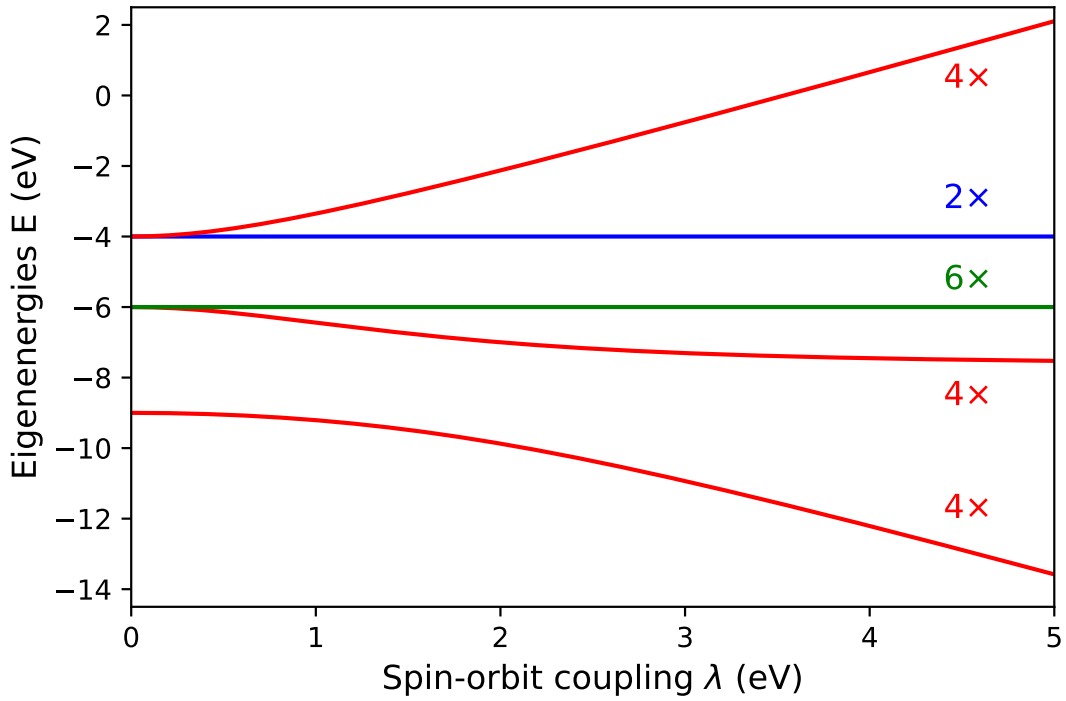

Figure D.3: The eigenenergies of the three electron case are shown for $U = 0, J_\mathrm{H} = 1$.

The energies of the $J = 0$ states can be described by the the polynomial equation

$$-864J_\mathrm{H}^3 - 456J_\mathrm{H}^2E + 60J_\mathrm{H}\lambda^2 - 76J_\mathrm{H}E^2 + 9\lambda^2E - 4E^3 = 0 \tag{D.8}$$

while the energies of the other two branches lie constant at

$$E_{J=\frac{1}{2}} = -4J_\mathrm{H} \tag{D.9}$$

$$E_{J=\frac{5}{2}} = -6J_\mathrm{H}. \tag{D.10}$$

D.4 t_{2g}^4

As shown in figure D.4, there are two nondegenerate ($J = 0$), two fivefold degenerate ($J = 2$) and one threefold degenerate ($J = 1$) branch.

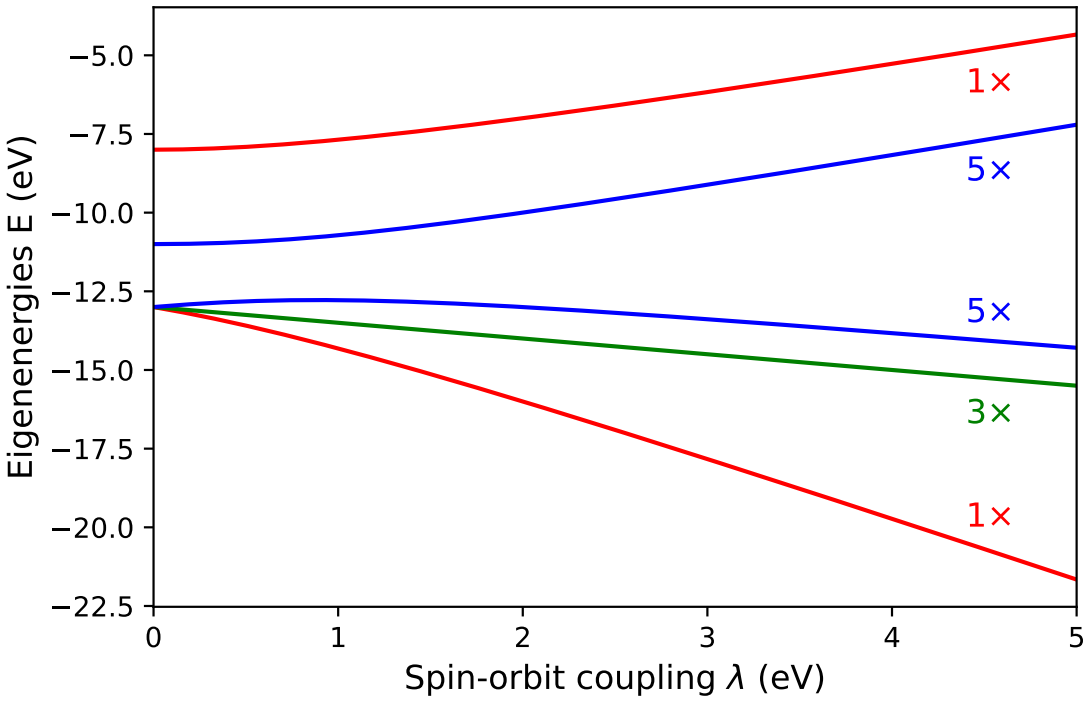

Figure D.4: The eigenenergies of the four electron case are shown for $U = 0, J_{\mathrm{H}} = 1$.

The energies of the states can be described by the functions

$$E_{J=0,upper} = J_{\mathrm{H}} \left(-\frac{21}{2} - \frac{1}{2}\frac{\lambda}{J_{\mathrm{H}}} + \frac{1}{2}\sqrt{9\left(\frac{\lambda}{J_{\mathrm{H}}}\right)^2 + 10\frac{\lambda}{J_{\mathrm{H}}} + 25} \right) \tag{D.11}$$

$$E_{J=2,upper} = J_{\mathrm{H}} \left(-12 + \frac{1}{4}\frac{\lambda}{J_{\mathrm{H}}} + \frac{1}{2}\sqrt{\frac{9}{4}\left(\frac{\lambda}{J_{\mathrm{H}}}\right)^2 - 2\frac{\lambda}{J_{\mathrm{H}}} + 4} \right) \tag{D.12}$$

$$E_{J=2,lower} = J_{\mathrm{H}} \left(-12 + \frac{1}{4}\frac{\lambda}{J_{\mathrm{H}}} - \frac{1}{2}\sqrt{\frac{9}{4}\left(\frac{\lambda}{J_{\mathrm{H}}}\right)^2 - 2\frac{\lambda}{J_{\mathrm{H}}} + 4} \right) \tag{D.13}$$

$$E_{J=1} = -13J_{\mathrm{H}} - \frac{1}{2}\lambda \tag{D.14}$$

$$E_{J=0,lower} = J_{\mathrm{H}} \left(-\frac{21}{2} - \frac{1}{2}\frac{\lambda}{J_{\mathrm{H}}} - \frac{1}{2}\sqrt{9\left(\frac{\lambda}{J_{\mathrm{H}}}\right)^2 + 10\frac{\lambda}{J_{\mathrm{H}}} + 25} \right). \tag{D.15}$$

D.5 t_{2g}^5

As shown in figure D.5, there is one fourfold degenerate ($J = 3/2$) and one doubly degenerate($J = 1/2$) branch.

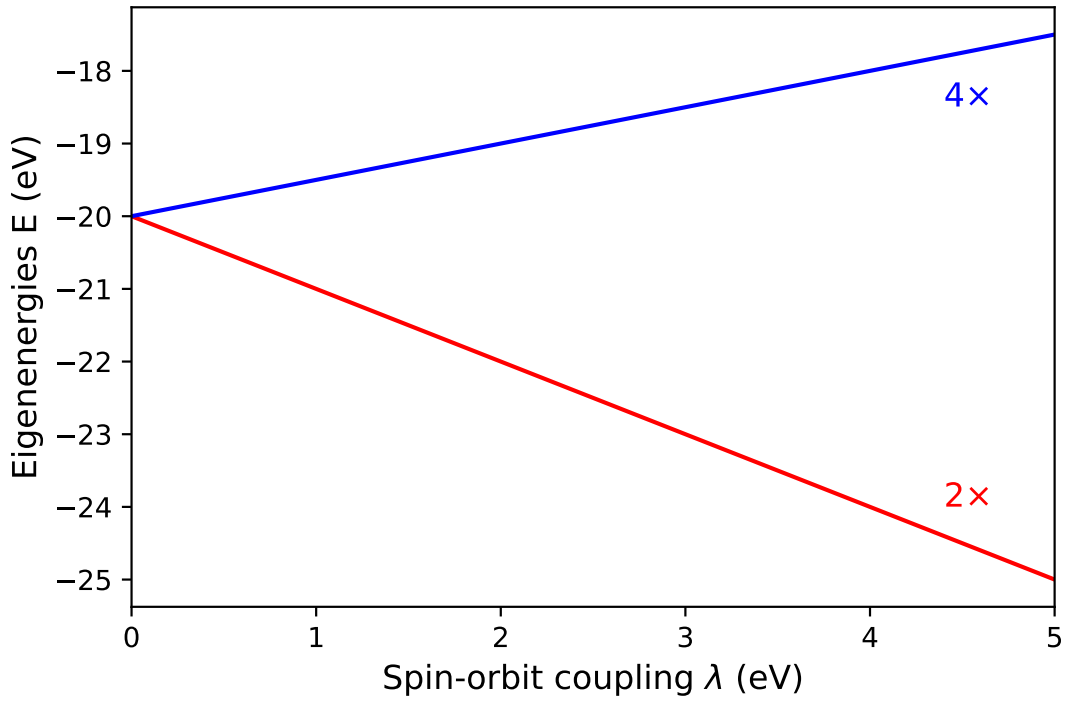

Figure D.5: The eigenenergies of the five electron case are shown for $U = 0, J_{\mathrm{H}} = 1$.

The energies of the states can be described by the linear functions

$$E_{J=\frac{3}{2}} = -20J_{\mathrm{H}} + \frac{1}{2}\lambda \tag{D.16}$$

$$E_{J=\frac{1}{2}} = -20J_{\mathrm{H}} - \lambda. \tag{D.17}$$

E Operators for the splitting at $J_{\mathrm{H}} = 0$

To describe the superexchange Hamiltonian for $J_{\mathrm{H}} = 0$, the fourfold degenerate ground state manifold was described by two doublets with (pseudo) spin-1/2 algebras. The fundamental operators used are listed below in their matrix form in the basis

$$\left\{\left|+\frac{3}{2}\right\rangle, \left|-\frac{3}{2}\right\rangle, \left|+\frac{1}{2}\right\rangle, \left|-\frac{1}{2}\right\rangle\right\}. \tag{E.1}$$

$$\sigma^{\mathrm{x}} = \begin{bmatrix} 0 & +1 & 0 & 0 \\ +1 & 0 & 0 & 0 \\ 0 & 0 & 0 & +1 \\ 0 & 0 & +1 & 0 \end{bmatrix} \quad \sigma^{\mathrm{y}} = \begin{bmatrix} 0 & -i & 0 & 0 \\ +i & 0 & 0 & 0 \\ 0 & 0 & 0 & -i \\ 0 & 0 & +i & 0 \end{bmatrix} \quad \sigma^{\mathrm{z}} = \begin{bmatrix} +1 & 0 & 0 & 0 \\ 0 & -1 & 0 & 0 \\ 0 & 0 & +1 & 0 \\ 0 & 0 & 0 & -1 \end{bmatrix} \tag{E.2}$$

$$\tau^{\mathrm{z}} = \begin{bmatrix} 1 & 0 & 0 & 0 \\ 0 & 1 & 0 & 0 \\ 0 & 0 & -1 & 0 \\ 0 & 0 & 0 & -1 \end{bmatrix} \quad \tau^{+} = \begin{bmatrix} 0 & 0 & 1 & 0 \\ 0 & 0 & 0 & 1 \\ 0 & 0 & 0 & 0 \\ 0 & 0 & 0 & 0 \end{bmatrix} \quad \tau^{-} = \begin{bmatrix} 0 & 0 & 0 & 0 \\ 0 & 0 & 0 & 0 \\ 1 & 0 & 0 & 0 \\ 0 & 1 & 0 & 0 \end{bmatrix} \tag{E.3}$$

Bibliography

[1] Herbert Goldstein, Charles P. Poole, and John L. Safko. *Classical Mechanics*. 3rd Edition. Addison Wesley, 2002. ISBN: 978-0-201-65702-9.

[2] Rudolf Gross and Achim Marx. *Festkörperphysik*. 2nd Edition. De Gruyter Oldenbourg, 2014. DOI: 10.1524/9783110358704.

[3] Adolfo Avella and Ferdinando Mancini. *Strongly Correlated Systems: Theoretical Methods*. 1st Edition. Springer Berlin, Heidelberg, 2011. DOI: 10.1007/978-3-642-21831-6.

[4] Daniel I. Khomskii. *Transition Metal Compounds*. Cambridge University Press, 2014. DOI: 10.1017/CBO9781139096782.

[5] Alexei Kitaev. "Anyons in an exactly solved model and beyond". In: *Annals of Physics* 321.1 (2006). January Special Issue, pp. 2–111. ISSN: 0003-4916. DOI: https://doi.org/10.1016/j.aop.2005.10.005. URL: https://www.sciencedirect.com/science/article/pii/S0003491605002381.

[6] G. Jackeli and G. Khaliullin. "Mott Insulators in the Strong Spin-Orbit Coupling Limit: From Heisenberg to a Quantum Compass and Kitaev Models". In: *Phys. Rev. Lett.* 102 (1 Jan. 2009), p. 017205. DOI: 10.1103/PhysRevLett.102.017205. URL: https://link.aps.org/doi/10.1103/PhysRevLett.102.017205.

[7] Yi Zhou, Kazushi Kanoda, and Tai-Kai Ng. "Quantum spin liquid states". In: *Rev. Mod. Phys.* 89 (2 Apr. 2017), p. 025003. DOI: 10.1103/RevModPhys.89.025003. URL: https://link.aps.org/doi/10.1103/RevModPhys.89.025003.

[8] Balents L. "Spin liquids in frustrated magnets". In: *Nature* 464 (7286 2010), pp. 199–208. DOI: 10.1038/nature08917.

[9] C. Broholm, R. J. Cava, S. A. Kivelson, D. G. Nocera, M. R. Norman, and T. Senthil. "Quantum spin liquids". In: *Science* 367.6475 (2020), eaay0668. DOI: 10.1126/science.aay0668. eprint: https://www.science.org/doi/pdf/10.1126/science.aay0668. URL: https://www.science.org/doi/abs/10.1126/science.aay0668.

[10] Manfred Sigrist and Kazuo Ueda. "Phenomenological theory of unconventional superconductivity". In: *Rev. Mod. Phys.* 63 (2 Apr. 1991), pp. 239–311. DOI: 10.1103/RevModPhys.63.239. URL: https://link.aps.org/doi/10.1103/RevModPhys.63.239.

[11] Sato Masatoshi and Yoichi Ando. "Topological superconductors: a review". In: *Rep Prog Phys* (2017). DOI: 10.1088/1361-6633/aa6ac7.

[12] Sergey V. Streltsov and Daniel I. Khomskii. "Jahn-Teller Effect and Spin-Orbit Coupling: Friends or Foes?" In: *Phys. Rev. X* 10 (3 Aug. 2020), p. 031043. DOI: 10.1103/PhysRevX.10.031043. URL: https://link.aps.org/doi/10.1103/PhysRevX.10.031043.

[13] P. Warzanowski, M. Magnaterra, G. Schlicht, Q. Faure, Ch. J. Sahle, P. Becker, L. Bohatý, M. Moretti Sala, G. Monaco, M. Hermanns, P. H. M. van Loosdrecht, and M. Grüninger. *Spin-orbit coupling in a half-filled t_{2g} shell: the case of $5d^3$ K_2ReCl_6*. 2023. arXiv: 2311.11419 [cond-mat.str-el].

[14] "transition element". In: (2019). DOI: doi:10.1351/goldbook.T06456. URL: https://doi.org/10.1351/goldbook.T06456.

[15] W. Pauli. "The Connection Between Spin and Statistics". In: *Phys. Rev.* 58 (8 Oct. 1940), pp. 716–722. DOI: 10.1103/PhysRev.58.716. URL: https://link.aps.org/doi/10.1103/PhysRev.58.716.

[16] Wolfgang Nolting. *Grundkurs Theoretische Physik 7*. 8th ed. Springer Spektrum Berlin, Heidelberg, 2015. DOI: 10.1007/978-3-642-25808-4.

[17] Jun John Sakurai and Jim Napolitano. *Modern quantum mechanics; rev. ed.* 2nd edition. Cambridge University Press, 2017.

[18] Albert Messiah. *Quantum Mechanics*. Dover Publications Inc., 2014.

[19] David J. Griffiths. *Introduction to Quantum Mechanics*. Cambridge University Press, 2017.

[20] Friedrich Hund. "Zur Deutung verwickelter Spektren, insbesondere der Elemente Scandium bis Nickel". In: *Zeitschrift für Physik* 33 (1925), pp. 345–371. URL: https://api.semanticscholar.org/CorpusID:122187870.

[21] Georgios L. Stamokostas and Gregory A. Fiete. "Mixing of $t_{2g} - e_g$ orbitals in $4d$ and $5d$ transition metal oxides". In: *Phys. Rev. B* 97 (8 Feb. 2018), p. 085150. DOI: 10.1103/PhysRevB.97.085150. URL: https://link.aps.org/doi/10.1103/PhysRevB.97.085150.

[22] Jahn H. A. and Teller E. "Stability of polyatomic molecules in degenerate electronic states - I—Orbital degeneracy". In: *Proc. R. Soc. Lond. A* (1937). DOI: 10.1098/rspa.1937.0142.

[23] Ching-Tarng Liang. "Kooperativer Jahn-Teller Effekt, orbitale Ordnung und Phasenuebergaenge". Dissertation. 2005. URL: http://dx.doi.org/10.17169/refubium-15741.

[24] Kliment I Kugel' and D I Khomskiĭ. "The Jahn-Teller effect and magnetism: transition metal compounds". In: *Soviet Physics Uspekhi* 25.4 (Apr. 1982), p. 231. DOI: 10.1070/PU1982v025n04ABEH004537. URL: https://dx.doi.org/10.1070/PU1982v025n04ABEH004537.

[25] Eva Pavarini, Erik Koch, Frithjof Anders, and Mark (eds.) Jarrell. *Correlated Electrons: From Models to Materials Modeling and Simulation*. Vol. 2. Verlag des Forschungszentrum Jülich, 2012. ISBN: 978-3-89336-796-2.

[26] G A Gehring and K A Gehring. "Co-operative Jahn-Teller effects". In: *Reports on Progress in Physics* 38.1 (Jan. 1975), p. 1. DOI: 10.1088/0034-4885/38/1/001. URL: https://dx.doi.org/10.1088/0034-4885/38/1/001.

[27] Junjiro Kanamori. "Electron Correlation and Ferromagnetism of Transition Metals". In: *Progress of Theoretical Physics* 30.3 (Sept. 1963), pp. 275–289. ISSN: 0033-068X. DOI: 10.1143/PTP.30.275. eprint: https://academic.oup.com/ptp/article-pdf/30/3/275/5278869/30-3-275.pdf. URL: https://doi.org/10.1143/PTP.30.275.

[28] Hubbard J. "Electron correlations in narrow energy bands". In: *Proc. R. Soc. Lond. A* (1963). DOI: 10.1098/rspa.1963.0204.

[29] Hugo U. R. Strand. "Correlated Materials - Models and Methods". Dissertation. 2013. URL: http://hdl.handle.net/2077/32118.

[30] Teresa Feldmaier. "Excitonic Antiferromagnetism in two-dimensional t_{2g}^4 Systems". Dissertation. 2019.

[31] Daniel Pranjic. "Superexchange and spin-orbit coupling for the half-filled t_{2g} shell". Masterarbeit. Universität Stuttgart, 2022.

[32] Craigt Smorynski. *History of Mathematics, A Supplement*. Springer New York, NY, 208. DOI: 10.1007/978-0-387-75481-9.

[33] Gautam Jha and Thomas Heine. "DFTB Parameters for the Periodic Table: Part III, Spin-Orbit Coupling". In: *Journal of Chemical Theory and Computation* 18.7 (2022). PMID: 35737969, pp. 4472–4481. DOI: 10.1021/acs.jctc.2c00376. eprint: https://doi.org/10.1021/acs.jctc.2c00376. URL: https://doi.org/10.1021/acs.jctc.2c00376.

[34] Judit Romhányi, Leon Balents, and George Jackeli. "Spin-Orbit Dimers and Noncollinear Phases in d^1 Cubic Double Perovskites". In: *Phys. Rev. Lett.* 118 (21 May 2017), p. 217202. DOI: 10.1103/PhysRevLett.118.217202. URL: https://link.aps.org/doi/10.1103/PhysRevLett.118.217202.

[35] George Jackeli and Giniyat Khaliullin. "Magnetically Hidden Order of Kramers Doublets in d^1 Systems: Sr_2VO_4". In: *Phys. Rev. Lett.* 103 (6 Aug. 2009), p. 067205. DOI: 10.1103/PhysRevLett.103.067205. URL: https://link.aps.org/doi/10.1103/PhysRevLett.103.067205.

Deutschsprachige Zusammenfassung

In der vorliegenden Arbeit wurde ein Modell-Hamiltonoperator untersucht, welcher die Eigenschaften einer halb gefüllten t_{2g} Schale in Übergangsmetallverbindungen beschreiben kann. Hierzu wurde zunächst das Problem eines einzelnen Ions betrachtet, bei welchem der Hamiltonoperator aus zwei Komponenten zusammengesetzt werden kann. Zum einen wurden die Effekte der Hundschen Kopplung durch einen Kanamori-Hubbard-Hamiltonian beschrieben, zum anderen die Spin-Bahn-Kopplung durch eine Wechselwirkung von Spin und Bahndrehimpuls der einzelnen Elektronen eingeführt. Hierbei zeigte sich, dass unabhängig von der Stärke der einzelnen Terme stets eine vierfach entartete Mannigfaltigkeit den Grundzustand bildete, deren Energie durch eine Nullstelle eines Polynoms dritten Grades beschrieben werden kann. Des Weiteren wurde die Grundzustandsmannigfaltigkeit vollständig beschrieben, wobei gezeigt wurde, dass eine Basis aus Eigenzuständen der beiden einzelnen Terme nicht ausreichend ist, um die Eigenzustände ihrer Summe zu beschreiben.

Hiernach wurde betrachtet, wie die Einführung des Jahn-Teller Effekts, einer Kopplung der elektronischen Zustände an das umgebende Gitter, Einfluss auf die Zustände nimmt und ob der Effekt zu einer Verzerrung der das Übergangsmetallion umgebenden Liganden führt. Hier wurde gezeigt, dass die Verzerrung mit steigender Spin-Bahn-Kopplung zunimmt, wobei die komprimierte geringfügig gegenüber der elongierten Geometrie bevorzugt wird.

Im zweiten Teil der Arbeit wurde untersucht, welchen Einfluss die Möglichkeit eines Elektronenaustauschs zwischen benachbarten Ionen durch Superaustausch auf die Grundzustandsmannigfaltigkeit hat. Hierbei konnte für die beiden Grenzfälle verschwindender Hundscher Kopplung respektive verschwindender Spin-Bahn-Kopplung eine analytische Beschreibung ermittelt werden. Für den Bereich kombinierter Effekte konnte gezeigt werden, dass eine störungstheoretische Berechnung zwar nicht immer, jedoch im Bereich physikalisch realistischer Parameter, eine nahezu perfekte Übereinstimmung mit der exakten Diagonalisierung des Hamiltonoperators erzielt.

Des weiteren wurde analysiert, inwiefern die Einführung eines Superaustausches die Auswirkungen des Jahn-Teller-Effektes verändert. In einem stark vereinfachenden Ansatz wurde gezeigt, dass sich die durch den Jahn-Teller-Effekt bedingten Symmetriereduktionen

im Zwei-Ionen-Modell bereits bei kleinerer Spin-Bahn-Kopplung bemerkbar machen können als beim One-Site Fall.

Danksagung

An dieser Stelle möchte ich zunächst allen danken, die zum Gelingen dieser Arbeit beigetragen haben:

- Prof. Dr. Maria Daghofer für die Gelegenheit, meine Masterarbeit am FMQ zu absolvieren und die hervorragende Betreuung dieser,
- Prof. Dr. Mathias Scheurer für die Übernahme des Mitberichtes,
- meinen Kollegen am Institut für die spannenden Diskussionen wissenschaftlicher und unwissenschaftlicher Natur, im Besonderen Pascal Strobel und Friedemann Aust, die mir bei fachlichen Fragen stets mit gutem Rat weiterhelfen konnten.

Da diese Arbeit auch das Ende meines Studiums markiert, möchte ich mich zudem bei all denen bedanken, die mich in den vergangenen sechs Jahren unterstützt und damit diesen Abschnitt meines Lebens maßgeblich geprägt haben. Zum einen möchte ich mich bei allen meinen Freunden bedanken, welche dafür gesorgt haben, dass die vergangenen sechs Jahre eben nicht nur aus Vorlesungen und Übungen, sondern auch aus der wunderbaren Zeit dazwischen bestanden. Ohne euch hätte mir das Studium nur halb so viel Freude bereitet.

Zum anderen und ganz besonders ist zudem meine Familie hervorzuheben, die mich zu jedem Zeitpunkt bedingungslos und auf vielfältige Art und Weise unterstützt haben. Ihr habt mich zu dem Menschen gemacht, der ich heute bin. Danke.

Erklärung

Ich versichere,

- dass ich diese Masterarbeit selbstständig verfasst habe,
- dass ich keine anderen als die angegebenen Quellen benutzt und alle wörtlich oder sinngemäß aus anderen Werken übernommenen Aussagen als solche gekennzeichnet habe,
- dass die eingereichte Arbeit weder vollständig noch in wesentlichen Teilen Gegenstand eines anderen Prüfungsverfahrens gewesen ist,
- und dass das elektronische Exemplar mit den anderen Exemplaren übereinstimmt.

Stuttgart, den 18. Dezember 2023 *Marco Schönleber*